

PHOTOLUMINESCENCE AND ELECTROLUMINESCENCE OF NEAR-INFRARED
EMITTING LANTHANIDE COMPLEXES IN CONJUGATED POLYMER HOSTS

By

BENJAMIN SCOTT HARRISON

A DISSERTATION PRESENTED TO THE GRADUATE SCHOOL
OF THE UNIVERSITY OF FLORIDA IN PARTIAL FULFILLMENT
OF THE REQUIREMENTS FOR THE DEGREE OF
DOCTOR OF PHILOSOPHY

UNIVERSITY OF FLORIDA

2003

You are worthy, Jehovah, even our God, to receive the glory and the honor and the power, because you created all things, and because of your will they existed and were created.”—Revelation 4:11.

ACKNOWLEDGMENTS

There are numerous people who deserve to be acknowledged because so many supported me in the mental, physical, spiritual and emotional sense and it would nearly take the length of this dissertation to completely relate all the support I have received.

My experience in graduate school can be likened to living on a ship. For the past four years, my advisor Professor “Captain” Kirk Schanze has taken me from deck hand to commanding the boat. He allowed me to navigate the waters of science with little interference. I worked on an amazing project which has sailed several seas found in science including physics and material science. Occasionally, I report back to shore to report to my other advisors that have helped me to navigate the waters safely including Prof. John Reynolds, Prof. James Boncella, Prof. David Tanner and Prof. Paul Holloway.

Others have been instrumental including some of my crew such as first mate Dr. Tae-Sik Kang and the other deck hands Nisha Ananthakrishnan, Garry Cunningham and Joonbo Shim. There were others that have closely assisted me in my work many times giving me the necessary tools to chart unexplored regions. They include Tim Foley, Alison Knefely, and Mohammed Bougetteya.

Besides my shipmates, many others have gained my deep respect at UF such as Dr. Khalil Abboud who gave me the privilege of special training in the art of x-ray crystallography. Also, Prof. Haniph Latchman provided me much useful guidance in many aspects of my life.

Dr. Schanze has always complemented his fleet with talent postdoctoral researchers that have helped me along the way including Mauricio Pinto, Yao Liu, Yibing “Ben” Shen, and Shujun Jiang. Also, he possesses a complement of talented graduate students that have aided me including those that have already moved on to other places such as Keith Walters, Joanne Bedlek-Anslow, Ed Whittle, Kevin Ley, and Yiting Li and those who come after me including Chunyan Tan, Ksenija Haskins-Glusac, Thomas Cardolaccia, Eric Silverman, Boris Kristal, Shengxia Liu, and Erkan Kose.

But even sailors come home once in a while. There the most patient person to tolerate me, my wife, Patty is there to greet me. She has been there to support me through the trials and tribulations of graduate school and parenthood. With her support and the support of our families, we have survived to the end. There are many, many other friends I would like to thank who have supported me. Finally, I must acknowledge Julie Walters who was the first real person I met in Gainesville and has ever since been a close supportive friend of Patty and me.

TABLE OF CONTENTS

	<u>Page</u>
ACKNOWLEDGMENTS	iii
LIST OF TABLES	viii
LIST OF FIGURES	ix
ABSTRACT	15
CHAPTER	
1 SOLUTION PHOTOPHYSICS OF NEAR-INFRARED EMITTING LANTHANIDE COMPLEXES.....	1
Background.....	1
Neodymium <i>tris</i> - β -Diketonates	4
Macrocyclics as the Coordinating Ligand for Near-Infrared Emitting Lanthanides	6
Near-Infrared Emitting Lanthanides Coordinated to Porphyrins	9
Synthesis of Lanthanide Monoporphyrinates	11
Photophysical Properties of Lanthanide <i>tris</i> - β -Diketonates	14
Absorption Properties of Lanthanide <i>tris</i> - β -Diketonates.....	15
Photoluminescent Properties of Lanthanide <i>tris</i> - β -Diketonates	16
Photophysical Properties of Lanthanide Monoporphyrinates in Solution	19
Axial Ligand Effects on the Absorption Properties of Ln(TPP)L	19
Metal Center Effects on the Absorption Properties of Ln(TPP)L	21
Near-Infrared Emission from Lanthanide Monoporphyrinates in CH ₂ Cl ₂	22
Visible Emission from Ln(TPP)L in CH ₂ Cl ₂	28
Solvent Effects on Near-Infrared Quantum Yield of Yb(TPP)L	34
Near-Infrared Emission from Other Lanthanide Porphyrin Emitters	38
Transient Absorption Spectroscopy of Ln(TPP)L Complexes	40
Conclusion	43
Experimental	43
2 NEAR-INFRARED EMISSION FROM LANTHANIDE COMPLEXES BLENDED INTO CONJUGATED POLYMER FILMS	45
Background.....	45
Energy Transfer between Conjugated Polymers and Visible Emitting Lanthanide Complexes in Polymer Blends.....	48

Near-Infrared Emission from Lanthanide <i>tris</i> - β -Diketonates Complexes Blended in PPP-R10 Films.....	55
Near-Infrared Emission from Yb <i>tris</i> - β -Diketonate Complexes Blended in PPP-OR11 Films.....	58
Quenching of PPP-OR11 Fluorescence by Lanthanide Monoporphyrinate Complexes.....	60
Near-Infrared Emission from Lanthanide Monoporphyrinate Complexes Blended in PPP-OR11 Films	64
Discussion.....	67
Conclusion	70
Experimental.....	70
 3 NEAR-INFRA-RED ELECTROLUMINESCENCE OF LANTHANIDE COMPLEXES IN CONJUGATED POLYMER BLENDS	72
Background.....	72
Poly(1,4-phenylenevinylene)s as Electroluminescent Emitters	73
Poly(1,4-phenylene)s as Electroluminescent Emitters	75
Electroluminescence Mechanisms.....	75
Lanthanide Complexes as Electroluminescent Emitters.....	78
Near-Infrared Emitting Lanthanide Based Devices.....	80
Electroluminescence from Lanthanide <i>tris</i> - β -Diketonates Blended in MEH-PPV	81
Concentration Effects of Yb(TPP)acac Blended into MEH-PPV on Device Performance	85
Near-Infrared Emission from Yb(TPP)acac as the Only Component in the Active Layer	89
Near-Infrared Emission from Er(TPP)acac in MEH-PPV	91
Electroluminescence of PPP-OR11	92
Near-Infrared Electroluminescence of Yb(TPP)TP Blended into PPP-OR11	95
Near-Infrared Electroluminescence of Yb(TPP)L(OEt) ₃ Blended into PPP-OR11	102
Near-Infrared Emission from Ln(TPP)L in Polystyrene	107
Near-Infrared Electroluminescence from Other Lanthanide TPP Complexes	109
Visible Emission of Lanthanide Complexes in Polystyrene.....	112
Dual Emitting Near-Infrared Devices.....	114
Discussion.....	115
Conclusion	124
Experimental.....	124
ITO Etching	125
Cleaning ITO	126
Spin Coating Hole Transport and Active Layers	127
Metal Electrode Deposition	127
Electroluminescent Device Measurements.....	129
 4 CONCLUSIONS	131
Near-Infrared Photoluminescence	131

Near-Infrared Electroluminescence	133
APPENDIX	
A CALCULATION OF EXTERNAL ELECTROLUMINESCENT QUANTUM EFFICIENCIES	134
Preparing the Detector	134
Calibrating the Detector	135
Measuring the Irradiance of an Electroluminescent Device	138
Electroluminescence Quantum Efficiency	140
B DRAWINGS	142
C ELECTROLUMINESCENT DATA PROCESSING	147
Worksheet: RawDataExtract	149
Worksheet: Radiance Data	150
Worksheet: Photon Data	150
Worksheet: Radiance Integrator	151
Worksheet: Photon Integrator	151
Worksheet: Correction Factors	152
Worksheet: Table Summary	153
Macro: DataExtractor	154
Macro: DataExtractorIntegrator	156
Macro: TableSummary	157
LIST OF REFERENCES	160
BIOGRAPHICAL SKETCH	175

LIST OF TABLES

<u>Table</u>	<u>page</u>
1-1. Near-infrared quantum yields and lifetimes of lanthanide <i>tris</i> - β -diketonates.....	4
1-2. Structures of Yanagida's ligands coordinated to lanthanides	5
1-3. Selected near-infrared quantum yields reported in the literature.	5
1-4. Natural radiative lifetimes and rates for lanthanides.....	6
1-5. Emission transitions of lanthanide <i>tris</i> - β -diketonates in benzene.	17
1-6. Photophysical properties of Ln(TPP)TP measured in CH ₂ Cl ₂	20
1-7. Photophysical properties of Ln(TPP)L(OEt) ₃ measured in CH ₂ Cl ₂	20
1-8. Near-infrared peak positions of Yb(TPP)TP at 5 nm resolution.....	27
1-9. Solvent effects on the near-infrared quantum yields of Yb(TPP)acac and Yb(TPP)TP.....	35
2-1. Critical Förster distances for lanthanide/conjugated polymer systems.	70
3-1. Near-infrared external EL efficiencies of 5, 10, 15 mol% concentrations of Yb(TPP)TP blended into PPP-OR11 at various current densities.	99
3-2. Near-infrared external EL efficiencies of 5, 10, 15 mol% concentrations of Yb(TPP)L(OEt) ₃ blended into PPP-OR11 at various current densities.	105
3-3. Maximum near-infrared external and internal EL efficiencies of PPP-OR11 and Yb(TPP)L blended into PPP-OR11 or PS.....	116
3-4. Apparent fraction of electron-hole recombination of PPP-OR11 and Yb(TPP)L blended into PPP-OR11 or PS.....	117
3-5. Summary of electroluminescent device fabrication.	129

LIST OF FIGURES

<u>Figure</u>	<u>page</u>
1-1. The electronic energy levels of trivalent lanthanide ions in fluoride glasses.....	2
1-2. Jablonski diagram showing the mechanism for ligand sensitized Yb ³⁺ luminescence.	3
1-3. Chemical structure of <i>m</i> -terphenyl.....	7
1-4. Structure of azamacrocyclic ligands used by Parker.....	9
1-5. Structure of various porphyrins.	10
1-6. Synthetic scheme used by Horrocks.....	12
1-7. Synthetic scheme of high-yield reactions of lanthanide monoporphyrins with easily modified axial ligand.	13
1-8. Chemical structures of lanthanide <i>tris</i> - β -diketonates studied..	14
1-9. Absorbance of Nd(TMHD) ₃ phen (---), Nd(DBM) ₃ phen (----), and Nd(DNM) ₃ phen(—) in chloroform.	16
1-10. Near-infrared emission scaled to show relative efficiencies of Ln(L) ₃ phen in benzene.....	18
1-11. Chemical structures of lanthanide tetraphenylporphyrin complexes with differing capping ligands.....	19
1-12. Absorption spectra of Yb(TPP)L in methylene chloride.	21
1-13. Molar absorptivity of Ln(TPP)TP in CH ₂ Cl ₂	23
1-14. Molar absorptivity of Ln(TPP)L(OEt) ₃ in CH ₂ Cl ₂	24
1-15. Visible and near-infrared emission of a) Yb(TPP)acac, b) Yb(TPP)L(OEt) ₃ , and c) Yb(TPP)TP in CH ₂ Cl ₂ when excited at 420 nm.	25
1-16. Near-infrared PL emission of Yb(TPP)TP (—) and Yb(TPP)L(OEt) ₃ (---)in CH ₂ Cl ₂ measured on an InGaAs detector	26

1-17. Photoluminescence of Yb(TPP)TP in CH ₂ Cl ₂ upon 420 nm excitation at 5 nm resolution.....	27
1-18. Visible emission of Ln(TPP)L(OEt) ₃ in CH ₂ Cl ₂ upon 420 nm excitation.....	29
1-19. Excitation spectra of Yb(TPP)L(OEt) ₃ in CH ₂ Cl ₂	30
1-20. Excitation spectra of Er(TPP)L(OEt) ₃ in CH ₂ Cl ₂	31
1-21. Excitation spectra of Ho(TPP)L(OEt) ₃ in CH ₂ Cl ₂	32
1-22. Excitation spectra of Tm(TPP)L(OEt) ₃ in CH ₂ Cl ₂	33
1-23. Visible emission from Ho(TPP)L(OEt) ₃ upon 330 nm emission.....	34
1-24. Representation of the radiative transition energies of Yb ³⁺ , Nd ³⁺ , and Er ³⁺ and the vibrational energies of common bonds found in organic systems.	38
1-25. Near-infrared emission of a) Er(TPP)TP and b)Er(TPP)L(OEt) ₃ in CH ₂ Cl ₂ upon exciting at 420 nm uncorrected for detector response.....	39
1-26. Near-infrared emission of Nd(TPP)TP in CH ₂ Cl ₂ upon exciting at 420 nm.	39
1-27. Transient absorptions of Ln(TPP)L.....	42
2-1. Structures of the conjugated poly(<i>p</i> -phenylene) polymers and the lanthanide complexes blended into the polymers.	47
2-2. Absorbance (solid line) and fluorescence (dashed line) of a) PPP-R10 and b) PPP-OR11 in chloroform.....	49
2-3. Absorption of films on quartz substrates of 0, 1, 2, 5, and 10 mol% of Eu(DBM) ₃ batho blended into PPP-R10.	51
2-4. Emission of polymer films that contain 0, 1, 2, 5, and 10 mol% Eu(DBM) ₃ batho in PPP-R10 upon excitation at 315 nm.	51
2-5. Normalized excitation spectra of ⁵ D ₀ → ⁷ F ₂ of Eu(DBM) ₃ batho (solid line) and PPP-R10 film containing 10 mol% Eu(DBM) ₃ batho (dashed line).	52
2-6. Absorption of spin cast films on quartz substrates of 0, 1, 2, 5, and 10 mol% of Eu(DNM) ₃ phen blended into PPP-R10.....	53
2-7. Emission of polymer films that contain 0, 1, 2, 5, and 10 mol% Eu(DNM) ₃ phen in PPP-R10 upon excitation at 315 nm.	54
2-8. Normalized excitation spectra of ⁵ D ₀ → ⁷ F ₂ emission of 1% (···) 2% (---), 5% (-·-·-), and 10% (— —) Eu(DNM) ₃ phen in PPP-R10.....	54

2-9. Near-infrared emission from spin-coated films of 10 mol% blends of the lanthanide complex with PPP-R10.....	56
2-10. Visible emission from the $^1D_2 \rightarrow ^3H_4$ transition of Pr^{3+} when a film of 10 mol% $Pr(DNM)_3phen$ blended with PPP-R10 is excited at 327 nm.....	57
2-11. The electronic levels of trivalent lanthanide ions in fluoride glasses	58
2-12. PL of films of PPP-OR11 blended with 0, 1, 2, 5, 10, 15, and 20 mol%.....	59
2-13. Fraction of PPP-OR11 fluorescence quenched by (●)Yb(DBM) ₃ phen and (▲)Yb(DNM) ₃ phen in spin-coated films prepared by blending the lanthanide complex into the polymer.....	59
2-14. Absorbance of spin cast films of Ln(TPP)TP blended into PPP-OR11.....	61
2-15. Visible emission of spin cast films of 0, 1, 2, 5, 10, 15, and 20 mol% of a) Er(TPP)TP and c) Ho(TPP)TP in PPP-OR11 when excited at 367 nm	62
2-16. Visible emission of spin cast films of 0, 1, 2, 5, 10, 15, and 20 mol% of a) Tm(TPP)TP and c) Yb(TPP)TP in PPP-OR11 when excited at 367 nm	63
2-17. Fraction of PPP emission quenched by (●) Ho(TPP)TP, (▼) Er(TPP)TP, (■) Tm(TPP)TP, and (◆) Yb(TPP)TP.....	63
2-18. Near-infrared emission of 1, 2, 5, 10, 15, and 20 mol% Yb(TPP)TP in PPP-OR11 upon excitation at 367 nm.....	65
2-19. Excitation spectra of 977 nm emission of 1, 2, 5, 10, 15, and 20 mol% Yb(TPP)TP in PPP-OR11 normalized to the PPP-OR11 intensity maximum.....	66
2-20. Near-infrared emission of 20 mol% Er(TPP)TP in PPP-OR11	66
2-21. Spectral overlap of PPP-OR11 emission (—) and the absorption of a) Ln(DBM) ₃ phen, b) Ln(DNM) ₃ phen and c) Ln(TPP)TP (---).	69
3-1. Chemical structure of aluminum <i>tris</i> -(8-hydroxyquinolate) (AlQ ₃) and a single-layer device architecture.....	73
3-2. Chemical structures of three common poly(<i>p</i> -phenylenevinylene)s	74
3-3. Sulphonium prepolymer route to PPV.	74
3-5. Structure of a multilayer light emitting diode	77
3-6. Examples of small-molecule hole transport materials.	78
3-7. Structure of hole transporting polythiophene PEDOT-PSS.....	79

3-8. Host polymer structures	81
3-9. Structure of EL device: glass/ITO/PEDOT-PSS (40 nm) / lanthanide complex and polymer host / Ca (5 nm) / Al (200 nm).....	82
3-10. Electroluminescence spectrum of ITO/PEDOT-PSS/MEH-PPV/Ca/Al recorded at 9 V.....	82
3-11. Structures of Yb tris- β -diketonates complexes blended into MEH-PPV.....	83
3-12. Electroluminescence spectrum at 9 V for 1:2 weight ratio of Yb(TTFA) ₃ phen to MEH-PPV device.....	84
3-13. Electroluminescence spectrum at 9 V for 1:1 weight ratio of Yb(DNM) ₃ phen to MEH-PPV device.....	85
3-14. Chemical structure of lanthanide tetraphenylmonoporphyrinate acetylacetonate. ..	86
3-15. Electroluminescence spectra of Yb(TPP)acac in MEH-PPV	87
3-16. Current response of electroluminescent devices at different voltages	90
3-17. Electroluminescence spectra of ITO/PEDOT/Yb(TPP)acac/Ca/Al device	91
3-18. Electroluminescence spectrum of 1:2 (weight ratio) Er(TPP)acac:MEH-PPV.....	92
3-19. Electroluminescence spectrum of PPP-OR11 at 6 V.	93
3-20. Current density (circles) and irradiance (triangles) of PPP-OR11 at different applied voltages.....	94
3-21. Efficiencies of ITO/PEDOT-PSS/PPP-OR11/Ca/Al devices verses current density	94
3-22 Chemical structures of lanthanide tetraphenylporphyrin complexes Ln(TPP) with differing capping ligands.....	95
3-23. Electroluminescence spectra measured from 4 to 10 V in 1 V increments.....	98
3-24. Current and radiance profiles of devices consisting of Yb(TPP)TP in PPP-OR11.	99
3-25. Log-log plot of near-infrared efficiency of a) 5 mol%, b) 10 mol%, and c) 15 mol% Yb(TPP)TP in PPP-OR11 verses current density.....	100
3-26. Log-log plot of near-infrared power output of a) 5 mol%, b) 10 mol%, and c) 15 mol% Yb(TPP)TP in PPP-OR11 verses input power.	101

3-27. Electroluminescence spectra of 15 mol% Yb(TPP)L(OEt) ₃ in PPP-OR11 from 5 to 12 V in 1 volt increments.	103
3-28. Current and radiance profiles of devices consisting of Yb(TPP)L(OEt) ₃ in PPP-OR11.	104
3-29. Log-log plot of near-infrared efficiency of a) 5 mol%, b) 10 mol%, and c) 15 mol% Yb(TPP)L(OEt) ₃ in PPP-OR11 versus current density.	105
3-30. Log-log plot of near-infrared power output of a) 5 mol%, b) 10 mol%, and c) 15 mol% Yb(TPP)L(OEt) ₃ in PPP-OR11 versus input power.	106
3-31. Current density (circles) and near-infrared irradiance (triangles) of 10 mol% Yb(TPP)L(OEt) ₃ in polystyrene (M _n : 280,000)	108
3-32. Electroluminescence from 6 V to 10 V for 10 mol% Yb(TPP)L(OEt) ₃ in polystyrene.	108
3-33. The electronic energy levels of Pr ³⁺ , Nd ³⁺ , Ho ³⁺ , Er ³⁺ , and Tm ³⁺ ions in fluoride glasses.	109
3-34. Electroluminescence of other near-infrared emitting lanthanides.	111
3-35. Visible EL at 9 V of 1:1 weight ratio of Ln(TPP)L(OEt) ₃ in PS: a) Er ³⁺ b) Ho ³⁺ c) Nd ³⁺ and d) Pr ³⁺	113
3-36. Electroluminescence of 10 mol% Yb(TPP)L(OEt) ₃ and 10 mol% Er(TPP)L(OEt) ₃ in PPP-OR11 at 7 V.	115
3-37. When Ln(TPP)L is dispersed into PPP-OR11, it may aggregate allowing charge hopping between Ln(TPP)L complexes to occur at lower concentrations (5 mol%) than estimated (15 mol%).	121
3-38. Darker areas indicated areas where ITO will be etched away when exposed to aqua regia vapors.	125
3-39. Masked ITO is suspended over aqua regia vapors for 6 minutes to etch away the exposed ITO.	126
3-40. ITO coated with polymer layers are placed face up on the inverted stage for electrode deposition.	128
3-41. Front and side view of device holder mounted on XY stage setup for EL device measurements on the Triax 180/CCD system.	130
4-1. Proposed ligands for coordination to lanthanides.	133
A-1. Irradiance (solid circles) at 50 cm from the detector of a 100 W QTH (S/N: EH-156) calibrated on September 18, 2002.	135

A-2. Fractional transmittance of 1% neutral density filter	136
A-3. Raw data collected by the CCD detector of 100 W QTH Lamp placed 250 cm away from 0.1 mm entrance slit width of monochromator.	137
A-4. Correction factors for ISA-SPEX Triax 180 spectrograph equipped with a liquid N ₂ cooled CCD detector.....	138
B-1. Dimensions of a Teflon holder for ITO glass during cleaning	142
B-2. Mounting stage for metal vapor deposition	143
B-3. Drawing of EL device holder.....	144
B-4. Mount for device holder to XY stage.....	145
B-5. Mask for metal deposition of electrodes	146

Abstract of Dissertation Presented to the Graduate School
of the University of Florida in Partial Fulfillment of the
Requirements for the Degree of Doctor of Philosophy

PHOTOLUMINESCENCE AND ELECTROLUMINESCENCE OF NEAR-INFRARED
EMITTING LANTHANIDE COMPLEXES IN CONJUGATED POLYMER HOSTS

By

Benjamin Scott Harrison

May 2003

Chair: Kirk S. Schanze

Major Department: Chemistry

The photoluminescent and electroluminescent properties of near-infrared emitting lanthanide monoporphyrinate complexes blended into conjugated polymers were investigated. The lanthanide monoporphyrinate complexes, Ln(TPP)L consisted of a lanthanide (Ln= Er³⁺, Nd³⁺, Pr³⁺, Tm³⁺, Yb³⁺) coordinated to 5,10, 15, 20-tetraphenylporphyrin (TPP) and a capping ligand, L. The capping ligand was either an acetylacetonate (acac), *tris*-pyrazoylborate (TP), or (cyclopentadienyl)tris(diethoxyphosphito-P)cobaltate) (L(OEt)₃) anion. The optical absorption properties of these complexes resembled “regular” metalloporphyrin absorption which was not significantly influenced with different coordinated lanthanide ions or capping ligands. The photoluminescent properties showed quenching of the porphyrin emission and sensitized near-infrared emission from Yb³⁺ (²F_{5/2}→²F_{7/2}, [977 nm]); Nd³⁺ (⁴F_{3/2}→⁴I_{11/2},

[880 nm]), $^4F_{3/2} \rightarrow ^4I_{13/2}$ [1060 nm], $^4F_{3/2} \rightarrow ^4I_{15/2}$ [1330 nm]); and Er^{3+} ($^4I_{13/2} \rightarrow ^4I_{15/2}$, [1520 nm]) was observed in CH_2Cl_2 . The photoluminescent quantum yields of the $Yb(TPP)TP$ and $Yb(TPP)(LOEt)_3$ were 3.2% and 2.4%, respectively.

Photoluminescent studies of $Ln(TPP)L$ blended into a bis-alkoxy poly(*p*-phenylene) (PPP-OR11) host show that energy transfer from the host to the lanthanide complex does occur resulting in sensitized near-infrared emission. Electroluminescence (EL) was observed from films containing $Ln(TPP)L$ in PPP-OR11. In all devices, the visible emission from the host was strongly suppressed. For devices where $Ln(TPP)L$ was Yb^{3+} , Nd^{3+} , or Er^{3+} , near-infrared emission was observed. For electroluminescent devices made with $Yb(TPP)TP$ in PPP-OR11, the external quantum efficiencies were typically 10^{-4} . Substituting PPP-OR11 with polystyrene improved the external quantum efficiencies to 10^{-3} suggesting that charge hopping between $Ln(TPP)TP$ may be more important than Förster energy transfer from polymer host to $Ln(TPP)$.

CHAPTER 1

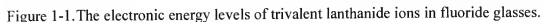
SOLUTION PHOTOPHYSICS OF NEAR-INFRARED EMITTING LANTHANIDE COMPLEXES

Background

Lanthanides are unique among the elements found on the periodic table because of their similar chemical reactivities yet diverse optical and magnetic properties. Their optical properties are different from other ions and molecular species because they absorb and emit light over narrow wavelength ranges. These unique optical properties arise because the inner-shell $4f$ orbitals are shielded by filled $5s$ and $5p$ valence orbitals. Effective shielding of $4f$ orbitals minimizes interactions with the surrounding environment, (i.e. ligands, solvent) also results in other optical properties including weak transition intensities, long lifetimes and transitions energies that are relatively insensitive to the coordinating ligands.

The wide variety of ultra-violet, visible, and near-infrared transitions of lanthanides were first described by Dieke.¹ Figure 1-1 shows an example of the energy states observed for lanthanide fluoride glasses.² The electronic structure observed results from spin-orbit coupling and crystal field effects on the lanthanide electronic states. A more detailed explanations of the complexities of $4f \rightarrow 4f$ transitions can be found in an excellent reference work on lanthanide chemistry edited by Gschneidner and Eyring.³

The forbidden nature of $f \rightarrow f$ transitions makes direct excitation difficult. The molar absorptivities of $f \rightarrow f$ transitions are typically $1\text{--}10 \text{ M}^{-1} \text{ cm}^{-1}$ compared with $d \rightarrow d$ transitions ($10^3 \text{ M}^{-1} \text{ cm}^{-1}$) of transition metals and allowed $\pi \rightarrow \pi^*$ transitions ($10^4\text{--}10^5 \text{ M}^{-1}$



1. The ligand is excited from the singlet ground state to a singlet excited state ($S_0 \rightarrow S_n$).
2. The S_n state decays into the lowest energy singlet excited state ($S_n \rightarrow S_1$) on the ligand.
3. The singlet state intersystem crosses into the ligand-based triplet state ($S_1 \rightarrow T_1$).
4. Energy transfer to the lanthanide then occurs.

5. The energy on the lanthanide can then undergo radiative decay resulting in lanthanide-centered luminescence.

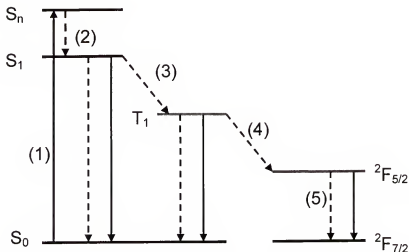


Figure 1-2. Jablonski diagram showing the mechanism for ligand sensitized Yb^{3+} luminescence. Solid lines indicate radiative transitions. Dashed lines represent non-radiative transitions.

Since this important discovery about ligand-sensitized lanthanide photoluminescence, intensive efforts have been put forth to improve lanthanide luminescent quantum efficiencies. For example, many groups have used β -diketonates as sensitizing ligands for lanthanides. Typically, three anionic β -diketonates coordinate through the carbonyl oxygen to the lanthanide. Commonly, lanthanide complexes have coordination numbers of seven to nine; therefore, to complete the coordination sphere, either water or another neutral coordinating ligand such as phenanthroline is coordinated to the lanthanide.

Most research in luminescent organolanthanide complexes has focused on visible emitters such as Eu^{3+} and Tb^{3+} for their use as inorganic phosphors in display technologies. Significantly less effort has been expended towards improving the

quantum efficiencies of near-infrared emitting lanthanides.⁵⁻⁸ Table 1-1 and Table 1-3 are compilations from the literature of near-infrared quantum yields and lifetimes of simple lanthanide *tris*- β -diketonates in their respective solvents. The next section gives a brief overview of significant work in near-infrared emitting lanthanide complexes.

Table 1-1. Near-infrared quantum yields and lifetimes of lanthanide *tris*- β -diketonates

Compound	λ / nm	Φ	τ / μ s	Solvent
Yb(TTFA) ₃	977	3.5×10^{-4}	5.7	Toluene
Yb(TTFA) ₃ phen	977	11.0×10^{-4}	10.4	Toluene
Yb(DBM) ₃ phen	977	1.3×10^{-3}	9	Toluene
Pr(TTA) ₃ •2H ₂ O	1000	1.8×10^{-4}	--	DMSO

Values for Yb³⁺ complexes are from references 9 and 10. Quantum yield data for Pr³⁺ complex can be found in reference 11.

Neodymium *tris*- β -Diketonates

Yanagida and co-workers have investigated the near-infrared luminescence of small molecule Nd³⁺ complexes for use in lasers.¹² In particular, they have focused on fluorinated ligands and other ligands that lack many high-frequency vibrational modes, such as found in C-H and O-H bonds, which contribute to non-radiative decay of excited states. Table 1-2 shows the structures of the coordinating anionic ligands used by Yanagida. Table 1-3 shows the quantum yield and lifetimes for these compounds in various solvents.¹³ The quantum yield represents the ratio of photons emitted to photons absorbed. The photoluminescent quantum yield can also be expressed as the ratio of the radiative rate, k_r , to the sum of the radiative and non-radiative rates (k_{nr}) as shown in equation 1-1.

$$\Phi = \frac{k_r}{k_r + k_{nr}} \quad 1-1$$

Table 1-2. Structures of Yanagida's ligands coordinated to lanthanides

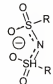
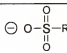
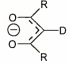
Ligand	Abbreviation	R
	pms	CF ₃
	pes	C ₂ F ₅
	pbs	C ₄ F ₉
	pos	C ₈ F ₁₇
	ms	CF ₃
	os	C ₈ F ₁₇
	dfa	CF ₃
	pom	C ₇ F ₁₅

Table 1-3. Selected near-infrared quantum yields reported in the literature.

	Q.Y. (%) DMSO- <i>d</i> 6	Q.Y. (%) Acetone- <i>d</i> 6	Q.Y. (%) acetone	Lifetime (μs) acetone- <i>d</i> 6
Nd(pos) ₃	3.3	3.2	3.0	13.0
Nd(pbs) ₃	3.3	2.5	0.8	2.0
Nd(pes) ₃ ·2H ₂ O	3.3	1.0	<0.01	--
Nd(pms) ₃ ·2H ₂ O	3.3	0.8	<0.01	--
Nd(bama) ₃	3.3	1.1	0.8	2.0
Nd(os) ₃ ·6H ₂ O	3.3	1.1	<0.01	2.0
Nd(ms) ₃ ·6H ₂ O	3.3	1.1	<0.01	4.0
Nd(pom) ₃ ·H ₂ O	3.2	0.8	<0.01	--
Nd(dfa) ₃ ·2H ₂ O	1.1	0.3	<0.01	1.7
Nd(NO ₃) ₃ ·6H ₂ O	3.3	<0.01	<0.01	<0.1

Comparing the lifetimes in Table 1-1 and Table 1-3 to the natural radiative lifetimes of the lanthanide ion in Table 1-4, it is evident that non-radiative pathways

dominate the deactivation of the excited state. The natural radiative rate of the near-infrared emitting lanthanide is in the order of milliseconds compared to the microsecond lifetimes observed in the lanthanide complexes.

Table 1-4. Natural radiative lifetimes and rates for lanthanides.

Ln	τ (ms)	k_r (s^{-1})
Yb ³⁺	2.0	500
Er ³⁺	14.0	71
Nd ³⁺	0.25	4000

Macrocyclics as the Coordinating Ligand for Near-Infrared Emitting Lanthanides

Although europium-based materials continue to be one of the most studied lanthanide systems, several groups have worked on macrocyclic systems containing near-infrared emitting lanthanides. These groups hoped to decrease non-radiative losses by designing ligands that minimize quenching by O-H and N-H oscillators with the view of use such molecules as biological probes or optical amplifiers.

Balzani and co-workers have shown that a dendritic antenna can be used to sensitize near-infrared emitting lanthanide ions.¹⁴ For example a solution containing a dendrimer bearing three branches of eight 5-dimethylamino-1-naphthalenesulphonamido (dansyl) units was titrated by Nd(NO₃)₃. Quenching of the dansyl units' fluorescence and emission from Nd³⁺ was observed. The near-infrared quantum yield was measured to be 2.7×10^{-3} in acetonitrile: dichloromethane (5:1) solution.¹⁴ Since Nd³⁺ and Er³⁺ both emit when coordinated to the dansyl units, and neither ion can easily participate in electron transfer reactions then energy transfer from the dendrimer was invoked to explain the near-infrared emission. However, for Yb³⁺ there is no spectral overlap of the dendrimer emission with a Yb³⁺ energy accepting level. To explain the observed near-infrared

emission, it was proposed that an electron transfers from the dendrimer and reduces Yb^{3+} to Yb^{2+} . Since the Yb^{2+} charge-transfer state lies above the $\text{Yb}^{3+} {}^2\text{F}_{5/2}$ state, upon back electron transfer Yb^{3+} can either be in the ${}^2\text{F}_{5/2}$ excited state or ${}^2\text{F}_{7/2}$ state.¹⁵ Interestingly, in the case of Eu^{3+} , which could participate in both electron and energy transfer quenching of the dansyl fluorophore, Eu^{3+} emission is not observed. This is explained as either a fast electron transfer processes (no redox transient species were observed) via a non-emissive Eu^{2+} state or energy transfer followed by a faster electron transfer process.¹⁵

Van Veggel and co-workers published a number of papers on lanthanide containing complexes coordinated with *m*-terphenyl based ligands.¹⁶⁻²⁰ Their attempts to improve lanthanide luminescence efficiency are based on the premise that encapsulation of the lanthanide ion prevents easy access of solvent from reaching the lanthanide. The basic structure of the *m*-terphenyl based ligand is shown in Figure 1-3. With a triplet energy of $24,600 \text{ cm}^{-1}$, this ligand is capable of sensitizing visible and near-infrared emission from nearly all of the lanthanides that luminesce.

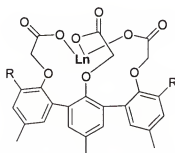


Figure 1-3. Chemical structure of *m*-terphenyl.

Focusing on the near-infrared complexes prepared containing Er^{3+} , Yb^{3+} , or Nd^{3+} , their lanthanide *m*-terphenyl complexes possessed lifetimes of 2.1, 1.2, and 9.1 μsec in

DMSO, respectively. Upon deuteration of the solvent these lifetimes increased to 3.5, 19.9, and 2.5 μsec , respectively, which corresponds to photoluminescence quantum yields of 2×10^{-4} , 7.8×10^{-3} , and 8.4×10^{-3} respectively.¹⁸ Deuteration of the ligand improved the quantum efficiencies to 4×10^{-4} for Er^{3+} , 3×10^{-2} for Yb^{3+} , and 2×10^{-2} for Nd^{3+} in DMSO-*d*6.¹⁶ Others have examined similar calixarenes coordinated to Er^{3+} , Yb^{3+} , or Nd^{3+} and found the quantum yields to be approximately a order of magnitude lower in non-deuterated solvents such as ethanol.²¹⁻²⁷ On the basis of their findings and others, the luminescence lifetimes, and hence the luminescence quantum yields, are significantly influenced by non-radiative deactivation by vibronic coupling of the 4f electronic states and high-energy oscillators in the local environment and deuteration of the ligand increases photoluminescence quantum efficiencies. Interestingly, several hetrobinuclear complexes exhibit near-infrared quantum yields as high as 6.1×10^{-3} in ethanol.²⁸

The importance of near-infrared emitting lanthanide for probing biological systems is evident in Parker's work who has studied lanthanide containing azamacrocyclic ligands based on cyclen (1,4,7,10-tetraazacyclododecane).²⁹⁻³⁴ Examples of these structures are shown in Figure 1-4. By functionalizing the arms of the macrocycle, in addition to modifying the compound's interactive properties with biological systems, the effects of the arms on lanthanide luminescence can be studied. Those studies confirmed that O-H oscillators as coordinated H_2O readily deactivate the excited states of Yb^{3+} and Nd^{3+} . The lifetime of Yb^{3+} containing azamacrocycles average about 0.8 μsec in H_2O and increases 2-10 times when measured in D_2O . The lifetimes of the analogous Nd^{3+} complexes increases from 0.16 to 0.33 μsec when going from H_2O to D_2O . This increase

in lifetime is attributed to the removal of coordinated water molecules, i.e. O-H oscillators, from the inner coordination sphere of the lanthanide by D₂O.

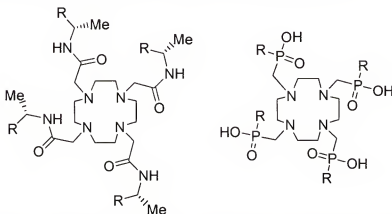


Figure 1-4. Structure of azamacrocyclic ligands used by Parker *et. al.*

Near-Infrared Emitting Lanthanides Coordinated to Porphyrins

Porphyrins are promising ligands for efficient energy transfer to near-infrared emitting lanthanide ions because their intense Soret bands lead to facile excitation and their low energy triplet states can readily excite the near-infrared emitting states of the lanthanide ions. Examples of porphyrins that have been coordinated to Ln³⁺ are shown in Figure 1-5. While porphyrin complexes of transition metals have been studied extensively, far fewer studies of porphyrins containing lanthanides have been published after their first appearance in 1976.³⁵

There have been scattered reports through the literature of near-infrared sensitized emission from lanthanide porphyrins.^{31,36,37} However, Tsviko, Solovev and Kachura launched a major effort to study the photophysical properties of lanthanide complexes of benzoporphyrins and etioporphyrins with an emphasis on investigation of their fast electronic relaxations.³⁸⁻⁴² They showed that the coordinated lanthanide rapidly deactivates the S₂ and S₁ excited states of the porphyrin via intersystem crossing to the

triplet state. This rapid intersystem crossing is due to spin-orbit coupling induced from the heavy atom effect of the lanthanides. As a result of fast intersystem crossing, visible emission from the porphyrin is quenched. However, the quenching is not 100% complete. It has been shown that weak emission arising from the $S_2 \rightarrow S_0$ and $S_1 \rightarrow S_0$ transitions does occur.⁴¹ The quantum yields for the near-infrared emission of Yb^{3+} etioporphyrin and Yb^{3+} benzoporphyrin where the axial ligand is either acetylacetonate or chloride have both been reported to be 5×10^{-3} with a lifetime of 12 μsec in benzene.⁴³

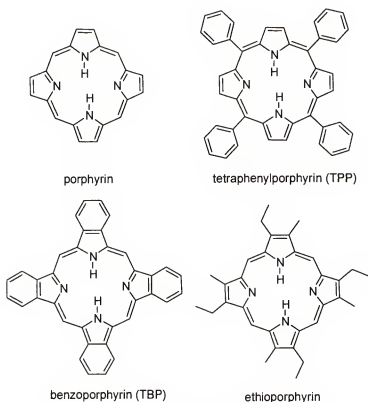


Figure 1-5. Structure of various porphyrins.

Solovev and Kachura also prepared Nd^{3+} containing tetra-*meso*-(*p*-tolyl)-porphyrin which upon visible excitation luminesced from the $^4\text{F}_{3/2} \rightarrow ^4\text{I}_{9/2}$ (875-940 nm) and the

$^4F_{3/2} \rightarrow ^4I_{11/2}$ transitions (1060 nm) of Nd^{3+} . The quantum yield of that complex was 2.4×10^{-4} in toluene.⁴⁴

For lanthanides whose energy accepting states are too high to accept energy from the porphyrin (Lu, Gd, La), the transient absorption shows similar transient profiles to Zn^{2+} and Pd^{2+} porphyrins with similar lifetimes thus showing that the triplet state is the lowest energy state in lanthanide-containing porphyrins. For Eu^{3+} , Tb^{3+} , Dy^{3+} , Ho^{3+} , Er^{3+} , and Tm^{3+} coordinated to etioporphyrin, the transient absorption matched the transient absorption of the non-energy accepting porphyrins mentioned above only with significantly shorter lifetimes. Thus, it was concluded that energy was efficiently transferred away from the porphyrin to the lanthanide. Quenching of the porphyrin emission by an energy transfer mechanism was not expected for Eu^{3+} since the energy accepting state of Eu^{3+} is too high in energy. However, the presence of a charge transfer deactivation pathway is a possibility since ligand-to-metal charge transfer quenching has been observed for Eu^{3+} .⁴⁵ Interestingly, an unusual transient absorption for Yb^{3+} containing porphyrins which had a derivative shape in the Q-band region was reported.³⁸ The lifetime of the transient was not dependant on oxygen concentration, but deuteration of the solvent did increase its lifetime. In addition the transient lifetime corresponded to the lifetime of the $Yb^{3+} {}^2F_{5/2} \rightarrow {}^2F_{7/2}$ emission. Taken together the observations suggested that the transient absorption was due to the Yb^{3+} based excited state.

Synthesis of Lanthanide Monoporphyrinates

While the porphyrin ligand is ideal for use as an efficient sensitizer of near-infrared emitters, the initial synthesis of the lanthanide porphyrin complexes resulted in low yields. The first reported synthesis of lanthanide monoporphyrinates involved distillation

at 220°C of acetylacetone from $\text{Ln}(\text{acac})_3$ in the presence of tetraphenylporphyrin to give lanthanide monoporphyrinate acetylacetonate complexes in 10-30% yield as shown in Figure 1-6.^{35,46,47} The low yields arise because the complexes hydrolyze during the lengthy chromatography times needed to isolate the products. This method effectively limits the choice of axial ligand to acac. The coordinated diketonate could be replaced by subsequent reactions, but even higher boiling solvents are required and low isolated product yields result.⁴⁸⁻⁵⁰ More recently, efforts to form lanthanide tetraphenylporphyrins and other porphyrin complexes have focused on amine elimination reactions of neutral lanthanide amides or alkyls with free base porphyrins^{51,52} or similar reactions between $\text{Li}\{\text{Ln}[\text{N}(\text{SiMe}_3)_2]_3\text{Cl}\}$ and substituted tetraphenylporphyrins.⁵³⁻⁵⁵

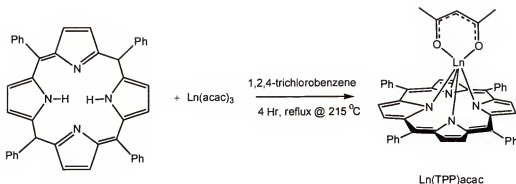


Figure 1-6. Synthetic scheme used by Horrocks *et al.*

Recently, a high-yield synthesis of a series of lanthanide (III) chloride tetraphenylporphyrinate complexes via nucleophilic displacement of Cl^- from anhydrous LnCl_3 by the TPP dianion was reported.⁵⁶ Using these $\text{Ln}(\text{TPP})\text{Cl}$ complexes as synthons a series of sterically saturated monoporphyrinate compounds were synthesized and characterized (Figure 1-7).

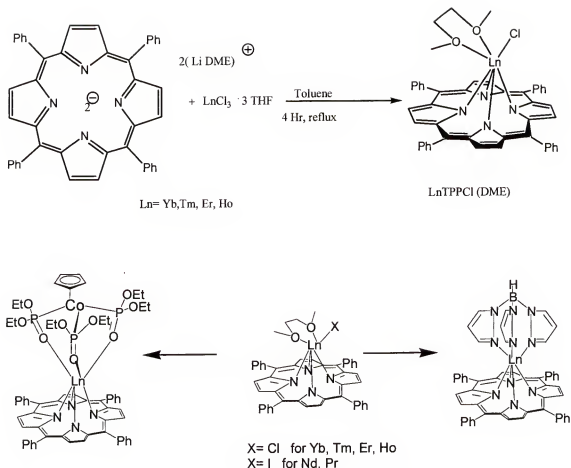


Figure 1-7. Synthetic scheme of high-yield reactions of lanthanide monoporphyrins with easily modified axial ligand.

Generation of near-infrared luminescence from metal complexes by photoexcitation or by application of an electric field has been area of growing interest.^{17,57-60}

Near-infrared sources have potential uses in both for biological and biomedical applications such as glucose monitoring⁶¹⁻⁶³ and immunoassay^{64,65} and for telecommunications. In this chapter, an overview of photophysical properties of near-infrared lanthanide emitters in solution is presented with the goal of incorporating these emitters in electroluminescent devices. We began by examine the photophysical properties of near-infrared emitting lanthanide *tris*- β -diketonate complexes followed by a

new series of lanthanide tetraphenylporphyrin complexes, $\text{Ln}(\text{TPP})\text{L}$. The effects of different axial ligands and lanthanide metal centers on the optical properties (absorption, transient absorption, visible and near-infrared photoluminescence) of $\text{Ln}(\text{TPP})\text{L}$ were thoroughly examined.

Photophysical Properties of Lanthanide *tris*- β -Diketonates

This work began by examining the basic photophysical properties of *tris*- β -diketonate complexes coordinated to near-infrared emitting lanthanides. Structures of the lanthanide *tris*- β -diketonates complexes studied consisted of three anionic 1,3-diketone ligands bound in a bidentate fashion to the lanthanide ion. Their structures are shown in Figure 1-8. To complete the coordination sphere of the lanthanide, phenanthroline was used. Phenanthroline helps prevent water from directly binding to the lanthanide. The structures of the complexes used are shown in Figure 1-8.

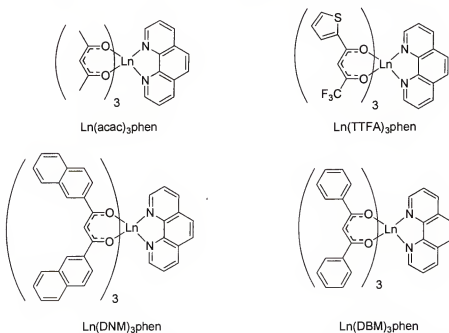


Figure 1-8. Chemical structures of lanthanide *tris*- β -diketonates studied. The lanthanide metal center was either Pr^{3+} , Nd^{3+} , Er^{3+} , or Yb^{3+} .

Absorption Properties of Lanthanide *tris*- β -Diketonates

All absorption measurements were made in dilute solutions of CH_2Cl_2 or CHCl_3 unless otherwise indicated. Figure 1-9 shows the UV/VIS absorptions of three Nd^{3+} *tris*- β -diketonates monophenanthroline complexes. The molar absorptivities (ϵ , $\text{M}^{-1}\text{cm}^{-1}$) were calculated using equation 1-2. A is the absorbance, c is the molar concentration (M) of the solution, and l is the cell path length (usually 1 cm).

$$A = \epsilon cl \quad 1-2$$

The absorption spectra are dominated by the $\pi \rightarrow \pi^*$ transitions of the ligands surrounding the lanthanide. The absorption corresponds very strongly with the β -diketonate ligand (not the phenanthroline ligand) because three β -diketonate ligands surround the metal as opposed to only one phenanthroline. It is observed, as expected, that increasing conjugation of the ligand red shifts the absorption of the complex. The $4f \rightarrow 4f$ transitions of Nd^{3+} or any of the lanthanides complexes prepared are not observed because of the low molar absorptivities ($1\text{-}10 \text{ M}^{-1}\text{cm}^{-1}$) of these transitions. Substituting Nd^{3+} for other trivalent lanthanides such as Eu^{3+} , Er^{3+} , Pr^{3+} , or Yb^{3+} , has little influence on the $\pi \rightarrow \pi^*$ transitions of the complexes. This indicates that the lanthanide metal center has little to no orbital interactions with the ligand other than electrostatic effects generated by the trivalent charge of each ion. This is reasonable to conclude because the $4f$ orbitals are well shielded by filled $5s$ and $5p$ orbitals.

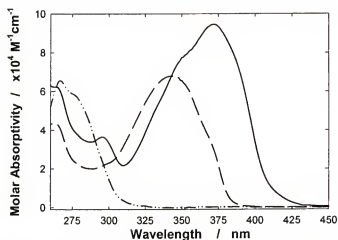


Figure 1-9. Absorbance of Nd(TMHD)₃phen (···), Nd(DBM)₃phen (---), and Nd(DNM)₃phen(—) in chloroform.

Photoluminescent Properties of Lanthanide *tris*- β -Diketonates

The photoluminescence emission spectra of eight different complexes in CH₂Cl₂ with identical absorbance when excited at 315 nm are shown in Figure 1-10. All emission spectra were collected from optically dilute solutions of CH₂Cl₂ or CHCl₃ unless otherwise indicated. A summary of the near-infrared transitions observed are shown in Table 1-5 including the quantum yields of these complexes.

Photoluminescence quantum yields (Φ_s) in solution were calculated using the equation 1-3 where A_{ref} and A_s are the absorbance of the relative standard and sample, respectively, n is the refractive index of the solvent; F_{ref} and F_s are the integrated area of the luminescence of the reference and sample, respectively; Φ_{ref} is the quantum yield of the standard used. Ruthenium (II) *tris*-bipyridine dichloride, Ru(bpy)₃ in water ($\Phi = 0.0379$) was used as a relative quantum yield standard for ytterbium complexes. The quantum yield measured for Yb(TTFA)₃phen ($\Phi = 1 \times 10^{-3}$, benzene) using a CCD detector was

then used as a relative standard for other near-infrared emitters measured using an InGaAs detector.

$$\Phi_S = \frac{10^{-A_{ref}} n_s^2 F_s}{10^{-A_s} n_{ref}^2 F_{ref}} \Phi_{ref} \quad 1-3$$

The quantum yields for the complexes are generally low but comparable to other reported values for lanthanide *tris*- β -diketonates (see Table 1-1). There is a decrease in quantum efficiency going from TTFA > DBM > DNM. This trend holds true regardless of metal center.

Table 1-5. Emission transitions of lanthanide *tris*- β -diketonates in benzene. The numbers in parentheses are the relative intensities of multiple peaks of the near-infrared spectrum.

Complex	Transitions	λ_{max} nm	Φ_{PL}
Er(DNM) ₃ phen	$^4I_{13/2} \rightarrow ^4I_{15/2}$ ^a	1531 ^a	4.3×10^{-6a}
Er(TTFA) ₃ phen	$^4I_{13/2} \rightarrow ^4I_{15/2}$ ^a	1531 ^a	1.0×10^{-5a}
Nd(DNM) ₃ phen	$^4F_{3/2} \rightarrow ^4I_{11/2}$	878 (0.7)	1.6×10^{-5}
	$^4F_{3/2} \rightarrow ^4I_{13/2}$	1061 (1.00)	
	$^4F_{3/2} \rightarrow ^4I_{15/2}$	1332 (0.15)	
Nd(DBM) ₃ phen	$^4F_{3/2} \rightarrow ^4I_{11/2}$	878 (0.60), 900 (0.54)	4.9×10^{-5}
	$^4F_{3/2} \rightarrow ^4I_{13/2}$	1061 (1.00)	
	$^4F_{3/2} \rightarrow ^4I_{15/2}$	1332 (0.12)	
Nd(TTFA) ₃ phen	$^4F_{3/2} \rightarrow ^4I_{11/2}$	877 (0.69), 894 (0.51)	1.9×10^{-4}
	$^4F_{3/2} \rightarrow ^4I_{13/2}$	1061 (1.00)	
	$^4F_{3/2} \rightarrow ^4I_{15/2}$	1332 (0.12)	
Pr(DNM) ₃ phen	$^3P_0 \rightarrow ^1G_4$ or $^1D_2 \rightarrow ^3F_4$	1016 (0.62), 1062(1.00)	3.4×10^{-6}
Yb(DNM) ₃ phen	$^2F_{5/2} \rightarrow ^2F_{7/2}$	977(1.00), 1008(0.73), 1034 (0.69)	2.1×10^{-4}
Yb(TTFA) ₃ phen	$^2F_{5/2} \rightarrow ^2F_{7/2}$	977(1.00), 1007(0.99), 1032(0.95)	1.0×10^{-3}

Φ_{PL} were measured relative to Ru(bpy)₃ ($\Phi=0.0379$, air saturated water)

^a Lower Limit. Values may be higher due to fall off in InGaAs detector response for wavelengths greater than 1550 nm.

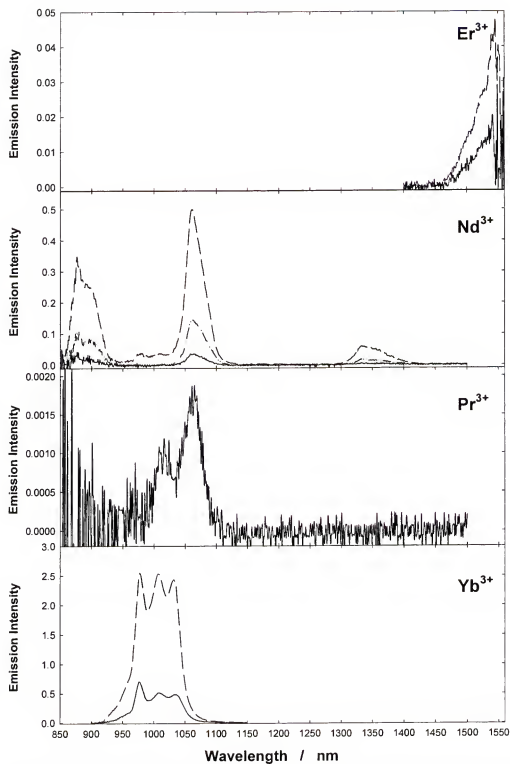


Figure 1-10. Near-infrared emission scaled to show relative efficiencies of $\text{Ln}(\text{L})_3\text{phen}$ in benzene where $\text{L} = (\text{---})$ DNM, (---) DBM, $(-\cdot-)$ TTFA.

Photophysical Properties of Lanthanide Monoporphyrinates in Solution

Lanthanide porphyrins are markedly different in structure and optical properties than lanthanide *tris*- β -diketonates. Figure 1-11 shows the structures of the lanthanide complexes studied in the present work. Each complex synthesized by Tim Foley or Alison Knefely has a lanthanide ($\text{Ln} = \text{Pr}^{3+}, \text{Nd}^{3+}, \text{Ho}^{3+}, \text{Er}^{3+}, \text{Tm}^{3+}, \text{or Yb}^{3+}$) coordinated to the four pyrrole nitrogens of the TPP ligand. A monoanionic bidentate or tridentate capping ligand completes the coordination sphere of the lanthanide ion. Summaries of the absorption, luminescence and near-infrared quantum yields of the $\text{Ln}(\text{TPP})\text{TP}$ and $\text{Ln}(\text{TPP})\text{L}(\text{OEt})_3$ complexes are presented in Table 1-6 and Table 1-7. All measurements were carried out in methylene chloride.

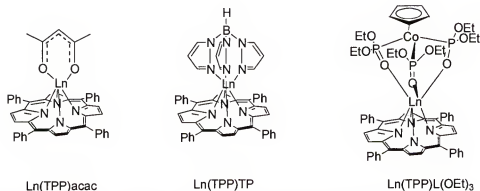


Figure 1-11. Chemical structures of lanthanide tetraphenylporphyrin complexes with differing capping ligands where acac is acetylacetonate, TP is *tris*-pyrazoylborate, and $\text{L}(\text{OEt})_3$ is (cyclopentadienyl) *tris*-(diethoxyphosphito-P)cobaltate).

Axial Ligand Effects on the Absorption Properties of $\text{Ln}(\text{TPP})\text{L}$

The axial ligands of transition metal metalloporphyrins are known to affect the metal's electronic properties.⁶⁶ Thus, the effect of axial ligand on the spectroscopy of the lanthanide porphyrins was examined. Figure 1-12 shows the absorption spectra of the

Table 1-6. Photophysical properties of Ln(TPP)TP measured in CH₂Cl₂.

Ln	$\lambda_{\text{abs}}/\text{nm}$ (log ϵ)	$\lambda_{\text{em}}/\text{nm}$	NIR Φ_{PL}
Ho ³⁺	402s(4.55), 423(5.69), 510(3.54), 552(4.27), 590(3.61), 627(3.32)	649, 715	--
Pr ³⁺	402s(4.87), 425(5.71), 450(3.94), 482(3.40), 515(4.03), 554(4.31), 593(3.86), 649(3.49)	652, 717	--
Tm ³⁺	402s(4.65), 423(5.80), 513(3.55), 551(4.43), 588(3.70), 626(3.28)	652, 718	--
Nd ³⁺	402s(4.67), 424(5.74), 516(3.66), 553(4.32), 592(3.76), 624(2.95)	651, 717, 882, 900, 932, 1069, 1111, 1324, 1354	2.4×10^{-3}
Er ³⁺	402s(4.68), 422(5.60), 514(3.71), 551(4.21), 590(3.63), 648(3.30)	653, 717, 1485, 1531	9×10^{-4}
Yb ³⁺	402s(4.85), 421(5.72), 513(3.58), 551(4.41), 588(3.77), 624(3.46)	652, 718, 932, 954, 977, 990, 1002, 1014, 1022, 1037	3.2×10^{-2}

Quantum yields were measured relative to ZnTPP ($\Phi = 0.033$, CH₂Cl₂)

Table 1-7. Photophysical properties of Ln(TPP)L(OEt)₃ measured in CH₂Cl₂.

Ln	$\lambda_{\text{abs}}/\text{nm}$ (log ϵ)	$\lambda_{\text{em}}/\text{nm}$	NIR Φ_{PL}
Ho ³⁺	405s(4.63), 427(5.72), 519(3.58), 597(3.85), 626(3.40), 649(3.31)	614, 656, 717	--
Pr ³⁺	409s(4.78), 428(5.81), 520(3.67), 561(4.32), 600(4.01)	656, 717	--
Tm ³⁺	405s(4.62), 426(5.71), 517(3.48), 557(4.27), 595(3.76), 624(3.15)	611, 655, 717	--
Nd ³⁺	409s(4.69), 429(5.76), 520(3.57), 561(4.39), 600(3.93)	655, 718, 829, 896, 947, 1069, 113, 1317, 1350, 1429	2×10^{-3}
Er ³⁺	406s(4.68), 427(5.68), 521(3.51), 558(4.34), 596(3.79), 625(3.06)	611, 655, 720, 1480, 1517, 1537	1×10^{-3}
Yb ³⁺	406s(4.60), 427(5.73), 521(3.67), 559(4.30), 596(3.76), 628(3.15)	612, 655, 719, 923, 956, 977, 1003, 1023, 1046	2.4×10^{-2}

Quantum yields were measured relative to ZnTPP ($\Phi = 0.033$, CH₂Cl₂)

ytterbium porphyrin complexes with the different axial ligands: acac, TP, and $\text{L}(\text{OEt})_3$. The absorption spectra exhibit the typical porphyrin features including the Soret band (~ 420 nm) and the correspondingly weaker Q-bands (~ 500 -600 nm). Upon coordination of the lanthanide to the porphyrin, the Soret band shifts from 412 nm in the free base porphyrin to ~ 425 nm in the complex. Overall, the absorption spectrum resembles a “regular” metalloporphyrin absorption spectrum such as $\text{Zn}(\text{TPP})$.⁶⁷ The absorption spectra of the acac and TP coordinated complexes are virtually identical. Coordination of the $\text{L}(\text{OEt})_3$ ligand does cause a 3 nm red shift in the absorption spectrum. A red-shift in the metalloporphyrin absorption can indicate the basicity of the ligands coordinated to the metal. Regardless, the capping ligand serves as an ancillary ligand with little effect on perturbing the π electron system of the porphyrin ring.

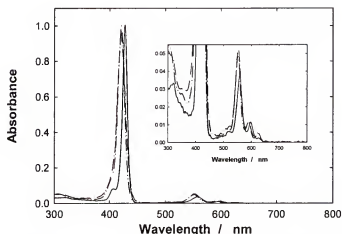


Figure 1-12. Absorption spectra of $\text{Yb}(\text{TPP})\text{L}$ in methylene chloride. The axial ligand, L is acac (\cdots), TP ($---$), or $\text{L}(\text{OEt})_3$ (\longrightarrow).

Metal Center Effects on the Absorption Properties of $\text{Ln}(\text{TPP})\text{L}$

Unlike transition metals, which can greatly affect the absorption properties of porphyrins, there is little change in the absorption bands between $\text{Ln}(\text{TPP})\text{L}$ complexes

as the lanthanide metal is varied. Figure 1-13 and Figure 1-14 show the absorption spectra of $\text{Ln}(\text{TPP})\text{TP}$ and $\text{Ln}(\text{TPP})\text{L}(\text{OEt})_3$ where the lanthanide metal center is either Er^{3+} , Ho^{3+} , Nd^{3+} , Pr^{3+} , Tm^{3+} , or Yb^{3+} . The absorption spectra of both ligand sets feature a sharp intense absorption around 420 nm corresponding to the porphyrin Soret band and a series of weaker absorbing Q bands between 500 and 650 nm. There is some variation in the intensity of the Q-bands upon changing metal center. The ratio of the Q(1,0) (~550 nm) to Q(0,0) (~600 nm) does increase along the lanthanide series. No $4f \rightarrow 4f$ transitions were observed since the Soret band is five orders of magnitude more intense than typical $4f \rightarrow 4f$ transitions. Thus, the lanthanide has little effect on the absorption properties of the complex, and the porphyrin ligand plays the dominant role in controlling the optical absorption properties of the complexes.

Near-Infrared Emission from Lanthanide Monoporphyrinates in CH_2Cl_2

The near-infrared photoluminescence properties are noticeably different and varied compared to the absorption properties. Figure 1-15 shows the near-infrared emission of $\text{Yb}(\text{TPP})\text{L}$ compounds. The near-infrared region consists of a sharp peak at 977 nm with additional broad bands of each side of the peak. In the broad peaks there are well defined peaks observed near 930 nm for $\text{Yb}(\text{TPP})\text{TP}$ and slightly bluer for $\text{Yb}(\text{TPP})\text{L}(\text{OEt})_3$ while this feature appears as shoulder in $\text{Yb}(\text{TPP})\text{acac}$. However, many of the low energy features (>1000 nm) of Yb^{3+} emission are attenuated due to the low sensitivity of the silicon based CCD detector. Figure 1-16 shows the PL emission of $\text{Yb}(\text{TPP})\text{TP}$ and $\text{Yb}(\text{TPP})\text{L}(\text{OEt})_3$ recorded on an InGaAs detector which has improved sensitivity in the near-infrared region.

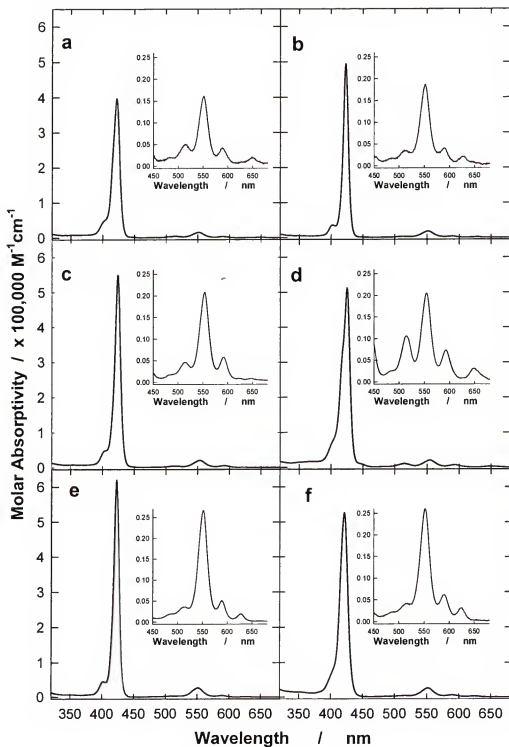


Figure 1-13. Molar absorptivity of $\text{Ln}(\text{TPP})\text{TP}$ in CH_2Cl_2 where Ln is a) Er^{3+} b) Ho^{3+} c) Nd^{3+} d) Pr^{3+} e) Tm^{3+} f) Yb^{3+}

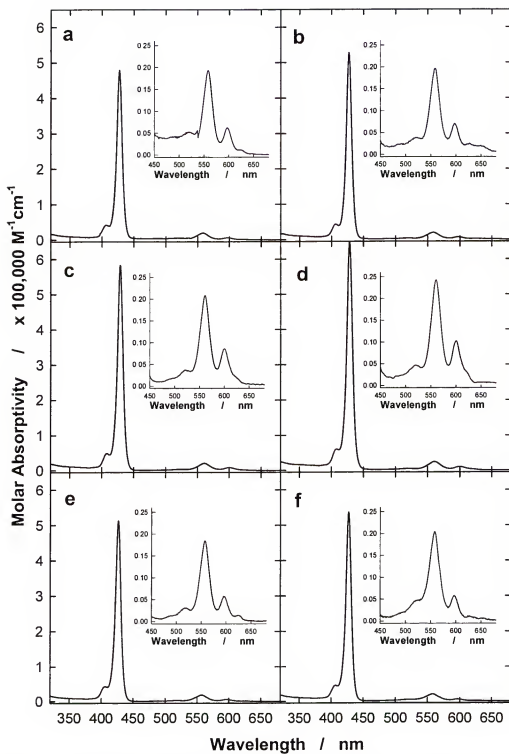


Figure 1-14. Molar absorptivity of $\text{Ln}(\text{TPP})\text{L}(\text{OEt})_3$ in CH_2Cl_2 where Ln is a) Er^{3+} b) Ho^{3+} c) Nd^{3+} d) Pr^{3+} e) Tm^{3+} f) Yb^{3+}

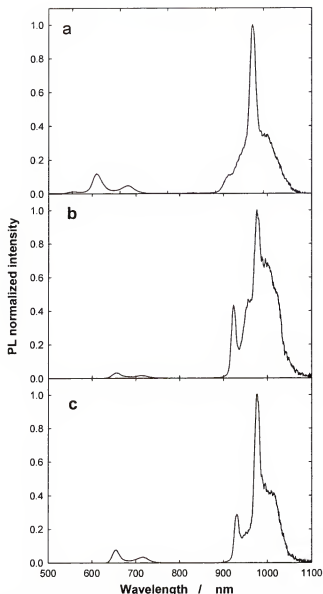


Figure 1-15. Visible and near-infrared emission of a) Yb(TPP)acac, b) Yb(TPP)L(OEt)₃, and c) Yb(TPP)TP in CH₂Cl₂ when excited at 420 nm.

The near-infrared quantum yields of Yb³⁺ porphyrins are generally higher than the Yb³⁺ *tris*- β -diketonate complexes. While the near-infrared quantum yield of Yb(TPP)acac is 1.6×10^{-3} in CH₂Cl₂, Yb(TPP)TP ($\Phi_{\text{PL}} = 3.2 \times 10^{-2}$) and Yb(TPP)L(OEt)₃ ($\Phi_{\text{PL}} = 2.4 \times 10^{-2}$) possess significantly higher quantum yields in solution than other many Yb³⁺ porphyrin complexes reported in the literature, e.g. (Yb(benzoporphine) $\Phi = 5 \times$

10^{-3} in benzene, $\tau=12 \mu\text{sec}$).^{43*} The higher quantum yield in solution is due to the steric bulk introduced by the TP and $\text{L}(\text{OEt})_3$ ligand preventing solvent from reaching the metal center and deactivating the excited state. Still, the quantum yields are much lower than unity showing that even with increased steric bulk non-radiative processes predominate in excited state deactivation.

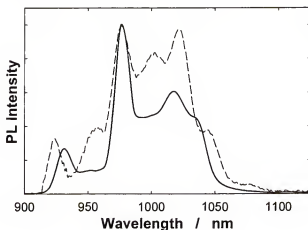


Figure 1-16. Near-infrared PL emission of $\text{Yb}(\text{TPP})\text{TP}$ (—) and $\text{Yb}(\text{TPP})\text{L}(\text{OEt})_3$ (---) in CH_2Cl_2 measured on an InGaAs detector. Excitation was at 420 nm and the emission slits were set at 5 nm band pass.

Additional emission peaks can be seen by recording the emission spectrum at higher resolution. Figure 1-17 shows the photoluminescence of $\text{Yb}(\text{TPP})\text{TP}$ scanned at 5 nm resolution. It is apparent that the $^2\text{F}_{5/2} \rightarrow ^2\text{F}_{7/2}$ transition is actually composed of 8 different peaks. The positions of these peaks are shown in Table 1-8. Early spectroscopic work into lanthanide β -diketonates deduced that the structured emission originated from crystal field splitting effects which is calculated to be in the order of hundreds of cm^{-1} .⁶⁸ Variable temperature work by others has shown that the higher

* While the ligand in the axial position was not reported, chloride or an acetylacetonate ligands was probably coordinated to Yb^{3+} based on other articles published by the authors.

crystal field state can be thermally populated at room temperature when the lifetime of the excited state is long enough.^{53,69} Thus peaks 1 and 3 may originate from different excited state energy levels but terminate to the same ground state energy level. This means that the $^2F_{5/2}$ state is split into at least two levels of 500 cm^{-1} apart in energy. However, this does not fully explain all the emission peaks observed since not all peaks have a matching peak with an energy difference of 500 cm^{-1} . For Yb^{3+} doped crystals, the splitting of Yb^{3+} has been attributed to both crystal field and vibronic bands.^{70,71} Thus, the origin of the low energy peaks may be a combination of crystal field effects and coupling to Ln-N vibrational modes.

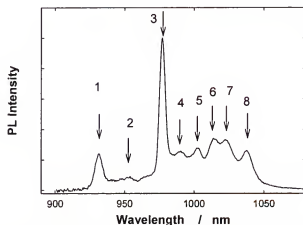


Figure 1-17. Photoluminescence of $\text{Yb}(\text{TPP})\text{TP}$ in CH_2Cl_2 upon 420 nm excitation at 5 nm resolution.

Table 1-8. Near-infrared peak positions of $\text{Yb}(\text{TPP})\text{TP}$ at 5 nm resolution.

Peak	$\lambda(\text{nm})$	$\nu(\text{cm}^{-1})$	Peak	$\lambda(\text{nm})$	$\nu(\text{cm}^{-1})$
1	932	10730	5	1002	9980
2	954	10480	6	1014	9860
3	977	10235	7	1022	9780
4	990	10100	8	1037	9640

Visible Emission from Ln(TPP)L in CH₂Cl₂

Excitation of the Ln(TPP)L complexes in the Soret or Q-bands of the complexes resulted in both visible and near-infrared emissions as previously shown in Figure 1-15. In the visible region from 600 to 750 nm, there are three emission bands. The weak ($\Phi_{PL} < 10^{-5}$) visible fluorescence at 645 and 719 nm matches the visible fluorescence of free-base tetraphenylporphyrin.⁷² The excited state lifetime of 8 ns supports the assignment that these two bands come from free TPP.

A weak emission band at 610 nm was observed in all the Ln(TPP)L(OEt)₃ complexes prepared as shown in Figure 1-18. The excitation spectra of all three emission bands help identify the origin of each emissive transition. The excitation spectra of the three visible emission peaks of Yb(TPP)L(OEt)₃, Er(TPP)L(OEt)₃, Ho(TPP)L(OEt)₃, and Tm(TPP)L(OEt)₃ are shown in Figure 1-19 through Figure 1-22. Comparison of the Soret bands observed in the excitation spectra show that the 610 nm emissions are red shifted 13 nm from the excitation spectra of the other emission bands. This is similar to the UV-VIS absorption band shift that occurs when TPP is coordinated to a metal. Also, the 720 nm band of Tm(TPP)L(OEt)₃ shows two peaks in the Soret region with a peak at 425 and 458 nm. This suggests that a more complex structure such as an aggregate is emitting. Thus the visible emitting bands at 654 and 720 nm correspond to the presence of a free base impurity while the emission band at 610 nm corresponds to emission from the lanthanide porphyrin.

Under higher energy excitation, additional weak emission bands can be seen from Ln(TPP)L. For example, Figure 1-23 shows emission bands from Ho(TPP)L(OEt)₃ upon

excitation at 330 nm at 370 and 445 nm. The 445 nm emission band is the mirror image of the Soret band absorption. Similar bands have been observed in $\text{Er}(\text{OEt})\text{TPP}$ and $\text{Gd}(\text{TBP})$ complexes.^{41,73} In both cases, this transition has been ascribed to fluorescence from the $S_2 \rightarrow S_0$ of the metalloporphyrin. Normally, $S_2 \rightarrow S_0$ emission is not observed in organics because the non-radiative rate for $S_2 \rightarrow S_1$ is large. However, $S_2 \rightarrow S_0$ can be observed if the radiative rate of the transition and/or the energy gap between S_2 and S_1 is large. For example, $S_2 \rightarrow S_0$ emission was observed in $\text{Zn}(\text{TBP})$ with a radiative rate of $1.5 \times 10^9 \text{ sec}^{-1}$ and has been described as a $\pi \rightarrow \pi^*$ excited state based on emission polarization studies.^{74,75} Therefore it is reasonable to conclude that the band at 445 nm is $S_2 \rightarrow S_0$ emission from the metalloporphyrin ring.

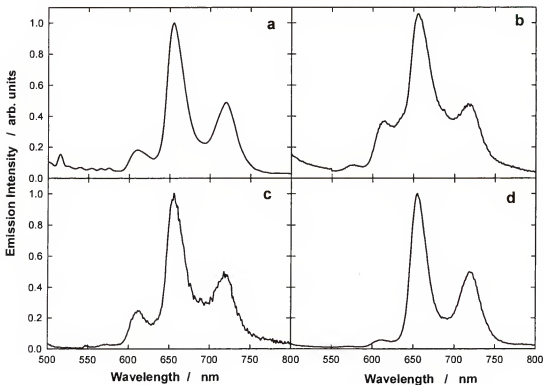


Figure 1-18. Visible emission of $\text{Ln}(\text{TPP})\text{L}(\text{OEt})_3$ in CH_2Cl_2 upon 420 nm excitation. Ln is a) Er^{3+} b) Ho^{3+} c) Tm^{3+} and d) Yb^{3+} .

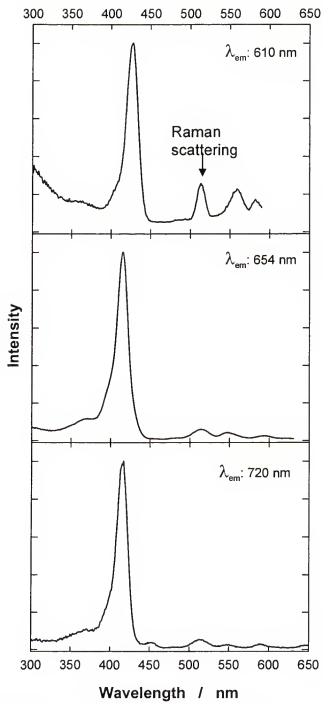


Figure 1-19. Excitation spectra of Yb(TPP)L(OEt)_3 in CH_2Cl_2 .

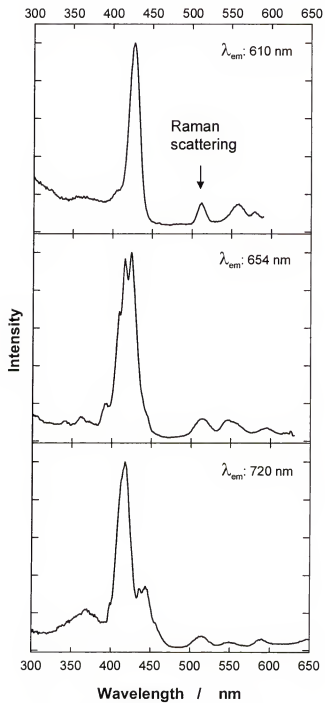


Figure 1-20. Excitation spectra of Er(TPP)L(OEt)_3 in CH_2Cl_2 .

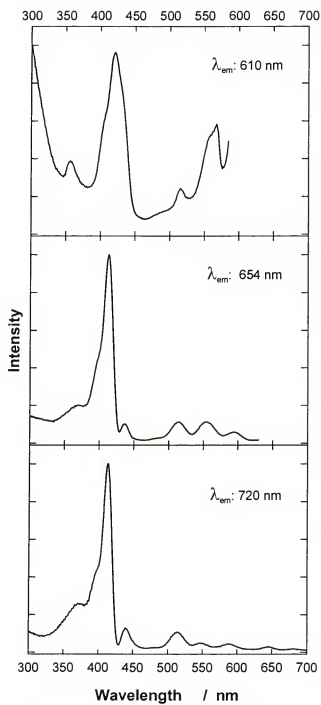


Figure 1-21. Excitation spectra of Ho(TPP)L(OEt)_3 in CH_2Cl_2 .

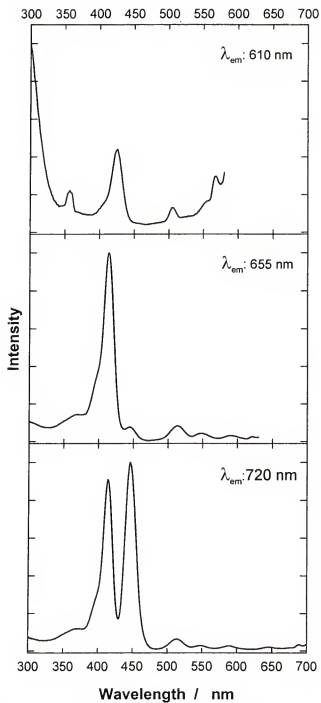


Figure 1-22. Excitation spectra of Tm(TPP)L(OEt)_3 in CH_2Cl_2 .

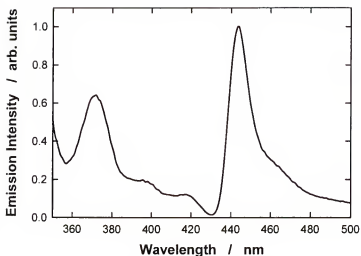


Figure 1-23. Visible emission from $\text{Ho}(\text{TPP})\text{L}(\text{OEt})_3$ upon 330 nm emission. Additional bands were observed at 653 and 719 nm as described previously.

The identity of the emission feature at 370 nm is unknown. Others who have made similar observations have suggested in the case of $\text{Ln}(\text{TBP})\text{acac}$ and $\text{Er}(\text{OEt})\text{TPP}$ that it is phosphorescence from the coordinate 1,3-diketone, such as 1,3-pentadione.^{73,76} Since the $\text{L}(\text{OEt})_3$ ligand also possesses a small conjugated ring, it would seem reasonable to conclude that the phosphorescence of the $\text{L}(\text{OEt})_3$ ligand would be in UV region. However, the absorption of cobalt cyclopentadiene dicarbonyl complexes absorb at 370 nm and thus phosphorescence from $\text{L}(\text{OEt})_3$ would be unexpected.

Solvent Effects on Near-Infrared Quantum Yield of $\text{Yb}(\text{TPP})\text{L}$

Solvents can play a significant role in the optical properties of compounds, and so the solvent effects on the absorption and emission properties of lanthanide TPP complexes were examined. The absorption properties of $\text{Yb}(\text{TPP})\text{acac}$ and $\text{Yb}(\text{TPP})\text{TP}$ are similar in various solvents. For both complexes the Soret peak gradually red-shifts

six nanometers when the solvent changes from CH_3CN to THF to CH_2Cl_2 to toluene, and finally to DMSO.

While the absorbance of $\text{Yb}(\text{TPP})\text{acac}$ varies by a few nanometers in different solvents, the solvent used have a more prominent effect on the near-infrared PL quantum yield of $\text{Yb}(\text{TPP})\text{acac}$ and $\text{Yb}(\text{TPP})\text{TP}$. Table 1-9 shows the quantum yields of $\text{Yb}(\text{TPP})\text{acac}$ and $\text{Yb}(\text{TPP})\text{TP}$ in several solvents. Generally, the quantum yields are low (<10%) because not only solvents but other non-radiative pathways deactivate the excited state. While solvents do play a role in deactivating the excited state, there was no correlation found between the number of C-H or O-H bonds of the solvent molecule and the photoluminescence quantum yield. $\text{Yb}(\text{TPP})\text{acac}$ photoluminescence appears more efficient in polar coordinating solvents such as DMSO as opposed to $\text{Yb}(\text{TPP})\text{TP}$ which has higher photoluminescence quantum efficiencies in non-polar, non-coordinating solvents such as CH_2Cl_2 and toluene.

Table 1-9. Solvent effects on the near-infrared quantum yields of $\text{Yb}(\text{TPP})\text{acac}$ and $\text{Yb}(\text{TPP})\text{TP}$.

Solvent	$\text{Yb}(\text{TPP})\text{acac}$ Φ_{PL} (%)	$\text{Yb}(\text{TPP})\text{TP}$ Φ_{PL} (%)
Toluene	0.14	5.3
Acetonitrile	0.39	1.3
Methanol	0.14	--
CH_2Cl_2	0.16	3.2
Acetone	0.43	--
THF	0.77	0.79
DMSO	2.1	2.0

Since the lanthanide is positioned above the ring of the porphyrin center, there remain several coordination sites where a solvent molecule can access the lanthanide ion. $\text{Yb}(\text{TPP})\text{acac}$ has a relatively small axial ligand which may allow trace amounts of water

present in the solvent to coordinate with the lanthanide metal center, which in turn lowers the radiative quantum yield. Coordination of water is known to play a role in deactivating the excited states of lanthanide ion by coupling to non-radiative O-H vibrational modes. However, in coordinating solvents, the solvent displaces the water thus removing the O-H oscillators from the proximity of the lanthanide therefore lowering the non-radiative rate.

Coordination of O-H and C-H oscillators to the lanthanide ion will increase the non-radiative rates of the lanthanide excited states particularly as the energy of the near-infrared transitions decrease. This is because the non-radiative rate increases exponentially as the energy gap decreases. Using Siebrand's approach for deriving the energy gap law for lanthanides, the non-radiative rate can be found using equation 1-4.⁷⁷

$$k_{nr} = \left(\frac{2\pi\rho_{nr}}{\hbar} \right) N_{\rho} J^2 \left(\frac{M_{\rho} \omega_{\rho}}{2\hbar} \right) F_{\rho} \quad 1-4$$

In equation 1-4, ρ_{nr} is the density of final vibrational states, J is the electronic coupling constant due to nuclear motion, $M_{\rho} \omega_{\rho}/2\hbar$ measures the coupling to the promoting modes, N_{ρ} is the number of modes and F_{ρ} is the Frank-Condon factor. The Frank-Condon factor can be described by equation 1-5.

$$F_{\rho} = \frac{\exp(-\frac{1}{2}k\Delta^2)(\frac{1}{2}k\Delta^2)^{\nu}}{\nu!} \quad 1-5$$

In equation 1-5, k is a constant, Δ is the difference in positions of the final and initial vibrational states and ν is composed of the energy between two states, ΔE_0 and maximum the oscillator of highest energy, ω_{\max} as shown in equation 1-6.

$$\nu = \frac{\Delta E_0}{2\hbar\omega_{\max}} - 1 \quad 1-6$$

Using Sterlings' approximation to expand the factorial in equation 1-5 and the approximations described by van Dijk and Schuurman for energy gaps of lanthanides corresponding to 1 to 3 vibrational quanta of the host, the non-radiative rate can be expressed by equation 1-7.

$$k_{nr} = \beta \exp[-(\Delta E_0 - 2\hbar\omega_{\max})\alpha] \quad 1-7$$

The α and β terms vary little between hosts. Thus, as the radiative energy gap decreases, the non-radiative rate increases exponentially. Figure 1-24 shows that the infrared emissive transitions of Yb^{3+} , Nd^{3+} , and Er^{3+} are within 2 to 3 vibrational quanta of common organic bonds. Therefore, it is not surprising that the quantum yields are low and the use of C-H bonds may limit greatly improving the quantum yields of these ions.

From Figure 1-24 it is clear that solvents containing O-H bonds will rapidly deactivate the excited states of the lanthanides. Since the lanthanide center is well shielded in $\text{Yb}(\text{TPP})\text{TP}$ by the TPP and TP ligand, water cannot readily access the excited lanthanide ion. Thus the PL quantum yield of $\text{Yb}(\text{TPP})\text{TP}$ in non-polar, non-coordinating solvents is larger compared to $\text{Yb}(\text{TPP})\text{acac}$. However, the quantum

yields of the two complexes remain approximately the same in coordinating solvents.

Therefore, the use of bulky ligands should help to improve the photoluminescence quantum efficiencies of near-infrared emitters, particularly in polar environments such as biological systems.

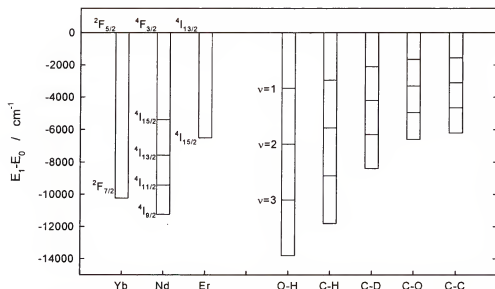


Figure 1-24. Representation of the radiative transition energies of Yb^{3+} , Nd^{3+} , and Er^{3+} and the vibrational energies of common bonds found in organic systems.

Near-Infrared Emission from Other Lanthanide Porphyrin Emitters

Figure 1-25 shows the $^4I_{13/2} \rightarrow ^4I_{15/2}$ Er^{3+} transition of $\text{Er}(\text{TPP})\text{TP}$ and $\text{Er}(\text{TPP})\text{L}(\text{OEt})_3$. Some structure is observed in the Er^{3+} emission which may be due to crystal field splitting effects. The emission is similar in shape to other Er^{3+} PL emissions reported however the low energy side appears attenuated. This is probably due to the fall off in sensitivity of the InGaAs detector. For $\text{Er}(\text{TPP})\text{TP}$ there are two peaks at 1485 and 1531 nm. No other Er^{3+} based emission was observed from the 760-1600 nm.

Neodymium emission in the near-infrared was observed from the $\text{Nd}(\text{TPP})\text{TP}$ complex. Figure 1-26 shows the near-infrared PL emission of $\text{Nd}(\text{TPP})\text{TP}$ in CH_2Cl_2 . In

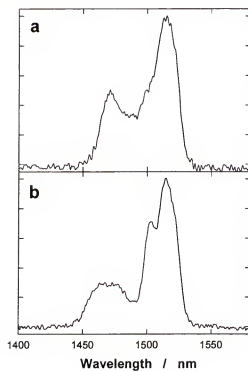


Figure 1-25. Near-infrared emission of a) Er(TPP)TP and b)Er(TPP)L(OEt)₃ in CH₂Cl₂ upon exciting at 420 nm uncorrected for detector response.

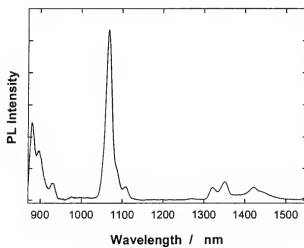


Figure 1-26. Near-infrared emission of Nd(TPP)TP in CH₂Cl₂ upon exciting at 420 nm.

solution, three transitions are observed from Nd^{3+} : $^4\text{F}_{3/2} \rightarrow ^4\text{I}_{11/2}$ (890 nm), $^4\text{F}_{3/2} \rightarrow ^4\text{I}_{13/2}$ (1060 nm), $^4\text{F}_{3/2} \rightarrow ^4\text{I}_{15/2}$ (1340 nm).

No photoluminescence near-infrared emissions from $\text{Tm}(\text{TPP})\text{L}$, $\text{Ho}(\text{TPP})\text{L}$, or $\text{Pr}(\text{TPP})\text{TP}$ have been observed in solution or in the solid state.

Transient Absorption Spectroscopy of $\text{Ln}(\text{TPP})\text{L}$ Complexes

Kachura and co-workers examined the transient absorptions (TA) of several lanthanide containing tetra(*p*-tolyl)porphyrin (TTP)³⁹ and benzoporphyrin (TBP) complexes.⁴¹ From their observations, they divided the lanthanides porphyrin complexes into three different classes based on their transient absorptions. The first class consisted of lanthanides which cannot accept energy from the porphyrin ligand, i.e. Gd^{3+} and Lu^{3+} . The TA of these complexes mimicked the transient profile of $\text{Zn}(\text{TTP})$.⁷⁸ Therefore, the long-lived (30 μsec) and broad transient from 600-800 nm which is observed is assigned to triplet-triplet absorption of the TTP ligand. The second class consisted of lanthanides, Tm^{3+} , Dy^{3+} , Ho^{3+} , and Er^{3+} , which can accept energy from TTP. This class of complexes is characterized by short-lived transient absorptions (<2 nsec). The third class is Yb^{3+} coordinated to TTP which has a long lived transient that equals the $^2\text{F}_{5/2} \rightarrow ^2\text{F}_{7/2}$ emission lifetime of $\text{Yb}(\text{TTP})\text{acac}$. $\text{Yb}(\text{TTP})\text{acac}$ complexes also differ from other lanthanide complexes because of the derivative shaped TA observed in the Q-bands region. However, no satisfying explanation was given by the authors to explain the long-lived transient absorption of the Yb complexes.

Transient absorption spectra for $\text{Yb}(\text{TPP})\text{L}$ and $\text{Nd}(\text{TPP})\text{TP}$ measured in argon-degassed CH_2Cl_2 are shown in Figure 1-27. The transient absorptions of $\text{Yb}(\text{TPP})\text{TP}$, $\text{Yb}(\text{TPP})\text{L}(\text{OEt})_3$, and $\text{Nd}(\text{TPP})\text{TP}$ all show a bleaching of the Soret band at

420 nm (not shown) and a net absorption around 440 nm. The transient lifetimes for the Yb^{3+} porphyrin complexes are $\tau = 57 \mu\text{sec}$. The Q-band region shows a derivative-shaped TA. The transient absorption of $\text{Nd}(\text{TPP})\text{TP}$ is also similar in profile and lifetime to the Yb^{3+} analogs. Interestingly, the lifetime of $\text{Yb}(\text{TPP})\text{L}(\text{OEt})_3$ of 40 μsec is within a factor of 2 of the transient absorption lifetime. Thus, transient absorption spectroscopy may at least for Yb^{3+} complexes provide a way of estimating the lifetime of the Yb^{3+} excited state. Besides Nd^{3+} and Yb^{3+} porphyrin complexes, no transient absorptions in the nanosecond timescale were detected for $\text{Er}(\text{TPP})\text{L}$, $\text{Tm}(\text{TPP})\text{L}$, and $\text{Ho}(\text{TPP})\text{L}$.

In all cases, coordination of a lanthanide to TPP results in rapid intersystem crossing of the $S_0 \rightarrow T_1$ state of TPP followed by energy transfer to the lanthanide. $\text{Er}(\text{TPP})\text{L}$, $\text{Tm}(\text{TPP})\text{L}$, and $\text{Ho}(\text{TPP})\text{TP}$ showed no long lived TA indicating that once the energy transferred to the lanthanide, it was rapidly deactivated by vibrational relaxation. This is reasonable since all three lanthanides have transitions that are roughly equal to a C-H bond vibration: Er^{3+} ($^4I_{11/2} \rightarrow ^4I_{13/2}$, 3700 cm^{-1}), Tm^{3+} ($^3\text{H}_4 \rightarrow ^3\text{H}_5$, 4300 cm^{-1}), and Ho^{3+} ($^5I_6 \rightarrow ^5I_7$, 3500 cm^{-1}). The TA of $\text{Yb}(\text{TPP})\text{L}$ and $\text{Nd}(\text{TPP})\text{L}$ complexes all show a long lifetime and derivative shaped region between 600-800 nm. While an electron transfer mechanism involving a $\text{Yb}^{3+}/\text{Yb}^{2+}$ redox process has been postulated to explain puzzling results for Yb^{3+} sensitization, Nd^{3+} , which cannot be reduced, also shows a TA absorption similar to $\text{Yb}(\text{TPP})\text{L}$ complexes.⁷⁹ Thus electron transfer cannot account for the observed behavior. Yb^{3+} or Nd^{3+} in their respective excited states may simply be exerting a different electronic influence of the π electron system of the porphyrin which

would account in a shift in the absorption of the excited lanthanide porphyrin complex rather than bleaching of the absorption upon laser excitation.

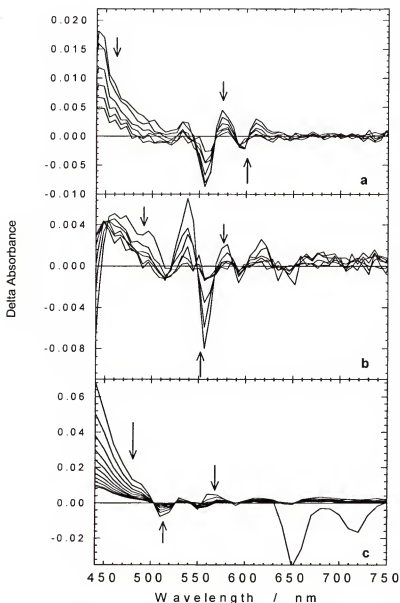


Figure 1-27. Transient absorptions of Ln(TPP)L. a) Yb(TPP)L(OEt)₃ (Transients are 8 μ sec after laser pulse) b) Yb(TPP)TP (Transients are 8 μ sec after laser pulse) c) Nd(TPP)TP (Transients are 16 μ sec after laser pulse). The first transient was recorded immediately after the laser pulse. All measurements were made in argon degassed CH₂Cl₂.

Conclusion

Lanthanide complexes containing Yb^{3+} , Nd^{3+} , and Er^{3+} have been shown to photoluminescence in the near-infrared. In general, lanthanide tetraphenylporphyrin complexes have higher near-infrared quantum yields than their β -diketonate analogs. The porphyrin ligand plays the lead role in controlling the absorption properties of the complexes while the lanthanide directs the emissive properties by accepting energy from the porphyrin ligand and generating near-infrared luminescence.

Improvement of the near-infrared quantum efficiency is achieved by effectively protecting the metal center from the surrounding environment. While not significantly affecting the absorption properties, the TP and $\text{L}(\text{OEt})_3$ capping ligand serve to effectively shield the metal center from coordinating water resulting in improved near-infrared quantum yields for Yb complexes on the order of 2 to 3 percent. In the future the near-infrared efficiency could be further improved if synthetic efforts are taken to remove C-H bonds from close proximity to the lanthanide ion such as deuteration or fluorination of the porphyrin and capping ligands.

Experimental

All photophysical studies were conducted in 1 cm square quartz cuvettes unless otherwise noted. All absorption, emission, and lifetime measurements were made in CH_2Cl_2 unless otherwise noted. Absorption spectra were obtained on a double-beam Cary-100 UV-visible spectrometer. Fluorescence spectra were measured on a SPEX Fluorolog-2 equipped with a water-cooled PMT detector or on a spectrometer consisting of an ISA-SPEX Triax 180 spectrograph equipped with a liquid N_2 cooled CCD detector (Hamamatsu CCD, EEV 1024x128 pixel, 400-1100nm). Near-infrared measurements

were measured on a SPEX Fluorolog-2 equipped with an LN₂ InGaAs detector (800-1600nm). All measurements were corrected for detector response. Emission quantum yields for the Yb complexes were measured by relative actinometry against H₂TPP ($\Phi=1.1 \times 10^{-1}$, CH₂Cl₂) or ZnTPP ($\Phi=3.3 \times 10^{-2}$, CH₂Cl₂). For the near-infrared emitters beyond 1,000 nm, Yb(TPP)TP was used as the standard ($\Phi=3.2 \times 10^{-2}$, CH₂Cl₂). Time-resolved emission decays were obtained by time-correlated single photon counting on an instrument that was constructed in-house. Excitation was effected by using either a pulsed LED source or a blue-pulsed diode laser (IBH instruments, Edinburgh, Scotland). The pulsed LED and diode laser sources have pulse widths of ca. 1 ns. Time-resolved emission was collected using a red sensitive, photon-counting PMT (Hamamatsu R928), and the light was filtered using 10 nm band-pass interference filters. Lifetimes were determined from the observed decays by using fluorescence lifetime deconvolution software. Nanosecond transient absorption spectra measurements were obtained on previously described instrumentation,⁸⁰ with the third harmonic of a Nd:YAG laser (355 nm, 10 ns fwhm, 5 mJ pulse⁻¹) as the excitation source. Samples were thoroughly degassed with argon. Primary factor analysis followed by first order (A→B) least-squares fits of the transient absorption data was accomplished with SPECFIT global analysis software (Spectrum Software Associates).

CHAPTER 2

NEAR-INFRARED EMISSION FROM LANTHANIDE COMPLEXES BLENDED INTO CONJUGATED POLYMER FILMS

Background

Intense efforts have been put forth to understand energy transfer processes in polymers such as saturated polymer backbones with pendent chromophores,^{81,82} polymers with main-chain polychromophores,⁸³⁻⁸⁵ and fully conjugated polymers⁸⁶⁻⁹². Also, there is increasing interest in studying the energy transfer processes in conjugated polymers and in blends of small molecules with conjugated polymers⁹³ such as poly(phenylene vinylenes),⁹⁴ poly(phenylene ethynyls)⁹⁵ and poly(*p*-phenylenes).⁹⁶ With a greater understanding of the energy transfer properties these blend systems can be a useful guide for their use in electroluminescent devices.

Small molecules have also been blended with conjugated polymers in order to tune the electroluminescent (EL) emission wavelengths and improve EL device efficiencies. In these applications, the role of the conjugated polymer is to transport charge and funnel energy to the dopant. This idea has been used by McGehee *et al.* by blending europium *tris*- β -diketonates in a cyano derivitized poly(*p*-phenylene) (PPP-CN).⁹⁷ Using the concept of spectral overlap of the PPP-CN emission with the absorption of the europium complex, they showed that energy transfer from polymer to lanthanide complex occurs. Expanding on this idea, we have carried out investigations in which a series of near-infrared emitting lanthanide *tris*- β -diketonates and monophyrinates were blended with

alkyl or alkoxy substituted poly(*p*-phenylenes). The structures of these materials used are shown in Figure 2-1. Before preparing electroluminescence devices using the polymer/lanthanide blends, blends were prepared where the energy transfer from the polymer to the lanthanide complex could be monitored by quenching of the PPP fluorescence and the resulting sensitization of the lanthanide luminescence by the polymer. These photoluminescence-based experiments served as a guide for determining the concentrations of the lanthanide complexes to be blended into the conjugated polymer for fabricating near-infrared emitting electroluminescent devices. This chapter provides an overview of this work where we fully characterized the UV, visible, and near-infrared PL properties of spin-coated thin films consisting of conjugated polymers blended with various types can concentrations of lanthanide complexes.

The two conjugated poly(*p*-phenylenes) used in this work have the same backbone structure but differ in the side chain that is directly bonded to the backbone. For PPP-R10 and PPP-OR11, the first atom of the 10 and 11 atom-long side chain is carbon and oxygen, respectively. The absorption and fluorescence properties of the two polymers in chloroform are shown in Figure 2-2. The alkyl substituted PPP-R10 has an absorption maximum at 310 nm and the emission maximum peaks in the UV at 370 nm. For PPP-OR11, the absorption maxima occur at 290 and 340 nm with a fluorescence maximum at 410 nm. The red-shift in the absorption and fluorescence of PPP-OR11 relative to PPP-R10 indicates that the HOMO-LUMO gap (i.e. the band gap) is small in the former. Comparative studies of 2,5-dialkyl and 2,5-dialkoxy poly(*p*-phenylene) have shown that regardless of the nature of the length (*n*-C₄, *n*-C₈, *n*-C₁₂, *i*-C₅) the electronic properties of the polymer depend on the atom directly attached to the backbone.⁹⁸ Thus, the HOMO-

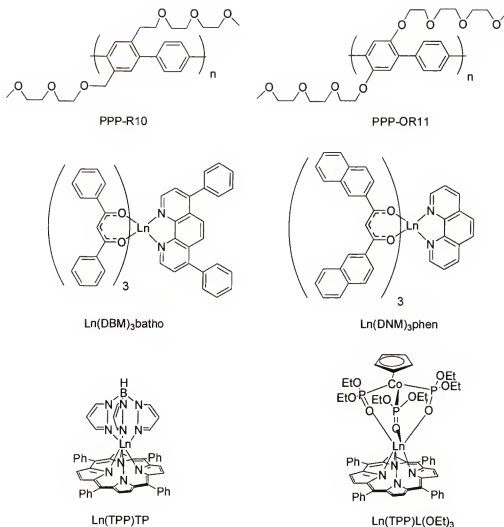


Figure 2-1. Structures of the conjugated poly(*p*-phenylene) polymers and the lanthanide complexes blended into the polymers.

LUMO gap decreases in energy from dialkyl to dialkoxy substitution has been explained in terms of increased planarity in the dialkoxy-substituted polymer resulting from reduced steric hindrance between phenylene rings bearing ether linkages relative to rings carrying alkyl linkages. This explanation has also been used to explain observations in polymers containing 1,4-bis(2-thienyl)phenylene and 1,4-bis(2-furanyl)phenylene repeat units.⁹⁹ Also for PPP-OR11, the electron-donating oxygen atoms serve to raise the

energy of the highest occupied molecular orbital (HOMO) thus decreasing the energy gap of the polymer. The difference in the band gap between PPP-OR11 and PPP-R10, which results in a significant difference in fluorescence wavelength, affords the opportunity to use these two polymers in comparative studies of energy transfer to lanthanide complexes. Specifically, we are able to examine the effect of spectral overlap between the polymer fluorescence and the lanthanide complex absorption on the energy transfer exchange.

Lanthanide *tris*- β -diketonates were used because their absorption properties have some spectral overlap with the fluorescence of the PPP polymers, particularly PPP-R10. Therefore, energy transfer from polymer to lanthanide complex is expected to occur. In addition, β -diketonates are known to sensitize the emitting states of europium, which emits in the visible region, thus it was expected that these ligands could also sensitize the near-infrared emission energy states of other lanthanides.

Energy Transfer between Conjugated Polymers and Visible Emitting Lanthanide Complexes in Polymer Blends

In initial experiments, visible emitting europium *tris*- β -diketonate complexes were blended into the conjugated polymers. While we waited for the arrival of an InGaAs detector that could be used for near-infrared measurements, these measurements were carried out on a spectrophotometer that operates only in the UV and visible. This approach provided us with the advantage of being able to simultaneously monitor quenching of the polymer emission and sensitization of the lanthanide complex. This allows one to easily compare the relative photoluminescence (PL) efficiencies of the emitting species in the film.

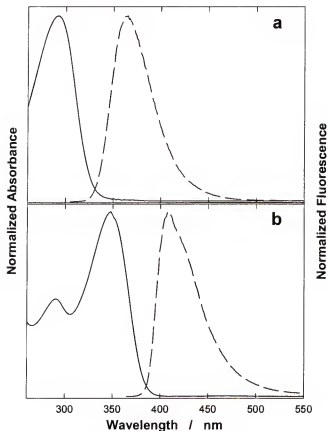


Figure 2-2. Absorbance (solid line) and fluorescence (dashed line) of a) PPP-R10 and b) PPP-OR11 in chloroform.

Films were prepared by first dissolving the polymer into chloroform and dividing the stock solution into five separate vials. To four of the vials, aliquots of varying size of the $\text{Eu}(\text{DBM})_3\text{batho}$ complex (concentration ~ 3 mM), also dissolved in chloroform, were pipetted into the polymer solution. Each of the resulting solutions was spin cast at 1000 rpm onto quartz slides. Quartz slides were used because the absorption of PPP-R10 would be obscured by the absorption of borosilicate glass which absorbs strongly below 300 nm. Concentrations used relate the number of molar equivalents of lanthanide complex relative to the molar equivalents of the polymer repeat unit.

The absorption spectra of the lanthanide polymer blends, corrected for absorption of the quartz substrate, are shown in Figure 2-3. For PPP-R10 a single absorption band corresponding to the $\pi \rightarrow \pi^*$ transition of the polymer is observed at 311 nm. However, below this wavelength, the absorption of the quartz attenuates the absorption signal and consequently additional polymer absorption features below 300 nm could be discerned. When the concentration of the lanthanide complex reaches 5 mol%, a new absorption band appears at approximately 360 nm. This absorption band corresponds to the $\pi \rightarrow \pi^*$ absorption band of the DBM ligand.

The photoluminescence of these films upon excitation at 315 nm are shown in Figure 2-4. Excitation at 315 nm was chosen because it gave the highest PL signal intensity, since the intensity of the xenon excitation lamp decreases sharply below this wavelength. As $\text{Eu}(\text{DBM})_3\text{batho}$ is blended into the film, the PPP-R10 fluorescence centered at 380 nm decreases and a series of peaks, the most intense of which is centered at 612 nm, appear in the 550-700 nm region. These new peaks correspond to the $^5\text{D}_0 \rightarrow ^7\text{F}_n$ transitions of Eu^{3+} , where n is 0 to 4. Quenching of the polymer fluorescence and emergence of the lanthanide emission upon increased lanthanide concentration indicates energy transfer from the polymer to the lanthanide is occurring in these polymer blends.

This premise is confirmed by the PL excitation spectra while monitoring the $^5\text{D}_0 \rightarrow ^7\text{F}_2$ transition of Eu^{3+} . Figure 2-5 shows the excitation spectra of $\text{Eu}(\text{DBM})_3\text{batho}$ in the solid state and $\text{Eu}(\text{DBM})_3\text{batho}$ blended with PPP-R10 at a loading of 10 mol%. The polymer blend shows a blue shift of the $\text{Eu}(\text{DBM})_3\text{batho}$ $\pi \rightarrow \pi^*$ absorption transition which suggests the polymer decreases the π - π stacking between the lanthanide

complexes. In addition, a new band at 330 nm is seen in the excitation spectrum (see arrow in Figure 2-5) which corresponds to the $\pi \rightarrow \pi^*$ absorption band of PPP-R10. This band is significant because it demonstrates that light absorbed by the polymer results in light emission from Eu^{3+} , which proves that energy transfer occurs.

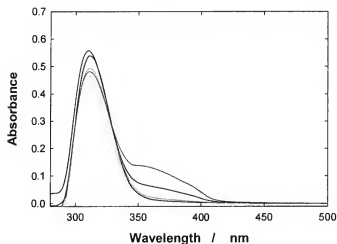


Figure 2-3. Absorption of films on quartz substrates of 0, 1, 2, 5, and 10 mol% of $\text{Eu}(\text{DBM})_3\text{batho}$ blended into PPP-R10. The absorbance at 370 nm increases with increases concentration of the lanthanide complex.

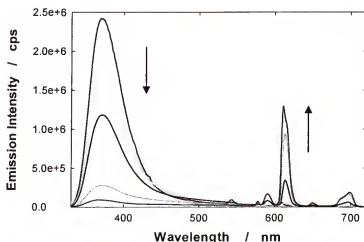


Figure 2-4. Emission of polymer films that contain 0, 1, 2, 5, and 10 mol% $\text{Eu}(\text{DBM})_3\text{batho}$ in PPP-R10 upon excitation at 315 nm. PPP-R10 fluorescence at 380 nm decreases and the Eu^{3+} emission increases at 612 nm with increasing dopant concentration.

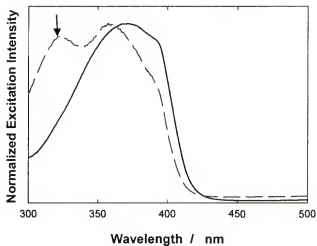


Figure 2-5. Normalized excitation spectra of $^5D_0 \rightarrow ^7F_2$ of $\text{Eu}(\text{DBM})_3\text{batho}$ (solid line) and PPP-R10 film containing 10 mol% $\text{Eu}(\text{DBM})_3\text{batho}$ (dashed line).

Next, we examined films that contained $\text{Eu}(\text{DNM})_3\text{phen}$ blended into PPP-R10. Because of the more extended π electron system of the DNM ligand relative to DBM, $\text{Eu}(\text{DNM})_3\text{phen}$ has a lower energy absorption than the DBM analog. This affords improved greater spectral overlap between the PPP-R10 fluorescence and the $\text{Eu}(\text{DNM})_3\text{phen}$ absorption and based on Förster energy transfer theory, improved spectral overlap is expected to lead to more efficient energy transfer. These films were prepared in a similar manner to the blended films of $\text{Eu}(\text{DBM})_3\text{batho}$ including spin casting onto quartz substrates. Figure 2-6 shows the absorption spectra of these films. In these films, the DNM absorption at 370 nm is also detectable at 5 mol% concentration.

Figure 2-7 shows the emission spectra of these films upon excitation into the polymer $\pi \rightarrow \pi^*$ band at 315 nm. As $\text{Eu}(\text{DNM})_3\text{phen}$ is blended into the film, the PPP-R10 fluorescence centered at 380 nm is quenched and the characteristic emission peaks of Eu^{3+} appear in the 550-700 nm region. Nearly complete quenching of the PPP-R10 PL occurs when the $\text{Eu}(\text{DNM})_3\text{phen}$ concentration is 10 mol%. Although, $\text{Eu}(\text{DNM})_3\text{phen}$

quenches PPP-R10 fluorescence more effectively than $\text{Eu}(\text{DBM})_3\text{batho}$, the Eu^{3+} emission from 10 mol% $\text{Eu}(\text{DNM})_3\text{phen}$ blended into PPP-R10 is only about one-half of the intensity of the same concentration of $\text{Eu}(\text{DBM})_3\text{batho}$ in PPP-R10. The decreased PL intensity is due to the lower quantum efficiency of $\text{Eu}(\text{DNM})_3\text{phen}$ compared to $\text{Eu}(\text{DBM})_3\text{batho}$.

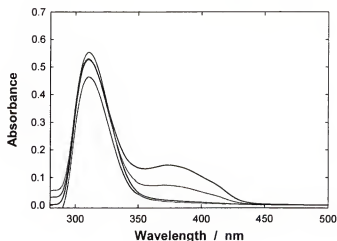


Figure 2-6. Absorption of spin cast films on quartz substrates of 0, 1, 2, 5, and 10 mol% of $\text{Eu}(\text{DNM})_3\text{phen}$ blended into PPP-R10. The absorbance at 370 nm increases with increases concentration of the lanthanide complex.

Excitation spectra of the $\text{Eu}(\text{DNM})_3\text{phen}/\text{PPP-R10}$ films show a band at 320 nm arising from PPP-R10 indicating that energy transfer from the polymer to the lanthanide complex occurs (See arrow in Figure 2-8). Compared to the neat metal complex film, the Eu complex-polymer blend shows a slight blue shift of the $\text{Eu}(\text{DNM})_3\text{phen } \pi \rightarrow \pi^*$ transition. This is not surprising since the polymer likely decreases aggregation of the complex by effectively diluting its concentration. Interestingly, the relative intensity of the polymer band to the Eu band in the excitation spectrum decreases as the concentration of $\text{Eu}(\text{DNM})_3\text{phen}$ increases. A change in the ratio is expected, since absorption by the

lanthanide increases as loading increases. There is also a small red-shift in the PPP-R10 band when the concentration is greater than 1mol%. However, it blue shifts again at 10 mol%. This may indicate that the Eu complex induces a morphology change in the polymer as the dopant concentration changes.

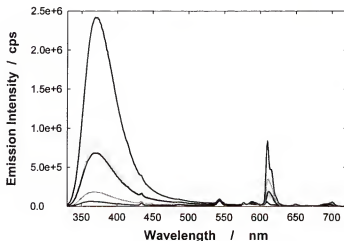


Figure 2-7. Emission of polymer films that contain 0, 1, 2, 5, and 10 mol% Eu(DNM)₃phen in PPP-R10 upon excitation at 315 nm. PPP-R10 fluorescence at 380 nm decreases and the Eu³⁺ emission increases at 612 nm with increasing dopant concentration.

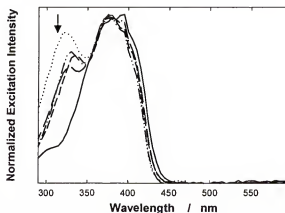


Figure 2-8. Normalized excitation spectra of $^5D_0 \rightarrow ^7F_2$ emission of 1% (···) 2% (---), 5% (- · - · -), and 10% (—) Eu(DNM)₃phen in PPP-R10. In addition a neat film of Eu(DNM)₃phen (solid line) was inspected. The new band at 330 nm which is seen in the polymer blends but not in pure Eu(DNM)₃phen, indicates that polymer to lanthanide energy transfer occurs.

**Near-Infrared Emission from Lanthanide
tris- β -Diketonates Complexes Blended in PPP-R10 Films**

In the work described in the preceding sections, we demonstrated that visible emitting lanthanide complexes to participate in energy transfer from poly(phenylene) polymers. By analogy it was expected that PPP-R10, or PPP polymers in general, could be blended with near-infrared emitting lanthanide complexes to sensitize long wavelength emission. In an effort to address this issue a series of blends were prepared in which near-infrared emitting lanthanide *tris*- β -diketonate complexes at 10 mol% concentration were blended with PPP-R10. The photoluminescence of spin cast films of the blends was examined by exciting at 315 nm. The PPP-R10 fluorescence was efficiently quenched by the lanthanide complexes and resulted in sensitization of the lanthanide-based emission. Figure 2-9 shows the near-infrared emission spectra of PPP-R10 films that contained 10 mol% Ln(DNM)₃phen.

Near-infrared emission was observed for Er³⁺ at 1520 nm (⁴I_{13/2}→⁴I_{15/2}) and Yb³⁺ at 977 nm (²F_{5/2}→²F_{7/2}). Three near-infrared transitions of Nd³⁺ were observed at 880, 1060, and 1333 nm which correspond to the ⁴F_{3/2}→⁴I_{11/2}, ⁴F_{3/2}→⁴I_{13/2}, and ⁴F_{3/2}→⁴I_{15/2}, respectively. Figure 2-9b shows the near-infrared emission from Nd(DBM)₃phen, and Nd(DNM)₃phen. From the graph it can be seen that the diketonate ligand does not perturb the emission energy of Nd³⁺ however, the PL from DBM complex films is more intense, suggesting that the quantum efficiency is higher for this complex. The greater quantum efficiency of the PL from the Nd(DBM)₃phen films must arise because of Nd(DBM)₃phen higher PL quantum yield and not Förster energy transfer from PPP-OR11 because spectral overlap is poorer in the Nd(DBM)₃phen/PPP-OR11 blends than Nd(DNM)₃phen/PPP-R10 blends.

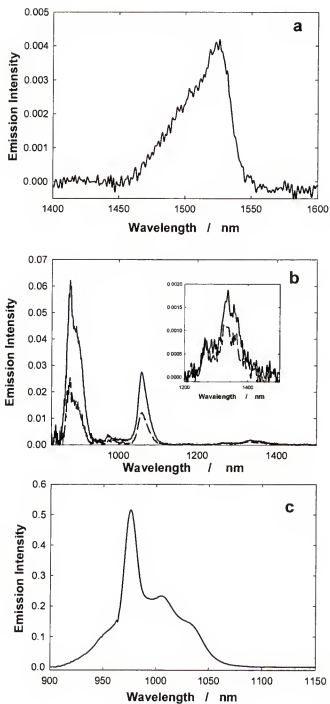


Figure 2-9. Near-infrared emission from spin-coated films of 10 mol% blends of the lanthanide complex with PPP-R10. a) Er(DNM)₃phen b) Nd(DNM)₃phen (—) and Nd(DBM)₃phen (···) and c) Yb(DNM)₃phen upon excitation at 327 nm.

Blends of $\text{Pr}(\text{DNM})_3\text{phen}$ in PPP-R10 did not exhibit detectable near-infrared emission at 1000 or 1300 nm, even though complete quenching of the polymer emission occurred. This was surprising since $\text{Pr}(\text{DNM})_3\text{phen}$ in CH_2Cl_2 was found to emitting in the near-infrared at 1000 and 1050 nm from $\text{Pr}^{3+} {}^1\text{D}_2 \rightarrow {}^3\text{F}_4$ transition. Instead of near-infrared, red emission from ${}^1\text{D}_2 \rightarrow {}^3\text{H}_4$ dominates at 635 nm (Figure 2-10). Since the ${}^1\text{D}_2$ is known to be the emitting level of several near-infrared transitions for Pr^{3+} (${}^1\text{D}_2 \rightarrow {}^3\text{F}_2$ at 850 nm, ${}^1\text{D}_2 \rightarrow {}^3\text{F}_4$ at 1000 nm, and ${}^1\text{D}_2 \rightarrow {}^1\text{G}_4$ at 1350 nm), near-infrared is expected. Thus in PPP-R10 films, near-infrared emission from $\text{Pr}(\text{DNM})_3\text{phen}$ is too weak to be observed. (The ${}^3\text{P}_0 \rightarrow {}^3\text{H}_6$ and ${}^3\text{P}_0 \rightarrow {}^3\text{H}_5$ transitions of Pr^{3+} also emit approximately at 630 nm, however, the triplet energy of the DNM ligand is lower in energy than the ${}^3\text{P}_0$ state and thus sensitization of the ${}^3\text{P}_0$ state is not expected. See Figure 2-11.)

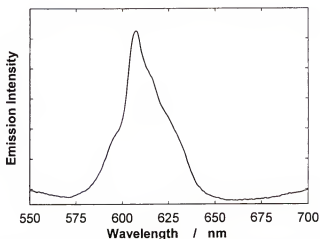
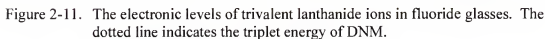


Figure 2-10. Visible emission from the ${}^1\text{D}_2 \rightarrow {}^3\text{H}_4$ transition of Pr^{3+} when a film of 10 mol% $\text{Pr}(\text{DNM})_3\text{phen}$ blended with PPP-R10 is excited at 327 nm.

Due to the improved spectral overlap between the PPP-OR11 fluorescence and the absorption of Yb(DNM)₃phen compared to Yb(DBM)₃phen, energy transfer is more efficient for Yb(DNM)₃phen. This is clearly seen in Figure 2-13 which shows that Yb(DNM)₃phen quenches PPP-OR11 more efficiently, and hence participates in more efficient energy transfer. Even at 5 mol% concentration, Yb(DNM)₃phen quenches 95% of PPP-OR11 fluorescence, but for Yb(DBM)₃phen the quenching is incomplete at even 20 mol% concentration.



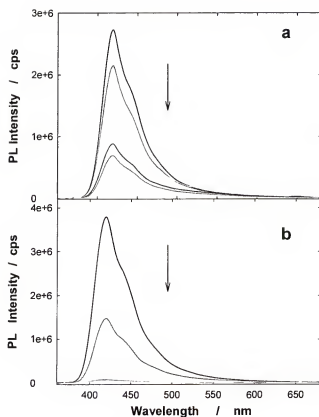


Figure 2-12. PL of films of PPP-OR11 blended with 0, 1, 2, 5, 10, 15, 20 mol% of a) Yb(DBM)₃phen and b) Yb(DNM)₃phen upon excitation at 330 nm.

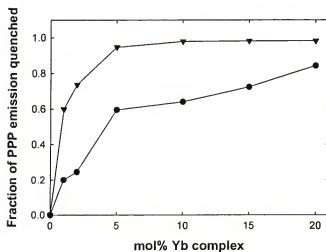


Figure 2-13. Fraction of PPP-OR11 fluorescence quenched by (●)Yb(DBM)₃phen and (▲)Yb(DNM)₃phen in spin-coated films prepared by blending the lanthanide complex into the polymer.

Quenching of PPP-OR11 Fluorescence by Lanthanide Monoporphyrinate Complexes

The spectral overlap between the emission of PPP-OR11 and the absorption of lanthanide tetraphenylporphyrin complexes, Ln(TPP)L is excellent and thus energy transfer is expected to be more efficient using Ln(TPP)L complexes than lanthanide *tris*- β -diketonates. In order to test this concept, spin-coated films were prepared by blending the desired concentration of lanthanide complex in a solution of PPP-OR11 dissolved in chloroform. The films were spin cast at 1000 rpm onto glass substrates. Figure 2-14 shows the absorption spectra of films of PPP-OR11 blended with Ln(TPP)TP at various concentrations.

In the film of pure PPP-OR11, absorption occurs at 330 nm (Figure 2-14a). Below 330 nm absorption of the substrate prevents any further details to be observed. By blending Ln(TPP)L into the polymer host, several new absorptions could be observed which correspond to the porphyrin Soret band at 427 nm and several weaker Q-bands at 554 and 591 nm. The Soret band gradually shifts from 427 nm at lower concentrations to 429 nm at 20 mol% suggesting some aggregation of the porphyrin may occur at high loading concentrations.

The polymer absorption band shows variations in intensity at different loading levels. This variation is due to differences in film thickness during spin coating. There is a linear correlation between the ratio of the two absorption bands and the concentration. Thus, the Ln(TPP)L to polymer ratio is not affected by the spin coating process and variations in polymer absorption are due to film thickness.

Quenching of the PPP-OR11 fluorescence by Ln(TPP)TP in the spin-coated blends is shown in Figure 2-15 and Figure 2-16. As the concentration of the lanthanide complex

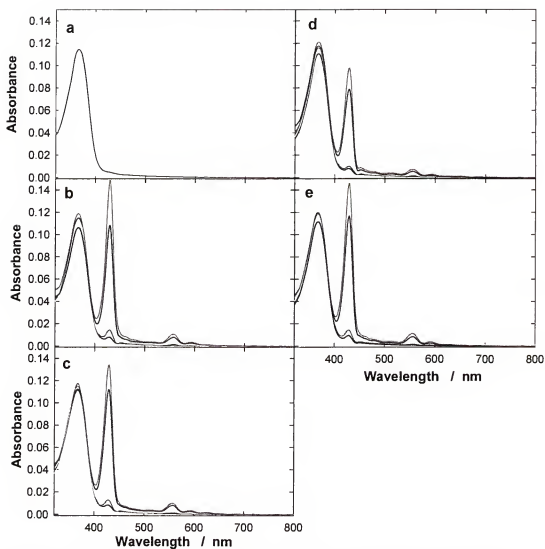


Figure 2-14. Absorbance of spin cast films of Ln(TPP)TP blended into PPP-OR11. a) PPP-OR11 on a glass substrate. Other graphs show the absorbance of Ln(TPP)TP blended in 1, 2, 5, 10, 15, and 20 mol% concentration with PPP-OR11: b) Ho(TPP)TP c) Yb(TPP)TP d) Er(TPP)TP e) Tm(TPP)TP.

is increased, there is a pronounced decrease in the PPP-OR11 fluorescence. At 5 mol% concentration, more than 95% of PPP-OR11 fluorescence is quenched by all Ln(TPP)TP complexes (Figure 2-17). The efficient quenching of the polymer fluorescence is believed to arise from the good spectral overlap of the PPP-OR11 fluorescence and the

absorption of the TPP ligand. The metal does not affect the efficiency of the quenching. However, even at the highest concentration of Ln(TPP)TP studied, some fluorescence from 400-500 nm is still observed from the film.

Aggregation of PPP-OR11 may account for the incomplete quenching. Balanda reported that PPP-OR11 aggregates in solutions used for GPC studies.¹⁰⁰ Thus it would not be surprising that in the solid state some of the PPP-OR11 polymer chains aggregate and thus cannot be quenched by Ln(TPP)TP. Coupled with a short lifetime, there may be insufficient time for energy transfer to the lanthanide to occur, and thus a small amount of unquenched polymer fluorescence occurs.⁹³

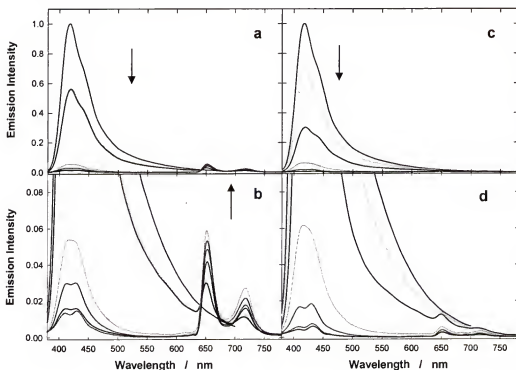


Figure 2-15. Visible emission of spin cast films of 0, 1, 2, 5, 10, 15, and 20 mol% of a) Er(TPP)TP and c) Ho(TPP)TP in PPP-OR11 when excited at 367 nm. Expansions of b) Er(TPP)TP and d) Ho(TPP)TP are also shown to highlight the increasing porphyrin emission. The arrows indicate the emission band intensity with increasing Ln(TPP)TP.

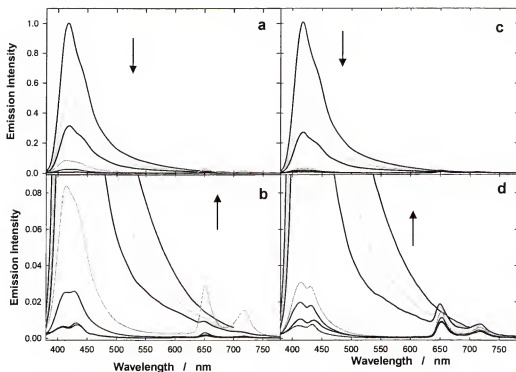


Figure 2-16. Visible emission of spin cast films of 0, 1, 2, 5, 10, 15, and 20 mol% of a) Tm(TPP)TP and c) Yb(TPP)TP in PPP-OR11 when excited at 367 nm. Expansions of b) Tm(TPP)TP and d) Yb(TPP)TP are also shown to highlight the increasing porphyrin emission. The arrows indicate the emission band intensity with increasing Ln(TPP)TP.

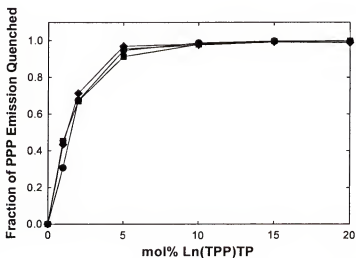


Figure 2-17. Fraction of PPP emission quenched by (●) Ho(TPP)TP, (▼) Er(TPP)TP, (■) Tm(TPP)TP, and (◆) Yb(TPP)TP.

The high energy fluorescence band appears to split at Ln(TPP)TP concentrations greater than 5 mol%. The $S_0 \rightarrow S_2$ absorption of the lanthanide porphyrin occurs in this region and is likely to cause the apparent splitting. Also noticeable at higher lanthanide porphyrin concentrations are two emission bands at 630 and 719 nm. These bands increase with increasing lanthanide concentration and originate from a non-metallated TPP impurity present with the Ln(TPP)TP complex.

Near-Infrared Emission from Lanthanide Monoporphyrinate Complexes Blended in PPP-OR11 Films

Quenching of the polymer fluorescence is accompanied by the appearance of near infrared emission from several of the lanthanide complexes. Near-infrared emission from Yb(TPP)TP was observed when blended into PPP-OR11 at as little as 2 mol% as is shown in Figure 2-18. The central transition at 977 nm corresponding to the $^2F_{5/2} \rightarrow ^2F_{7/2}$ is clearly observed. Additionally, high and low energy bands resulting from crystal field splitting of the $^2F_{5/2} \rightarrow ^2F_{7/2}$ states are also observed. The near-infrared intensity increases linearly with concentration as shown in inset of Figure 2-18 which indicates that concentration quenching is not observed over this concentration range. This is contrary to many inorganic solid-state materials where self-quenching of lanthanides is observed at relatively low concentrations.¹⁰¹

The PL excitation spectra of the blends also confirm that energy transfer to the lanthanide complex occurs when the polymer is excited (Figure 2-19). The two bands at 420 and 550 nm correspond to the Soret and Q-band absorption of the TPP ligand, respectively. The band at 360 nm corresponds to the $\pi \rightarrow \pi^*$ absorption band of PPP-

OR11, thus supporting the idea that energy transfer from the polymer chain to the porphyrin ligand occurs and eventually sensitizes near-infrared emission of Yb^{3+} .

Near-infrared photoluminescence from $\text{Er}(\text{TPP})\text{TP}$ in PPP-OR11 required much higher concentrations of $\text{Er}(\text{TPP})\text{TP}$ than $\text{Yb}(\text{TPP})\text{TP}$. In the film with the highest concentration of $\text{Er}(\text{TPP})\text{TP}$ (20 mol%) used, a weak emission of the $^4\text{I}_{13/2} \rightarrow ^4\text{I}_{15/2}$ transition at 1517 nm was observed as shown in Figure 2-20. Even though PPP-OR11 quenching by $\text{Er}(\text{TPP})\text{TP}$ was comparable to $\text{Yb}(\text{TPP})\text{TP}$, higher concentrations of $\text{Er}(\text{TPP})\text{TP}$ are required because the photoluminescence quantum efficiency of $\text{Er}(\text{TPP})\text{TP}$ is considerably lower compared to its Yb^{3+} analog (see Table 1-6) and also because of poor sensitivity InGaAs detector in the 1500-1600 nm region.

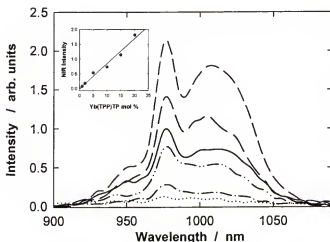


Figure 2-18. Near-infrared emission of 1, 2, 5, 10, 15, and 20 mol% $\text{Yb}(\text{TPP})\text{TP}$ in PPP-OR11 upon excitation at 367 nm. The inset shows that the lanthanide intensity increases linearly with concentration.

Photoluminescence in the near-infrared region was not detected from $\text{Ho}(\text{TPP})\text{TP}$ or $\text{Tm}(\text{TPP})\text{TP}$ blended into PPP-OR11 films. Near-infrared emission from Ho^{3+} $^5\text{I}_6 \rightarrow ^5\text{I}_8$ (1.2 μm) or $^3\text{H}_5 \rightarrow ^3\text{H}_6$ (1.2 μm) was not observed in the spectral regions that could be detected. There are several other near-infrared transitions of Ho^{3+} i.e. $^5\text{I}_7 \rightarrow ^5\text{I}_8$,

(2.0 μm), and $^5\text{I}_6 \rightarrow ^5\text{I}_7$ (2.8 μm), and Tm^{3+} i.e. $^1\text{F}_4 \rightarrow ^3\text{H}_6$ (1.8 μm) and $^3\text{H}_4 \rightarrow ^3\text{H}_5$ (2.3 μm), which are beyond the wavelength range of our InGaAs detector and thus could not be observed.

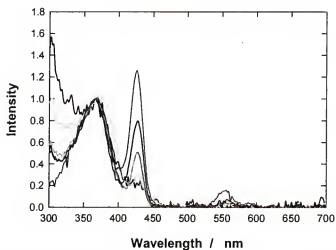


Figure 2-19. Excitation spectra of 977 nm emission of 1, 2, 5, 10, 15, and 20 mol% Yb(TPP)TP in PPP-OR11 normalized to the PPP-OR11 intensity maximum. The TPP absorption bands increased with increased loading of Yb(TPP)TP.

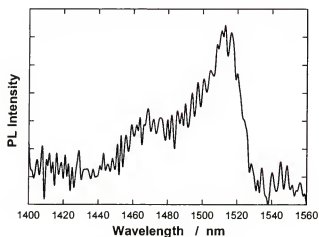


Figure 2-20. Near-infrared emission of 20 mol% Er(TPP)TP in PPP-OR11 excited at 367 nm.

Discussion

In general, the mechanism of energy transfer from the polymer to the lanthanide complex followed by near-infrared emission is believed to occur as follows: Light absorption produces the PPP-OR11 singlet exciton which is then transferred to the β -diketonate or TPP ligand exciting it to the $^1\pi \rightarrow \pi^*$ state. Intersystem crossing occurs producing the $^3\pi \rightarrow \pi^*$ state of the ligand, which subsequently induces the lanthanide-based excited state which then relaxes via emission of a visible or near-infrared photon.

Visible and near-infrared emissions have been observed in films of the lanthanide complexes blended in conjugated polymers. Förster energy transfer theory can be used to analyze the energy transfer efficiency.¹⁰² Figure 2-21 shows the spectral overlap between the absorption of three different lanthanide complexes with the fluorescence spectrum of PPP-OR11. Qualitatively, the spectral overlap increases from $\text{Ln}(\text{DBM})_3\text{L} < \text{Ln}(\text{DNM})_3\text{L} < \text{Ln}(\text{TPP})\text{L}$ in PPP-OR11. Quantitatively, the extent of Förster transfer between a donor and an acceptor can be determined by examining the Förster radius, R_0 , which is the distance between the donor and acceptor where the efficiency of energy transfer is 50%. R_0 can be calculated using the following equation:

$$R_0^6 = \frac{0.5291\Phi_D k^2}{n^4 N_A} \Omega \quad 2-1$$

where k^2 is an orientation factor (2/3 for a randomly oriented molecules), n is the refractive index of the medium (assumed to be 1.7 for PPP), N_A is Avogadro's number, Φ_D is the PL efficiency of the donor, and Ω is the spectral overlap integral defined by:

$$\Omega = \int_0^{\infty} \epsilon_A(\lambda) F_D(\lambda) \lambda^4 d\lambda \quad 2-2$$

where $\epsilon_A(\lambda)$ is the molar absorptivity spectrum of the acceptor, λ is wavelength, and $F_D(\lambda)$ is the normalized emission spectrum as shown in equation 2-3.

$$\int_0^{\infty} F_D(\lambda) d\lambda = 1 \quad 2-3$$

The R_0 for the systems studied are shown in Table 2-1. The R_0 values show that PPP-OR11 blended with Ln(TPP)L should provide the most efficient Förster energy transfer for a given concentration in the blend. The R_0 value of 4.6 nm computed for the Ln(TPP)L/PPP-OR11 blend agrees well with 4.8 nm reported for TPP dispersed in poly(9,9-dioctylfluorene) (PFO).⁹⁶ The calculated R_0 value of 2.6 nm for Ln(TPP)L blended in MEH-PPV also compares well with 2.5 nm reported for TPP blended in MEH-PPV.¹⁰³

However, the R_0 values calculated using Förster energy transfer theory assumes only long-range dipole-dipole interactions. It is expected that it would underestimate the energy transfer distances in these systems, because singlet excitons in the PPP material can rapidly diffuse from their point of formation. For example, Holmes *et. al.* have suggested that excitons formed on poly(phenylene vinylene) can migrate up to 8 nm from the point of formation.⁹⁴ Thus, the exciton can migrate very rapidly throughout the conjugated polymer backbone. Since a much higher concentration than expected is necessary to quenched PPP fluorescence compared to others work with PFO and TPP, this may be an indication that the Yb(TPP)TP is not homogeneously dispersed throughout

the polymer film.⁹⁶ Aggregation of Ln(TPP)TP was not readily observed in PPP-OR11 using fluorescence microscopy. Further work using TEM may more accurately determine if aggregation of Yb(TPP)TP occurs in the polymer host.

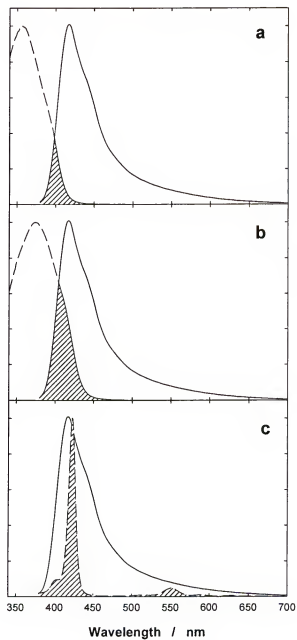


Figure 2-21. Spectral overlap of PPP-OR11 emission (—) and the absorption of a) Ln(DBM)₃phen, b) Ln(DNM)₃phen and c) Ln(TPP)TP (---). The shaded region indicates the area of spectral overlap.

TABLE 2-1. CRITICAL FÖRSTER DISTANCES FOR LANTHANIDE/CONJUGATED POLYMER SYSTEMS.

Blend Composition	R_0 / nm
PPP-R10/ Ln(DBM) ₃ phen	2.7
PPP-R10/ Ln(DNM) ₃ phen	3.1
PPP-OR11/ Ln(DBM) ₃ phen	1.4
PPP-OR11/ Ln(DNM) ₃ phen	2.7
PPP-R10/ Ln(TPP)L	3.7
PPP-OR11/ Ln(TPPL)	4.6
MEH-PPV/ Ln(TPP)L	2.6

Conclusion

Concepts of spectral overlap and Förster energy transfer can be used as a guide for preparing materials which should have improved electroluminescent properties. Using this approach it shows that the most efficient energy transfer should occur in PPP-OR11/Ln(TPP) blend systems. Photoluminescence work indicates that by blending 5 mol% or higher concentration of lanthanide TPP or DNM ligand results in complete quenching (>95% quenching) of the polymer fluorescence.

Experimental

Films of the conjugated polymers and lanthanide complexes were prepared by first dissolving the polymer in chloroform (2 mg/mL) and then adding aliquots of a solution of the lanthanide complex also dissolved in chloroform. The resulting solutions were spin

cast onto glass or quartz substrates at 800 rpm for 30 sec and the films were allowed to air dry overnight.

Absorption spectra recorded were the average of 3-5 scans measured on different areas of the film. Emission spectra were measured by exciting the film perpendicular to the glass substrate and collecting the emission using front-face geometry. Emission spectra were the average of 5 measurements recorded on different areas of the film. A PMT detector was used for visible measurements and an InGaAs detector was used for near-infrared measurements. Detailed descriptions of the instruments used are described in Chapter 1.

CHAPTER 3

NEAR-INFRARED ELECTROLUMINESCENCE OF LANTHANIDE COMPLEXES IN CONJUGATED POLYMER BLENDS

Background

Differing from photoluminescence, where photons are absorbed and emitted by molecules, electroluminescence (EL) is a process where an applied electric field generates an excited species which upon relaxation emits photons. Electroluminescence was first described by Destriau using microcrystals of ZnS suspended in an insulating medium sandwiched between two electrodes.^{104,105} Since then a multitude of inorganic materials have been prepared and commercialized which are capable of producing a wide variety of wavelengths of light.

Electroluminescence of organic materials was first described in anthracene crystals in 1963.^{106,107} However because of the low efficiencies and high-field strengths required, research into organic based electroluminescent materials waned until Tang and Van Slyke prepared single-layer devices by vapor depositing aluminum *tris*-(8-hydroxyquinolate) (AlQ₃) (Figure 3-1) onto indium-tin-oxide (ITO) followed by vapor deposition of an aluminum electrode.¹⁰⁸ Upon application of an electric field, green emission from AlQ₃ was observed.

Another significant milestone in organic based LEDs was the fabrication of the first polymer light-emitting diode (PLED) in 1990.¹⁰⁹ The Cambridge group prepared a thin film of poly(*p*-phenylenevinylene) (PPV) and sandwiched it between two electrodes

Al/Al₂O₃ and Al to produce a yellow green light when a voltage was applied. Their work has since triggered an explosion of interest into polymeric LEDs particularly in two conjugated polymer types: poly(*p*-phenylene vinylene)s (PPVs) and poly(*p*-phenylene)s (PPPs). Since then there has been extensive research on PLEDs and these devices are at the point of commercialization.¹¹⁰⁻¹¹³

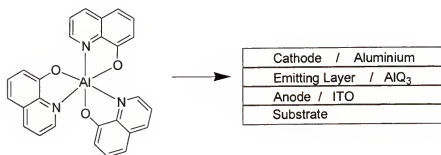


Figure 3-1. Chemical structure of aluminum *tris*-(8-hydroxyquinolate) (AlQ₃) and a single-layer device architecture.

Poly(1,4-phenylenevinylene)s as Electroluminescent Emitters

Poly(1,4-phenylenevinylene)s (PPV) are one of the most studied classes of conjugated polymers (Figure 3-2). Upon photoexcitation, PPVs generally fluoresce in the 500 to 700 nm region giving an orange to red colored emission. The photoluminescence spectrum of PPV generally matches the electroluminescence spectrum suggesting that the emitting excited state produced in PPV is the same regardless of the method of excitation.

Without any substituents on its backbone, PPV is an insoluble and unprocessable polymer. Thus PPV is typically deposited onto the substrate as a polymer precursor which is soluble in organic solvents. The precursor is converted to PPV upon heating as shown in Figure 3-3. Substituting the PPV backbone is also an effective way to affect its

solubility properties. For example, poly(2-(2'-ethylhexyloxy)-5-methoxy-1,4-phenylene vinylene) (MEH-PPV), an orange emitter, possesses side chains which allows the polymer to be dissolved in common organic solvents such as CHCl_3 and toluene and can be spin coated into a thin film.^{114,115} Chemical modification can also affect its electronic properties. For example, by attaching electron withdrawing cyano groups to the vinylene bonds of a substituted PPV, a red emitting polymer (CN-PPV) was obtained which when incorporated into an electroluminescent device showed internal quantum efficiencies up to 4%.¹¹⁶

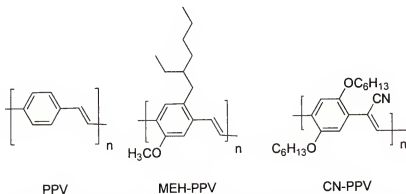


Figure 3-2. Chemical structures of three common poly(*p*-phenylenevinylene)s.

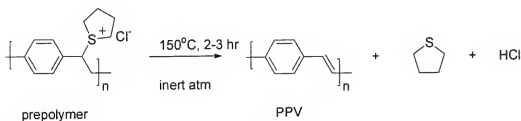


Figure 3-3. Sulphonium prepolymer route to PPV.

Poly(1,4-phenylene)s as Electroluminescent Emitters

Blue emitting polymer LEDs have been a particularly attractive area of interest because of the difficulty in producing blue emitting inorganic semiconductors. Poly(*p*-phenylene)s possess band gaps of 2.7-3.0 eV and are known blue PL emitters making them ideal candidates for use in blue emitting LEDs. In fact, the first example of a blue emitting PLED reported used poly(*p*-phenylene) (PPP) (Figure 3-4).^{117,118} Unsubstituted PPP like unsubstituted PPV has poor processing characteristics. Substitution of alkyl or alkoxy sidechains improves the solubility of the polymer as well as altering the electronic properties of the polymer.¹⁰⁰ Substituted poly(fluorene)s (PFO) are also interesting variations of PPP with promising properties such as efficient quantum efficiencies, high charge-carrier mobilities, and good processability.¹¹⁹

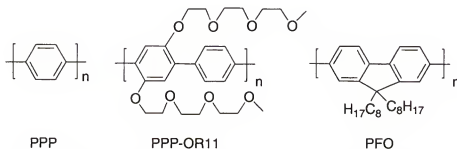


Figure 3-4. Examples of blue emitting electroluminescent poly(*p*-phenylene)s

Electroluminescence Mechanisms

While electroluminescence in its simplest form is the conversion of electrons into photons, the process of electroluminescence can be broken into four steps: (1) introduction of energy into the device, (2) movement of the carriers, (3) excitation of the radiative material and (4) radiative relaxation of the excited material. There are several possible mechanisms proposed which account for electroluminescence. One such

mechanism requires accelerating electrons with enough kinetic energy to cause excitation of the molecule by impact of hot carriers. This is known as intrinsic electroluminescence which has been demonstrated by Bernanose¹²⁰ in organic containing cellophane films and in perylene and anthracene crystals.¹²¹ However, it is difficult to generate intrinsic electroluminescence in organic materials because high ac voltages are usually required, which often leads to electrical breakdown before electroluminescence is obtained.

A more common method of introducing charge carriers into organic materials is to sandwich the electroactive material between electrodes, which upon application of an electric field inject charge into the material. The cathode usually consists of a low work function material which can easily inject electrons into the lowest unoccupied molecular orbital (LUMO), which is analogous to the conduction band (E_c) in semiconductors, of the electroactive material. In chemical terms, injection of electrons reduces the electroactive material. Usually, the cathode is made of calcium, magnesium, or aluminum. Once electrons are injected, they drift to the electrode of more positive potential. At the same time, the anode injects holes into the highest occupied molecular orbital (HOMO) of the active material, which is analogous to the valence band (E_v) in semiconductors. Injection of holes actually corresponds to the removal of electrons from the electroactive material, i.e. oxidation of the electroactive material. Once injected, holes drift toward the more negative cathode. Commonly, the anode is indium tin oxide (ITO) because of its high work function and good transmission properties in the visible region. Electrons and holes recombine in the active material producing an excited state on the emitting material which can decay radiatively or non-radiatively.

Recombination of electrons with holes can cause the electron configuration of the excited material to be either in a singlet state ($S = \frac{1}{2}$) or triplet state ($S = 1$). According to simple spin statistics 25% of the excitons produced are in the singlet state and the remaining 75% will be in triplet states. This means that electroluminescent devices with fluorescent emitters (i.e. emission from the singlet) are limited to a maximum of 25% efficiency, since radiative decay requires the excited species be in a singlet state. Intersystem crossing from the triplet- to singlet-state can be neglected in most organic materials due to a low transition probability, thus fluorescent emitters can only use singlet states formed upon electron hole recombination. Yet, emissive materials which can use the triplet states could theoretically allow device efficiency to reach 100%.

Electronic configuration of the excited state alone is not the only obstacle which must be overcome to maximize device efficiency. It is important that the electron and hole mobilities be nearly equal in the device to effectively recombine on the desired material. However, in most organic materials, the hole mobility typically far exceeds the electron mobility. Therefore, more complicated device architectures can be used to increase or retard carrier mobilities. An example of this is shown Figure 3-5.

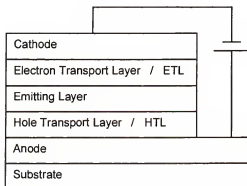


Figure 3-5. Structure of a multilayer light emitting diode

Electron transport layers (ETL) and hole transport layers (HTL) serve to improve the electron and hole mobility to the device, respectively, while at the same time impeding the transport of the opposite carrier. The hole transport layer usually consists of small molecules typically containing amines with low ionization potentials and a small electron affinity associated with a large energy gap. These properties allow hole transport to occur while at the same time blocking electrons from migrating to the anode. Examples of small molecule hole transporters are shown in Figure 3-6. These molecules typically are vapor deposited onto the anode. For polymer based HTL, the most commonly used polymer is poly(3,4-ethylenedioxy-thiophene) doped with polystyrene sulfonic acid whose chemical structure is shown in Figure 3-7. This polymer can be purchased commercially as an aqueous suspension which can easily be spin coated onto ITO.

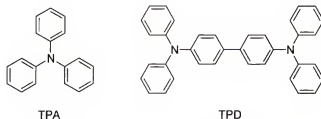


Figure 3-6. Examples of small-molecule hole transport materials. TPA is triphenylamine and TPD is (N, N'-diphenyl-N,N'-bis(3-methylphenyl)1,1'-biphenyl-4,4'-diamine).

Lanthanide Complexes as Electroluminescent Emitters

A typical characteristic of OLEDs, particularly in polymer based devices, is broad emission. This is because the excited state can decay into a multitude of ground state vibrational levels resulting in a broad emission. For polymers, other factors such as intra- or interchain interactions can further broaden the emission characteristics. Broad

emission can be undesirable because it prevents good color purity needed for certain applications such as displays. Tuning the EL emission properties via chemically modifying the emitting material can be difficult and time consuming since chemical modification can affect (possibly adversely), the processing properties, carrier mobilities, or device efficiencies. While elaborate device architectures have been used to improve color purity and device efficiency, lanthanide emitters blended into conjugated polymers are promising alternatives. For example McGehee *et al.* showed that devices prepared with visible emitting europium *tris*- β -diketonates can be blended into a blue emitting poly(*p*-phenylene) giving line-like Eu^{3+} emission.⁹⁷ In those devices energy transfer from PPP to Eu^{3+} was invoked as an explanation of the quenching of polymer fluorescence and sensitization of Eu^{3+} luminescence. Energy transfer has been demonstrated to be an important factor in metal complex doped conjugated polymer systems.^{57,58,97,122} Efficient Förster energy transfer from a conjugated polymer host to a lanthanide complex dopant requires sufficient spectral overlap between the emission spectrum of the polymer and the absorption spectra of the lanthanide complex.¹²³⁻¹²⁷

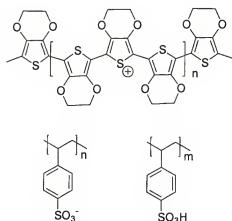


Figure 3-7. Structure of hole transporting polythiophene PEDOT-PSS

Lanthanide metal ions are unique in that their $4f$ orbitals are shielded by filled $5s$ and $5p$ orbitals. This shielding prevents the $4f$ orbitals from interacting with the environment thus allowing the lanthanide to maintain its atomic-like emission properties even in the solid state which is an advantage compared to broadly emitting polymers for display technologies. An additional advantage of lanthanides is that efficient excitation of the lanthanide occurs through the triplet state of the surrounding ligands. This allows the possibility of using both singlet and triplet excitons created by electron-hole recombination to be used in radiative processes.

Near-Infrared Emitting Lanthanide Based Devices

Although most previous investigations have focused on electroluminescent devices that emit in the visible region, there is considerable potential for LEDs that emit in the near-infrared and mid-infrared spectral regions; in particular for optical communication,^{128,129} medical and biological,^{130,131} and sensor applications.¹³² Lanthanide ions such as Nd^{3+} , Er^{3+} and Yb^{3+} are known near-infrared emitters having excellent luminescence properties due to the characteristics of the f - f transitions, which include specific, narrow bandwidth emission in the 800 - 1600 nm region. Previously, near-infrared emitting materials and devices have been prepared using lanthanide compounds, such as small molecule lanthanide complexes¹³³ and blends of conjugated polymers with lanthanide chelates.⁵⁷ Near-infrared electroluminescent (EL) devices using molecular lanthanide complex films, which were fabricated by vacuum deposition, have been constructed and shown to emit light at the wavelengths characteristic of the lanthanide ions.^{59,60,134,135}

Using the concepts mentioned, this chapter presents a summary of work done preparing electroluminescent devices consisting of near-infrared emitting Ln(III) complexes blended into MEH-PPV or an oligoether functionalized poly(*p*-phenylene) as shown in Figure 3-8. It will be shown that while Förster energy transfer between the polymer host and lanthanide complex may occur, charge hopping between lanthanide porphyrin complexes may be the dominant charge transporting pathway in these devices.

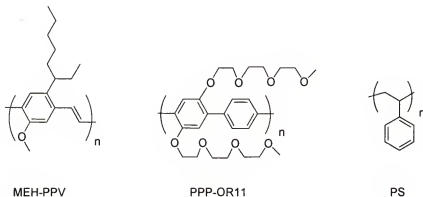


Figure 3-8. Host polymer structures

Electroluminescence from Lanthanide *tris*- β -Diketonates Blended in MEH-PPV

Before the lanthanide complexes were blended with MEH-PPV, a device was prepared to show the EL properties of the host polymer. Electroluminescent devices were prepared by spin coating a thin layer of PEDOT-PSS (Bayer Baytron P VP 4083) onto cleaned ITO. The device was subsequently dried in vacuo at 150°C for 4 hours to remove any residual solvent. Then the active layer was spin-coated followed by deposition of Ca and Al and finally encapsulation with a commercially purchased epoxy material. The device architecture is shown in Figure 3-9.

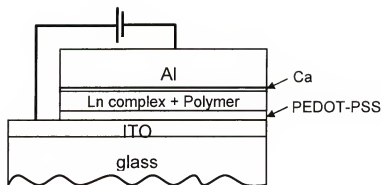


Figure 3-9. Structure of EL device: glass/ITO/PEDOT-PSS (40 nm) / lanthanide complex and polymer host / Ca (5 nm) / Al (200 nm).

Figure 3-10 shows the electroluminescence emission of a pure 750Å thick MEH-PPV device at 9 V. The device showed a broad orange emission peak at 560 nm which corresponds to the MEH-PPV fluorescence peak in the photoluminescence spectrum. While the EL spectrum of MEH-PPV tails into the near-infrared region (>770 nm), there is no emission detected at 980 nm where the first near-infrared emitting complex emitted.

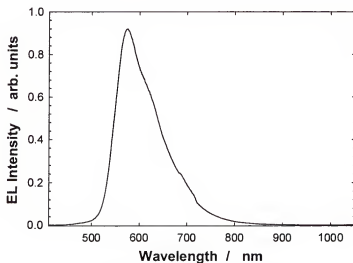


Figure 3-10. Electroluminescence spectrum of ITO/PEDOT-PSS/MEH-PPV/Ca/Al recorded at 9 V. Turn-on voltage was 3 V for this 750Å film.

Ytterbium containing β -diketonates complexes were initially blended into MEH-PPV because they emit in the near-infrared at 977 nm which could be conveniently recorded using a CCD detector. The structures of the lanthanide complexes used are shown in Figure 3-11. First, devices were prepared with $\text{Yb}(\text{TTFA})_3\text{phen}$ blended with MEH-PPV. $\text{Yb}(\text{TTFA})_3\text{phen}$ has one of the highest photoluminescence quantum yields known for Yb^{3+} complexes ($\Phi=0.003$) but its absorption spectrum does not overlap with the emission spectrum of MEH-PPV. Therefore, no energy transfer from the host polymer to the lanthanide complex was expected.

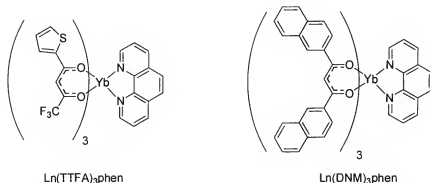


Figure 3-11. Structures of Yb tris- β -diketonates complexes blended into MEH-PPV.

Figure 3-12 shows the EL spectrum recorded at 9 V of 1:2 weight ratio of $\text{Yb}(\text{TTFA})_3\text{phen}$:MEH-PPV. The MEH-PPV fluorescence dominates the emission peaking at 560nm. A weak emission from $\text{Yb}(\text{TTFA})_3\text{phen}$ is observed at 977 nm. Since there is no spectral overlap, Förster energy transfer from MEH-PPV to $\text{Yb}(\text{TTFA})_3\text{phen}$ was not expected to occur. The electroluminescence spectrum supports this with a large host emission and weak near-infrared emission. The Yb^{3+} emission observed probably results from electron-hole recombination that occurs directly on $\text{Yb}(\text{TTFA})_3\text{phen}$.

Next, $\text{Yb}(\text{DNM})_3\text{phen}$ was blended into MEH-PPV. $\text{Yb}(\text{DNM})_3\text{phen}$ possesses a more conjugated ring system and thus absorbs light at longer wavelengths. Figure 3-13 shows the electroluminescence of $\text{Yb}(\text{DNM})_3\text{phen}$ blended into MEH-PPV. Even though some spectral overlap occurs between MEH-PPV and the lanthanide complex and the doping level of the lanthanide complex is high (1:1 weight ratio), the electroluminescence is still dominated by host polymer emission with a visible radiance output 27 times the near-infrared radiance.

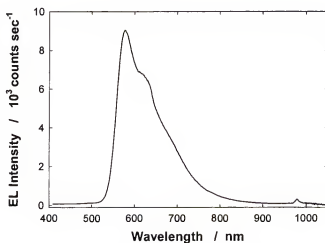


Figure 3-12. Electroluminescence spectrum at 9 V for 1:2 weight ratio of $\text{Yb}(\text{TTFA})_3\text{phen}$ to MEH-PPV device. MEH-PPV emission dominates with a relatively small amount of $^2\text{F}_{5/2} \rightarrow ^2\text{F}_{7/2}$ emission from Yb^{3+} observed at 977 nm.

While the near-infrared EL is low, the $\text{Yb}(\text{DNM})_3\text{phen}$ devices shows more near-infrared emission relative to the visible emission than MEH-PPV/ $\text{Yb}(\text{TTFA})_3\text{phen}$ devices. This is significant because the photoluminescence quantum yield of $\text{Yb}(\text{DNM})_3\text{phen}$ is 5 times lower than $\text{Yb}(\text{TTFA})_3\text{phen}$. Thus if the complexes were equally excited by an electric field, $\text{Yb}(\text{DNM})_3\text{phen}$ should emit with significantly lower efficiency than $\text{Yb}(\text{TTFA})_3\text{phen}$. Two possibilities can account for this; either more

efficient Förster energy transfer from MEH-PPV to Yb(DNM)₃phen occurs because of improved spectral overlap or improved charge trapping by the DNM ligand occurs thus enhancing electron/hole recombination.¹³⁶

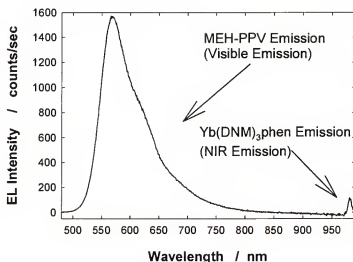


Figure 3-13. Electroluminescence spectrum at 9 V for 1:1 weight ratio of Yb(DNM)₃phen to MEH-PPV device. MEH-PPV emission dominates with a relatively small amount of $^2F_{5/2} \rightarrow ^2F_{7/2}$ emission from Yb³⁺ observed at 977 nm.

Concentration Effects of Yb(TPP)acac Blended into MEH-PPV on Device Performance

Since the porphyrin ligand has Q-bands near 600 nm which overlap with the emission of MEH-PPV, it is expected that more efficient energy transfer from the polymer to the TPP ligand compared to simple β -diketonate ligands would occur. To explore this idea Ln(TPP)acac was prepared according to published procedures^{35,56,137} and blended at several different concentrations into MEH-PPV. The structure of Ln(TPP)acac is shown in Figure 3-14.

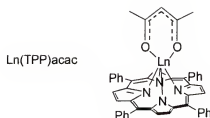


Figure 3-14. Chemical structure of lanthanide tetraphenylmonoporphyrinate acetylacetonate.

Devices were prepared from consisting of pure MEH-PPV, 5, 10 15, and 20 mol%. (Mole percentage represents the fraction of the number of moles of Yb(TPP)acac to moles of MEH-PPV repeat unit.) In addition, a device with an active layer consisting of exclusively Yb(TPP)acac was prepared. The usual device configuration consisted of ITO coated with PEDOT-PSS and the polymer/lanthanide active layer was spin-casted (typically 40-50 nm thick) onto the hole transport layer.

Finally, calcium and aluminum were deposited and the device was encapsulated with epoxy. Figure 3-15 shows the electroluminescence spectra of 5, 10, 15, and 20 mol% Yb(TPP)acac in MEH-PPV at several different voltages. In all devices the dominant emission occurs at 977 nm which corresponds to the $^2F_{5/2} \rightarrow ^2F_{7/2}$ transition of Yb^{3+} . Below 20 mol% Yb(TPP)acac, weaker emission occurs between 500-600 nm. This visible emission is from MEH-PPV not completely quenched and TPP impurity. The overall emission intensity appears to decrease with increasing Yb(TPP)acac concentration.

Figure 3-16 shows the electrical characteristics along with the relative emission areas of the visible and near-infrared emission regions of the spectrum. The current-voltage characteristics are typical of PLEDs. The device consisting of only MEH-PPV turned on at 3 V and the current increased with the voltage until 8 V (500 mA cm^{-2}) after

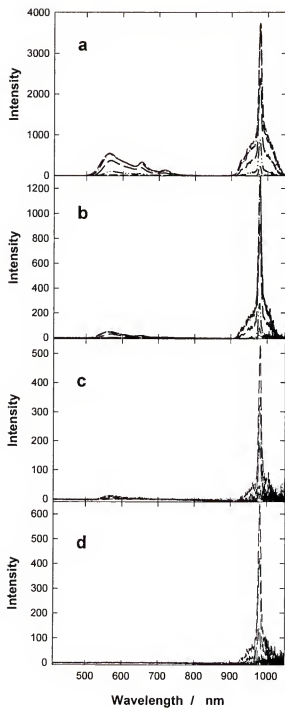


Figure 3-15. Electroluminescence spectra of Yb(TPP)acac in MEH-PPV. a) 5 mol%, b) 10 mol%, c) 15 mol%, and d) 20 mol% Yb(TPP)acac in MEH-PPV at 3,4,5,7,9, and 11 volts.

which the current began to gradually increase beyond this voltage. The visible radiance was detectable at 3 V and began to increase in parallel with the current. After reaching 8 V, the visible radiance decreased even though the current continued to increase.

For 5 mol% Yb(TPP)acac/MEH-PPV the current profile is similar to MEH-PPV. Visible emission appears at 4 V and near-infrared emission is detected at 3 V. As the concentration of Yb(TPP)acac increases, there is an increase in the turn on voltage for near-infrared emission from 4 V for 5 mol% to 5 V for 20 mol%. This is accompanied by an increase in the applied potential needed to reach comparable current densities. For a current density of 100 mA cm^{-2} , the voltage rises from 4 V for MEH-PPV only to 5 V for 5 and 10 mol% then to 6 V for 15 mol%, and finally 8 V for 20 mol%. This indicates that the resistance of the film increases and suggests that TPP plays a role in the charge transport through the polymer film.

As the concentration of Yb(TPP)acac increases, the ratio of near-infrared to visible radiance increases and the voltage at which visible light is detected increases from 4 V to 10 V for 5 to 20 mol%, respectively. The increase in the voltage required for visible light to be detected is due to excitons or charge carriers formed on the polymer being transferred from MEH-PPV to Yb(TPP)acac instead of being utilized for polymer fluorescence.

The decrease in the visible and near-infrared radiances at high current densities is due to device degradation. Lowering the voltage does not regain the previous emission intensities. Since a large number of triplet excitons are formed from electron-hole recombination, it is not surprising that photochemical changes of the device material can occur in these devices thus leading to undesirable effects such as carbonyl formation and

other defects in the film.^{138,139} Upon increasing the current density, there is a hypsochromic shift in the MEH-PPV emission peak position. The emission peak position does not return to its original λ_{max} upon lowering the current suggesting that permanent chemical changes such as reduction in conjugation length by defect formation are occurring.

Near-Infrared Emission from Yb(TPP)acac as the Only Component in the Active Layer

Since Yb(TPP)acac plays a role in controlling charge transport, a device was prepared by spin casting Yb(TPP)acac as the only active layer. While the film quality was poorer than films of polymer blends, the spin cast film of Yb(TPP)acac was of sufficient quality to prepare an EL device. Figure 3-17 shows the electroluminescence spectra of this device as a function of voltage. The device has the following device architecture: ITO/PEDOT-PSS/Yb(TPP)acac/Ca/Al. The *i*-V and radiance characteristics of the Yb(TPP)acac only devices are shown in Figure 3-16f. At 5 V, a weak near-infrared emission was observed at 977 nm, which corresponds to the $^2F_{5/2} \rightarrow ^2F_{7/2}$ transition of Yb^{3+} , which peaks in intensity around 12 V. Near-infrared emission is the dominant emission from these devices. There is no visible emission from the free TPP impurity which is observed when Yb(TPP)acac is blended with a polymer.

Since no polymer is present, charge hopping from one porphyrin ring to another must account for the EL observed. This is not surprising since vapor deposited OLEDs must use a similar mechanism for charge transport. While the polymer may not be necessary for near-infrared electroluminescence, it still plays a role in enhancing the device efficiency. Since this device was prepared in conjugation with devices containing

Yb(TPP)acac blended into MEH-PPV, a comparison between the relative intensities can be drawn. Overall, the devices with 5 to 10 mol% Yb(TPP)acac in MEH-PPV had greater near-infrared outputs than the pure device.

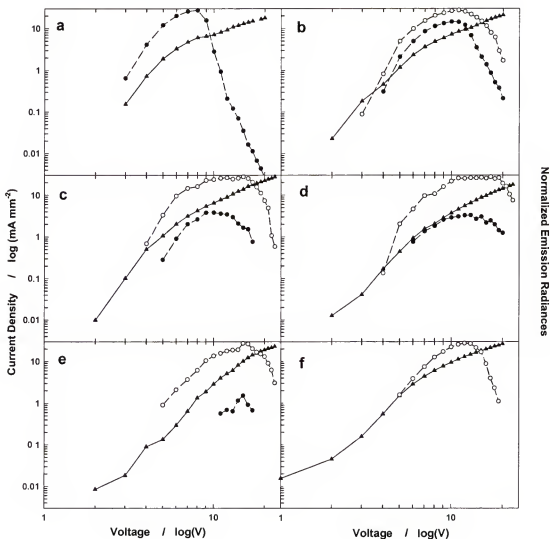


Figure 3-16. Current response of electroluminescent devices at different voltages. Current density data are triangles. a) MEH-PPV, b) 5 mol%, c) 10 mol%, d) 15 mol%, e) 20 mol%, and f) pure Yb(TPP)acac film with Ca/Al electrodes. Relative visible (filled circles) and near-infrared emission (empty circles) area are also indicated.

Increasing the concentration of Yb(TPP)acac in MEH-PPV to 15 mol%, reached a minimum in near-infrared irradiance. The neat film only produced 20% of the near-infrared intensity of the 5 mol% device. This suggests that one way the host enhances near-infrared emission is by minimizing self-quenching effects. Therefore, while Förster energy transfer of excitons formed on MEH-PPV is a feasible method of exciting Yb(TPP)acac, this experiment has shown that it is not the only possible pathway for Yb(TPP)acac sensitization.

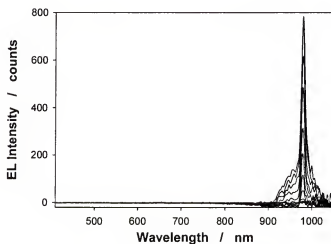


Figure 3-17. Electroluminescence spectra of ITO/PEDOT/Yb(TPP)acac/Ca/Al device from 6-12 V.

Near-Infrared Emission from Er(TPP)acac in MEH-PPV

Other near-infrared wavelengths can be achieved by substituting the lanthanide coordinated to TPP. A device containing 1:2 weight ratio of Er(TPP)acac blended into MEH-PPV was prepared in a similar fashion as to devices containing Yb(TPP)acac blended into MEH-PPV. Upon application of an electric field near-infrared emission was observed at 1520 nm corresponding to the $^4I_{13/2} \rightarrow ^4I_{15/2}$ transition of Er^{3+} (Figure 3-18).

No other Er^{3+} based emission was observed. A visible red emission was observed by eye, corresponding to the fluorescence of free-base tetraphenylporphyrin impurities present.

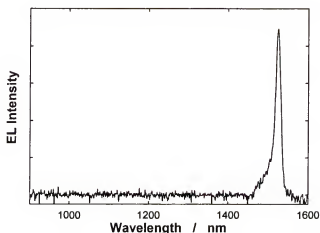


Figure 3-18. Electroluminescence spectrum of 1:2 (weight ratio) $\text{Er}(\text{TPP})\text{acac}:\text{MEH-PPV}$ at 9 V. A red emission was also seen. No other Er^{3+} based emissions were observed.

Electroluminescence of PPP-OR11

Photoluminescence studies suggested that good spectral overlap of the emission from PPP-OR11 with the absorption of the porphyrin ligand should result in more efficient energy transfer from polymer to lanthanide complex resulting in less residual visible fluorescence. Before electroluminescence studies could be carried out on blends of PPP-OR11 with lanthanide complexes, the electrical and EL properties of the polymer itself were studied. Devices were prepared with the following architecture: ITO/PEDOT-PSS/PPP-OR11/Ca/Al with approximately 50 nm thickness. Once the device turns-on, a blue emission was observed peaking at 420 nm as shown in Figure 3-19. This blue emission matches closely the photoluminescence spectrum of PPP-OR11 films. Thus the electroluminescence observed results from a similar singlet $\pi \rightarrow \pi^*$ excited state which

can be created by photoexcitation. The emission intensity of the device increases with increasing voltage and peaks at 9 V followed by a decrease in emission at higher voltages. Figure 3-20 shows the i - V and irradiance characteristics of devices made with PPP-OR11 as the active layer. The current initially increases slowly, presumably due to leakage current, but at 6 V, the current increases rapidly with increasing voltage. Upon turning on at 5 V, the irradiance was $4 \mu\text{W cm}^{-2}$, and by 9 V the average irradiance reaches $70 \mu\text{W cm}^{-2}$ at 140 mA cm^{-2} .

The electroluminescence efficiency of the PPP-OR11 device as a function of current density is shown in Figure 3-21. From the graph it is apparent that the efficiency increases until approximately 30 mA cm^{-2} peaking at 2.6×10^{-3} after which the efficiency remains constant until about 100 mA cm^{-2} and then rapidly decreases possible through photo-oxidation of PPP or other irreversible degradation pathways.¹⁴⁰

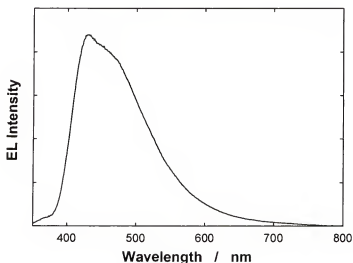


Figure 3-19. Electroluminescence spectrum of PPP-OR11 at 6 V.

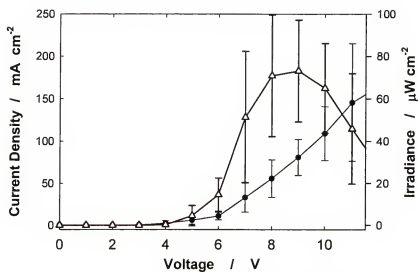


Figure 3-20. Current density (circles) and irradiance (triangles) of PPP-OR11 at different applied voltages. The error bars represent the standard deviations of five measurements.

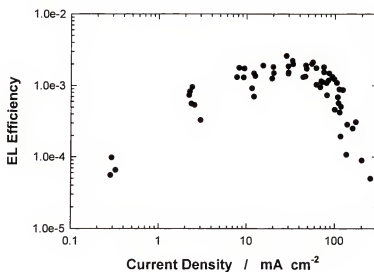


Figure 3-21. Efficiencies of ITO/PEDOT-PSS/PPP-OR11/Ca/Al devices versus current density.

Near-Infrared Electroluminescence of Yb(TPP)TP Blended into PPP-OR11

Devices were prepared with Yb(TPP)TP (Figure 3-22) blended into PPP-OR11. Yb(TPP)TP is expected to give higher external electroluminescence efficiency because the photoluminescence quantum yield of Yb(TPP)TP is higher than that of Yb(TPP)acac (See Table 1-9). This is significant because the electroluminescence quantum yield is directly proportional to the photoluminescent quantum yield.¹⁴¹ Therefore, devices were prepared with Yb(TPP)TP blended into PPP-OR11. In addition, the concentration of Yb(TPP)TP was varied from 5, 10, and 15 mol% to observe the effects of dopant concentration on device performance.

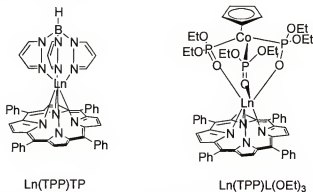


Figure 3-22 Chemical structures of lanthanide tetraphenylporphyrin complexes Ln(TPP) with differing capping ligands TP = tris-pyrazoylborate or L(OEt)₃ = (cyclopentadienyl) tris(diethoxyphosphito-P)cobaltate.

Electroluminescence spectra of devices containing Yb(TPP)TP blended into PPP-OR11 are shown in Figure 3-23. At all concentrations, Yb³⁺ is the predominate emitter in the devices with a near-infrared emission at 977 nm. As the concentration of Yb(TPP)TP in PPP-OR11 increases, the spectral shape of the Yb³⁺ begins to show a defined emission band at 920 nm. The ²F_{5/2} energy state of Yb³⁺ in a non-symmetric environment is split into three crystal field states. The splitting of these states is on the order of a few hundred wavenumbers. With a sufficiently long excited state lifetime at room temperature,

thermal equilibrium is established between the lowest excited and second lowest excited states which results in emission of a higher energy band at 920 nm.

Emission in the visible region is significantly weaker than the near-infrared emission, but there are interesting features when closely examined. At 5 mol% a very weak emission from PPP-OR11 is observed from 400-500 nm. At higher Yb(TPP)TP concentration, this band disappears indicating that emission from PPP-OR11 is completely quenched at concentrations at 10 mol% or above. Very weak bands between 550 and 620 nm in the 15 mol% are probably ring fluorescence from the metallated porphyrin. Between 620 and 800 nm, several things may be contributing to the luminescence including aggregate fluorescence from a free base porphyrin impurity present or phosphorescence from the metallated porphyrin ring. Yb(OEP)OH (OEP= octaethylporphyrin) has been shown to phosphoresce at 710 nm.³⁶ The analogous Gd complex shows phosphorescence at 710, 740 and 790 nm.³⁶ (The extra phosphorescence bands arise due to the fact that energy accepting levels of Gd^{3+} are much higher in energy than the triplet energy of porphyrin ligand preventing energy transfer to occur. In addition, Gd^{3+} enhances intersystem crossing from the porphyrin singlet to triplet state due to the heavy atom effect.) Therefore, the additional features observed between 620 and 800 nm in the electroluminescence spectrum may be due to ring phosphorescence from the Yb(TPP)TP complex.

The current-voltage (*i*-V) profiles and irradiances of the devices are shown in Figure 3-24 along with the current-voltage profile of the host material itself. The turn-on voltages for the devices are 6 V for the PPP-OR11 only, 5 and 10 mol% devices. The 15 mol% device has a turn-on voltage of 4 V. Devices with increasing amounts of

Yb(TPP)TP exhibit lower resistivity, as reflected by the fact that the current density increases with increasing Yb(TPP)TP at the same voltage. This strongly suggests that the porphyrin complex plays an important role in charge transport in the device.

The near-infrared irradiance of the devices increases with Yb(TPP)TP concentration. For example, at 9 V the 5 mol% devices emit with a near-infrared irradiance of $1.6 \mu\text{W cm}^{-2}$ and passing an average current of 100 mA cm^{-2} . At 10 mol%, the irradiance and current increase to $5.0 \mu\text{W cm}^{-2}$ and 160 mA cm^{-2} at 9 V, respectively. Finally, at 15 mol%, devices emit $10.0 \mu\text{W cm}^{-2}$ with a current of 315 mA cm^{-2} at 9 V. Overall, the increase in near-infrared radiance is accompanied by a corresponding increase in current.

The near-infrared efficiencies at 5, 10, and 15 mol% Yb(TPP)TP in PPP-OR11 at several selected current densities are shown in Table 3-1. Additional efficiency verses current density data are plotted in Figure 3-25. At 5 mol% the efficiency of the device is approximately 3×10^{-5} . There is a significant amount of scatter in the device data at this concentration, however, as the concentration is increased, the scatter decreases. At 10 mol% the near-infrared efficiency peaks at approximately 10 mA cm^{-2} with a value of 1.8×10^{-4} and decreases with increasing current. For 15 mol% the near-infrared efficiency peaks between $30\text{-}50 \text{ mA cm}^{-2}$ with a value of 1.3×10^{-4} . Above 100 mA cm^{-2} , there is a decrease in the near-infrared efficiency which can partially be attributed to device degradation.

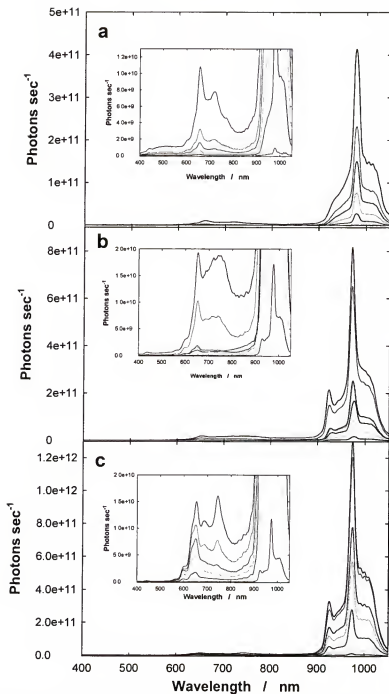


Figure 3-23. Electroluminescence spectra measured from 4 to 10 V in 1 V increments. a) 5 mol%, b) 10 mol%, and c) 15 mol% Yb(TPP)TP in PPP-OR11. The insets are expansions of the visible region. The intensity increases with increasing voltage.

Table 3-1. Near-infrared external EL efficiencies of 5, 10, 15 mol% concentrations of Yb(TPP)TP blended into PPP-OR11 at various current densities.

	5 mA cm ⁻²	10 mA cm ⁻²	30 mA cm ⁻²	50 mA cm ⁻²	100 mA cm ⁻²
5 mol%	2.4×10^{-5}	1.4×10^{-5}	2.4×10^{-5}	5.0×10^{-5}	5.2×10^{-5}
10 mol%	1.2×10^{-4}	1.8×10^{-4}	1.6×10^{-4}	1.0×10^{-4}	8.0×10^{-5}
15 mol%	4.5×10^{-5}	6.1×10^{-5}	1.3×10^{-4}	1.3×10^{-4}	1.2×10^{-4}

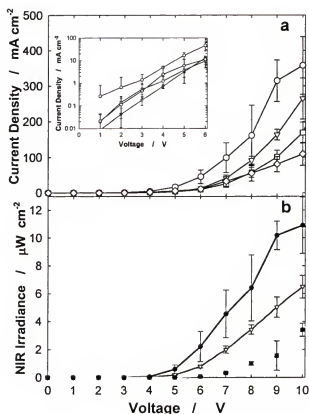


Figure 3-24. Current and radiance profiles of devices consisting of Yb(TPP)TP in PPP-OR11. a) Current density of 5 (squares), 10 (triangles), 15 (circles) mol% of Yb(TPP)TP in PPP-OR11 with the i-V profile of PPP-OR11 (diamonds) included. Inset shows the log(current) versus voltage. b) Near-infrared irradiance of 5 (squares), 10 (triangles), 15 (circles) mol% of Yb(TPP)TP in PPP-OR11.

Power output verses power input plots of these devices are shown in Figure 3-26. Power input increases linearly until 2000 mW cm^{-2} . After 2000 mW cm^{-2} , the output power increased sublinearly.

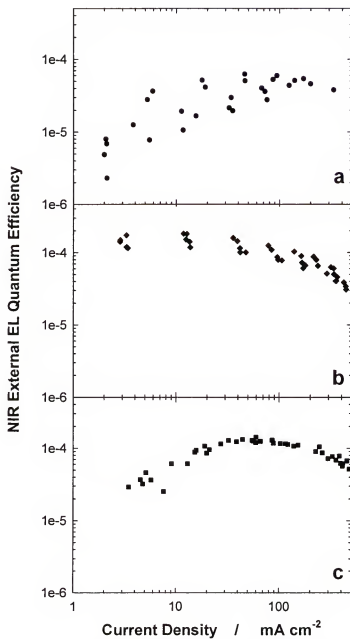


Figure 3-25. Log-log plot of near-infrared efficiency of a) 5 mol%, b) 10 mol%, and c) 15 mol% Yb(TPP)TP in PPP-OR11 verses current density.

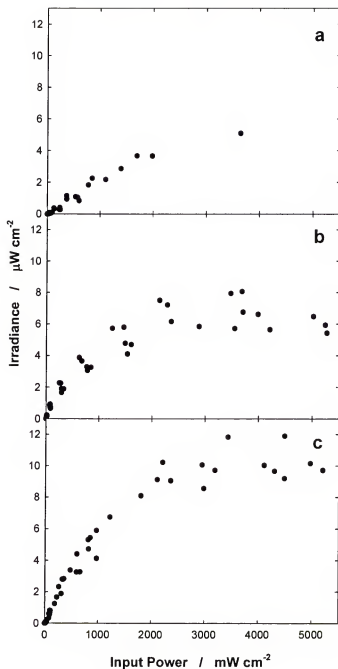


Figure 3-26. Log-log plot of near-infrared power output of a) 5 mol%, b) 10 mol%, and c) 15 mol% Yb(TPP)TP in PPP-OR11 versus input power.

The power efficiency of the devices is on the order of 10^{-6} . Commercial GaAs LEDs emitting at similar wavelengths typically have power efficiencies of 10^{-2} .¹⁴² Thus

inorganic near-infrared emitting LEDs have a significantly higher power efficiencies than organic LEDs.

Near-Infrared Electroluminescence of Yb(TPP)L(OEt)₃ Blended into PPP-OR11

Devices were next prepared by blending Yb(TPP)L(OEt)₃ (Figure 3-22) with PPP-OR11. The concentration of Yb(TPP)L(OEt)₃ was varied from 5, 10, and 15 mol%. An example of the electroluminescence spectra of a device containing 15 mol% Yb(TPP)L(OEt)₃ in PPP-OR11 is shown in Figure 3-27. Graphs of the current and irradiance verses applied potential are shown in Figure 3-28. The electroluminescence spectra at this concentration show complete quenching of the PPP-OR11 emission and predominately near-infrared emission from Yb³⁺ at 977 nm. The ²F_{5/2}→²F_{7/2} emission of Yb(TPP)L(OEt)₃, like Yb(TPP)TP, is split into several peaks due to crystal field effects. Between 600 and 800 nm there are several bands observed. These bands are composed of Yb(TPP)L(OEt)₃ ring fluorescence and phosphorescence and fluorescence from a free base TPP impurity. The feature at 440 nm is attributed to the S₂→S₀ transition of the porphyrin ring. The turn-on voltages for the devices are 6 V for the 5 mol% and 4 V for the 10 mol% and 15 mol% devices. Devices that contain increasing amounts of Yb(TPP)L(OEt)₃ exhibit lower resistivity, as shown by the fact that the current density increases with increasing Yb(TPP)L(OEt)₃ concentration at the same voltage. This strongly suggests that the porphyrin ligand plays a controlling role as a charge carrier in the device. The current densities of Yb(TPP)L(OEt)₃ devices however are similar to the devices prepared with Yb(TPP)TP. This suggests that the axial ligand has little influence on charge transport in the device.

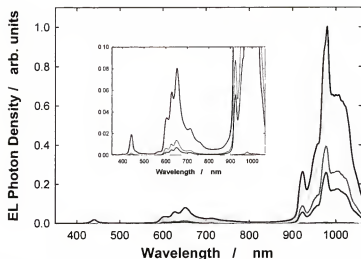


Figure 3-27. Electroluminescence spectra of 15 mol% Yb(TPP)L(OEt)₃ in PPP-OR11 from 5 to 12 V in 1 volt increments.

The efficiencies of devices made with Yb(TPP)L(OEt)₃ blended in PPP-OR11 peak between 30-50 mA as shown in Table 3-2 and Figure 3-29. The electroluminescence efficiencies of the near-infrared emission increase with increasing concentration of Yb(TPP)L(OEt)₃ with values of 2.3×10^{-5} , 3.5×10^{-5} , and 8.0×10^{-5} at 30 mA cm^{-2} for 5, 10 and 15 mol%, respectively. They peak around 30 mA cm^{-2} and decrease with increasing current density. Similar to Yb(TPP)TP blended into PPP-OR11, there is a significant amount of scatter in the efficiency data at low concentrations of Yb(TPP)L(OEt)₃. However, as the concentration of Yb(TPP)L(OEt)₃ increases, the scatter in the data begins to decrease and becomes apparent that the near-infrared efficiency decreases with increasing current density. Thus the L(OEt)₃ ligand may prevent the aggregation necessary for charge hopping to occur.

The decrease in near-infrared efficiency with increasing current density is due to two possible factors. First, because the lifetime of the lanthanide excited state is long, approximately 40 μsec for Yb(TPP)L(OEt)₃, at very high current densities saturation of

the emissive sites can occur.⁵³ Work by others has shown that the decrease in efficiency, which occurs at a much lower current density than saturation, is due to triplet-triplet annihilation.¹⁴³ A second possibility is permanent degradation of the device through chemical reactions.

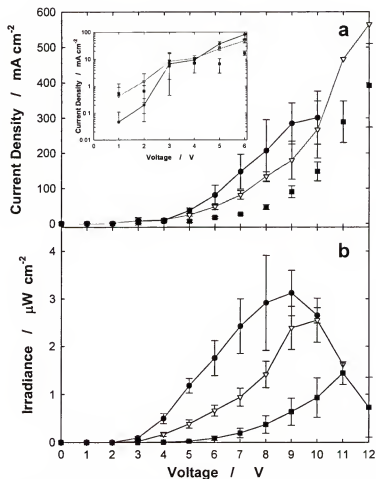


Figure 3-28. Current and radiance profiles of devices consisting of Yb(TPP)L(OEt)₃ in PPP-OR11. a) *i*-V plot with various 5 (squares), 10 (triangles), 15 (circles) mol% of Yb(TPP)L(OEt)₃ in PPP-OR11. b) near-infrared radiance of 5 (squares), 10 (triangles), 15 (circles) mol% of Yb(TPP)L(OEt)₃ in PPP-OR11.

Table 3-2. Near-infrared external EL efficiencies of 5, 10, 15 mol% concentrations of Yb(TPP)L(OEt)₃ blended into PPP-OR11 at various current densities.

	5 mA cm ⁻²	10 mA cm ⁻²	30 mA cm ⁻²	50 mA cm ⁻²	100 mA cm ⁻²
5 mol%	2.3×10^{-6}	5.1×10^{-6}	2.3×10^{-5}	2.9×10^{-5}	2.5×10^{-5}
10 mol%	1.4×10^{-5}	2.7×10^{-5}	3.5×10^{-5}	3.5×10^{-5}	3.2×10^{-5}
15 mol%	1.6×10^{-4}	1.3×10^{-4}	8.0×10^{-5}	7.2×10^{-5}	4.8×10^{-5}

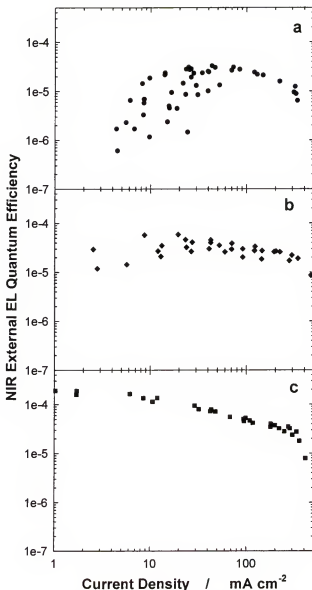


Figure 3-29. Log-log plot of near-infrared efficiency of a) 5 mol%, b) 10 mol%, and c) 15 mol% Yb(TPP)L(OEt)₃ in PPP-OR11 versus current density.

The power efficiencies of these devices, a typical value used by engineers, are low, generally around 10^{-6} . A plot of output power verse input power shows that most of the input energy is not converted into near-infrared light but is non-radiatively dissipated.

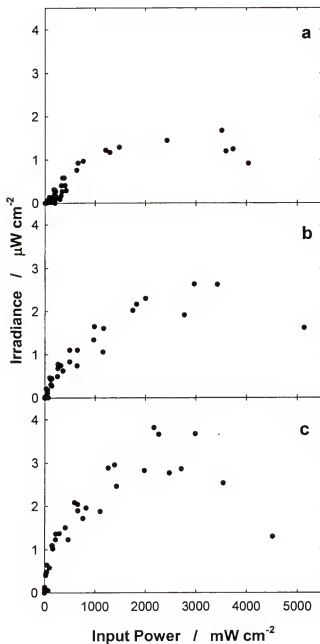


Figure 3-30. Log-log plot of near-infrared power output of a) 5 mol%, b) 10 mol%, and c) 15 mol% Yb(TPP)L(OEt)₃ in PPP-OR11 verses input power.

Near-Infrared Emission from Ln(TPP)L in Polystyrene

Better insight into the role Ln(TPP) plays in the device was gathered by replacing PPP-OR11 with a non-electroactive and non-fluorescent polymer. Polystyrene (PS) (Aldrich, M_n 280,000) was chosen for comparison with PPP-OR11 because instead of the conjugated phenylene rings of PPP-OR11, PS possesses phenyl rings that are not conjugated between rings. PS is a wide-bandgap material and is generally considered to be an electrical insulator. By contrast, due to the relatively narrower band-gap PPP-OR11 is a semiconductor. Figure 3-31 shows the *i*-V and near-infrared irradiance of a device consisting of Yb(TPP)L(OEt)₃ blended into PS. The device begins to pass current with detectable near-infrared emission at 6 V. Above 7 V the current increases rapidly and the near-infrared irradiance follows suit. The irradiance peaks at $22 \mu\text{W cm}^{-2}$ at 220 mA cm^{-2} . The current passing through the device is much lower than devices prepared with PPP-OR11 has the host.

The EL spectra of this device are shown in Figure 3-32 and near-infrared emission from Yb(TPP)L(OEt)₃ is clearly observed at 977 nm. The near-infrared emission arises from the $^2F_{5/2} \rightarrow ^2F_{7/2}$ transition of Yb³⁺. Visible emission is also observed at 430 nm and between 600-750 nm which is the result of weak porphyrin ring fluorescence or a free TPP impurity. The average EL efficiency of this unoptimized device was 3.1×10^{-4} . This experiment clearly shows that porphyrins play a very significant—if not the dominant role—in charge transport in the PPP-OR11 device.¹⁴⁴

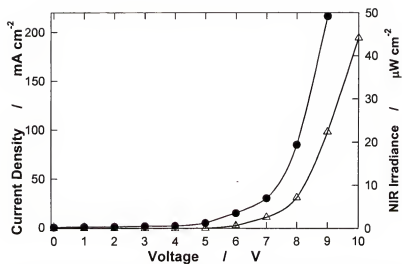


Figure 3-31. Current density (circles) and near-infrared irradiance (triangles) of 10 mol% Yb(TPP)L(OEt)₃ in polystyrene (M_n : 280,000)

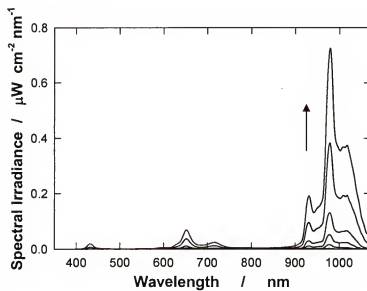


Figure 3-32. Electroluminescence from 6 V to 10 V for 10 mol% Yb(TPP)L(OEt)₃ in polystyrene.

Near-Infrared Electroluminescence from Other Lanthanide TPP Complexes

Other lanthanides besides Yb^{3+} are known to emit in the near-infrared. By changing the lanthanide coordinated to the TPP, tuning of the near-infrared emission can be achieved. Figure 3-33 shows the energy state diagram of other near-infrared emitting lanthanide ions coordinated to TPP and the triplet energy of TPP, specifically $\text{Zn}(\text{TPP})$.¹⁴⁵ Devices prepared by blending 10 mol% $\text{Ln}(\text{TPP})\text{L}$ with PPP-OR11 or PS.

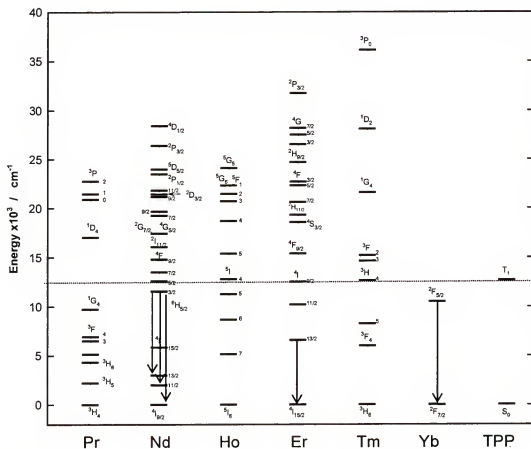


Figure 3-33. The electronic energy levels of Pr^{3+} , Nd^{3+} , Ho^{3+} , Er^{3+} , and Tm^{3+} ions in fluoride glasses. Triplet energy of TPP is based on ZnTPP and is indicated by the dotted line.¹⁴⁵ The arrows show the lanthanide-based near-infrared electroluminescence observed.

Nd(TPP)L(OEt)₃ blended into polystyrene shows three near-infrared transitions which include emission at 880 nm ($^4F_{3/2} \rightarrow ^4I_{9/2}$), 1060 nm ($^4F_{3/2} \rightarrow ^4I_{11/2}$), and 1300 nm ($^4F_{3/2} \rightarrow ^4I_{13/2}$) (Figure 3-34a). Near-infrared emission was detected at as little as 6 V. Er(TPP)L(OEt)₃ blended in PS shows a single emission peak at 1520 nm corresponding to the $^4I_{13/2} \rightarrow ^4I_{15/2}$ transition of Er³⁺ (Figure 3-34b). The shape of the lower energy side of the Er³⁺ emission may be affected because the rapid drop off in sensitivity of the InGaAs detector used at 1560 nm. Also, no other near-infrared Er³⁺ emissions were detected. This is surprising since the $^4I_{11/2}$ energy state matches well with the TPP triplet level (12,700 cm⁻¹) and $^4I_{11/2} \rightarrow ^4I_{15/2}$ transition at 970 nm is a known emissive transition. No near-infrared emission was detected for Pr(TPP)TP at 1,000 or 1,300 nm. For near-infrared emission from Pr³⁺ to occur either, the 1D_2 or 1G_4 state must be populated (see the energy diagram above). Energy transferred from the porphyrin ligand would populate the 1G_4 state. Since the 1G_4 state is within 3000 cm⁻¹ of the 3F_4 state, rapid deactivation via coupling to vibrational modes of C-H bonds can prevent the 1G_4 state from emitting in the near-infrared. The Tm³⁺ transition in the near-infrared at 1800 nm is too far in the near-infrared to be detected using our liquid nitrogen cooled InGaAs detector. However, in the regions that electroluminescence could be detected, other Tm³⁺ based luminescence, such as the $^3H_6 \rightarrow ^3H_5$ transition, at 1200 nm was not observed. Ho(TPP)TP in PPP-OR11 emitted a very weak emission at 1,200 nm. (Figure 3-34c) The weakness of the emission arises from the 5I_6 state rapidly relaxing to the 5I_7 state which is only 2,000 cm⁻¹ lower in energy. $^5I_7 \rightarrow ^5I_8$ is the transition from the lowest excited state which would have an emission at 2,000 nm which is far beyond the sensitivity range of our detectors.

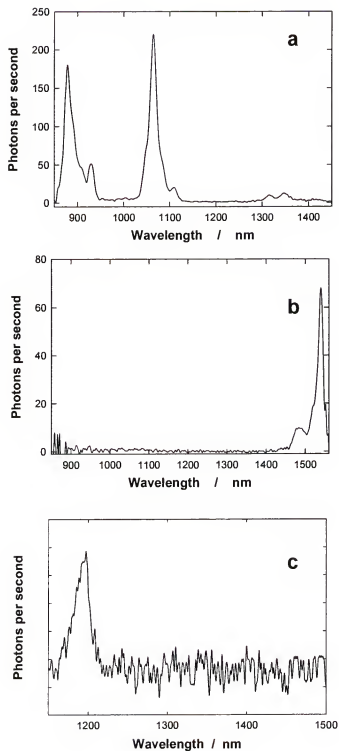


Figure 3-34. Electroluminescence of other near-infrared emitting lanthanides. a) 10 mol% Nd(TPP)TP in polystyrene at 9 V. b) 10 mol% Er(TPP)TP in polystyrene at 12 V. c) 20 mol% Ho(TPP)TP in PPP-OR11 at 9 V.

Visible Emission of Lanthanide Complexes in Polystyrene

While near-infrared electroluminescence has been the main area of interest, usually these devices emit in the visible region also. The visible electroluminescence spectra at 9 V for 1:1 weight ratio Ln(TPP)TP blended into polystyrene are shown in Figure 3-35. All four complexes show a series of emission peaks between 550 and 750 nm which come from the porphyrin dopant itself since the host does not emit. For Er(TPP)L(OEt)₃ in PS (Figure 3-35a), there are four bands observed with peak maxima occurring at 453, 617, 639, 662, and 725 nm. The peaks at 662 and 725 nm are from an impurity of free base TPP. The other peaks at 617 and 639 nm are emission from the metalloporphyrin ring, since none of the transitions correspond with Er³⁺ *f*→*f* transitions and are similar to the fluorescence observed from closed shell transition metal metalloporphyrin such as ZnTPP. The very weak emission peak at 453 nm is the S₂→S₀ transition from the porphyrin.

The electroluminescence of Ho(TPP)L(OEt)₃ in polystyrene (Figure 3-35b) shows a very different emission pattern than the other complexes with peaks at 450 nm, a shoulder at 608 nm, and 633 nm with a shoulder at 658 nm. The band at 715 nm which is found in all the other complexes is missing. The position of the band suggests metallated porphyrin fluorescence, however, the photoluminescence emission of Ho(TPP)L(OEt)₃ in this region is similar to the fluorescence of the other lanthanide porphyrins. This visible emission may be from the ⁵F₅→⁵I₈ transition of Ho³⁺ which would occur at 645 nm, which is in the same region where this new emission band occurs. Transient electroluminescence lifetime measurements should confirm if this band is lanthanide based because the lifetime would be in the microsecond timescale. Interestingly, this

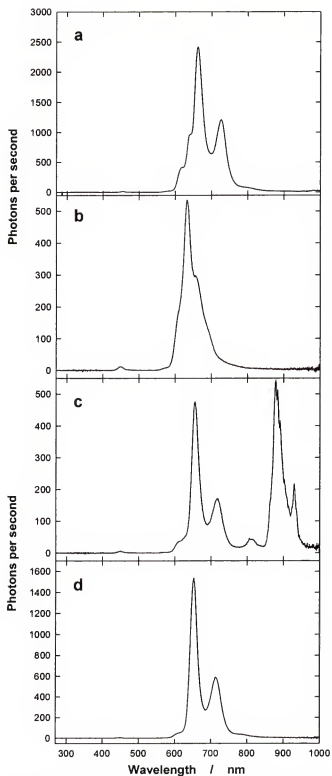


Figure 3-35. Visible EL at 9 V of 1:1 weight ratio of $\text{Ln}(\text{TPP})\text{L}(\text{OEt})_3$ in PS: a) Er^{3+} b) Ho^{3+} c) Nd^{3+} and d) Pr^{3+}

emission band is $\sim 4,000\text{ cm}^{-1}$ above the lowest energy triplet of the porphyrin. Thus, direct excitation of $\text{Ho}^{3+} {}^5\text{F}_8$ through the porphyrin's lowest energy triplet probably does not occur.

$\text{Nd}(\text{TPP})\text{L}(\text{OEt})_3$ in polystyrene (Figure 3-35c) has similar peak pattern to $\text{Er}(\text{TPP})\text{L}(\text{OEt})_3$ and $\text{Pr}(\text{TPP})\text{L}(\text{OEt})_3$ except three peaks at 814, 878, and 930 nm. These peaks correspond to the ${}^4\text{F}_{3/2} \rightarrow {}^4\text{I}_{9/2}$ transition of Nd^{3+} . This transition is split by crystal field effects for similar reasons to the splitting observed in Yb^{3+} . In this case the ${}^4\text{I}_{9/2}$ state splits into a maximum of five crystal field states of which three are clearly observed.

$\text{Pr}(\text{TPP})\text{L}(\text{OEt})_3$ in polystyrene (Figure 3-35d) has EL emission peaks at 448, 610, 653, and 718 nm. No other Pr^{3+} based emission is observed.

Dual Emitting Near-Infrared Devices

A common method of enhancing Er^{3+} emission at 1550 nm is energy transfer from Yb^{3+} .^{146,147} A device was prepared by blending 10 mol% of $\text{Yb}(\text{TPP})\text{L}(\text{OEt})_3$ and 10 mol% $\text{Er}(\text{TPP})\text{L}(\text{OEt})_3$ into PPP-OR11. The electroluminescence spectrum from the visible to near-infrared region as shown in Figure 3-36 is a composite of spectra recorded by a CCD detector (400-1100 nm) and an InGaAs detector (1000-1550 nm). The visible region consists of four peaks. The highest energy peak found at 430 nm is the weak $\text{S}_2 \rightarrow \text{S}_0$ emission from the metalloporphyrin. The next peak found at 602 nm is $\text{S}_1 \rightarrow \text{S}_0$ fluorescence from the metallated porphyrin ring. The two peaks at 649 and 719 nm are the fluorescence from a small amount of free base tetraphenylporphyrin impurity.

At 977 nm ${}^2\text{F}_{5/2} \rightarrow {}^2\text{F}_{7/2}$ emission of Yb^{3+} with an external quantum efficiency of 4.4×10^{-5} is observed. At 1520 nm the EL emission from Er^{3+} has an external quantum efficiency of 7.8×10^{-7} . These quantum efficiencies underestimate the true external

quantum efficiencies of each emitter since no attempt was made to determine the actual number of electron injected that when to each Ln(TPP) complex. This experiment suggests that Yb(TPP)TP and Er(TPP)TP act as independent emitters in the device and that energy transfer from Yb³⁺ to Er³⁺ is inefficient.

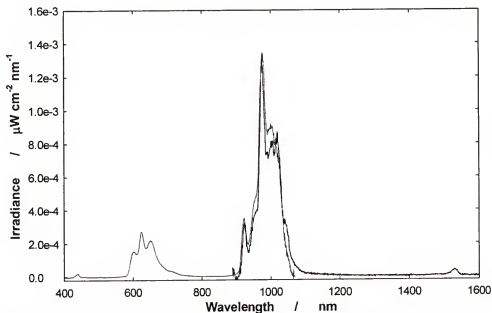


Figure 3-36. Electroluminescence of 10 mol% Yb(TPP)L(OEt)₃ and 10 mol% Er(TPP)L(OEt)₃ in PPP-OR11 at 7 V.

Discussion

To determine the internal quantum efficiencies of our near-infrared devices, the external quantum efficiency, Φ_{ext} measured can be related to the internal quantum efficiency, Φ_{int} by equation 3-1 which corrects for the fraction of photons lost due to total internal reflection within the film and therefore do not reach the detector.

$$\Phi_{int} = 2n^2 \Phi_{ext} \quad 3-1$$

Assuming a refractive index, n , of 1.6 for a PPP polymer,¹⁴⁸ the internal EL efficiencies of the Yb(TPP)L devices are tabulated in Table 3-3. The internal efficiencies are on the order of 10^{-4} to 10^{-3} for the devices containing Yb(TPP)L in PPP-OR11. This compares well with the external efficiency of 3×10^{-4} estimated for a vapor deposited Yb(DBM)₃phen device⁵⁹ and 1.5×10^{-4} reported for device consisting of a near-infrared emitting ionic dye (LDS 821) in PVK.¹⁴⁹

Table 3-3. Maximum near-infrared external and internal EL efficiencies of PPP-OR11 and Yb(TPP)L blended into PPP-OR11 or PS.

Concentration	Yb(TPP)TP External	Yb(TPP)TP Internal	Yb(TPP)L(OEt) ₃ External	Yb(TPP)L(OEt) ₃ Internal
5 mol% in PPP	5.2×10^{-5}	2.7×10^{-4}	2.9×10^{-5}	1.5×10^{-4}
10 mol% in PPP	1.8×10^{-4}	9.2×10^{-4}	3.5×10^{-5}	1.8×10^{-4}
15 mol% in PPP	1.2×10^{-4}	6.7×10^{-4}	1.6×10^{-4}	8.2×10^{-4}
10 mol% (relative to PPP) in PS	--	--	3.1×10^{-4}	1.6×10^{-3}
Visible EL Efficiency of PPP-OR11 Only: External: 1.2×10^{-3} Internal: 6.1×10^{-3}				

Equation 3-1 can be modified to calculate the fraction of useful electron and hole recombinations that occur by relating the internal quantum efficiency to the fraction of electrons and holes which recombine on the active species, η_{eh} and the photoluminescence quantum efficiency of the emitter, Φ_{PL} , as shown in equation 3-2 to give equation 3-3.

$$\Phi_{int} = \eta_{eh} \Phi_{PL} \quad 3-2$$

$$\eta_{e/h} = \frac{2n^2\Phi_{ext}}{\Phi_{PL}} \quad 3-3$$

If the photoluminescence efficiencies of the lanthanide complexes in the polymer films are similar to the values determined in solution (Table 1-6 and Table 1-7), then the fraction of electron-hole pair recombination can be calculated as reported in Table 3-4. These numbers represent the apparent fraction of electrons and holes that recombine to produce useful excited states. For PPP-OR11 due to spin statistics 75% of the electron-hole recombination events that occur on the polymer is believed to result in triplet excitons which do not contribute to light output from the device. From the table it is apparent that as the porphyrin concentration increases, the probability of useful electron-hole recombination increases.

Table 3-4. Apparent fraction of electron-hole recombination of PPP-OR11 and Yb(TPP)L blended into PPP-OR11 or PS.

Concentration	Yb(TPP)TP ($\Phi_{PL} = 3.2 \times 10^{-2}$)	Yb(TPP)L(OEt) ₃ ($\Phi_{PL} = 2.4 \times 10^{-2}$)
5 mol% in PPP	8.4×10^{-3}	6.3×10^{-3}
10 mol% in PPP	2.9×10^{-2}	7.5×10^{-3}
15 mol% in PPP	2.1×10^{-2}	3.4×10^{-2}
10 mol%(relative to PPP) in PS	--	6.7×10^{-2}

Φ_{PL} of PPP-OR11 was determined to be 0.8 in the solid state thus the fraction of charge recombination for PPP-OR11 only is 7.6×10^{-3} .

Charge injected into the active layer will probably be transported along the PPP-OR11 chains at low concentration of Yb(TPP)L. There are three possible fates of the charge while on PPP-OR11. First, the charge bridges the two electrodes and is annihilated at the opposite electrode. This is the most likely scenario because hole

transport is more rapid than electron transport in conjugated polymers. For example, the hole and electron mobilities of polyfluorene, a blue emitting conjugated polymer that is structurally similar to PPP-OR11, are approximately $10^{-4} \text{ cm}^2 \text{ V}^{-1} \text{ sec}^{-1}$ and $10^{-7} \text{ cm}^2 \text{ V}^{-1} \text{ sec}^{-1}$, respectively.¹⁵⁰ This shows that hole transport mobility in the polymer is about 1000 greater than electron mobility. Although the carrier mobilities of PPP-OR11 have not been measured for PPP-OR11, it is likely that similar results would be obtained.

Thus for PPP-OR11, the majority of holes are annihilated at the cathode before encountering an electron with the host. A second possible fate of carriers in PPP-OR11 is the charge recombines with the opposite carrier and excites the polymer, after which the exciton formed can either radiatively decay or transfers to a nearby Ln(TPP)L complex. The third scenario involves the charge being trapped by the lanthanide porphyrin complex. The Ln(TPP)L molecules are excited by direct charge trapping of the holes on Ln(TPP)L followed by electron capture and recombination on Ln(TPP)L instead of exciton formation on the host followed by energy transfer. This conclusion was drawn for EL devices involving platinum (II) 2, 3, 7, 8, 12, 13, 17, 18-octaethyl-21H, 23H-porphyrin Pt(OEP) blended into poly(9,9-dioctylfluorene) (PFO).¹⁵¹ Thus, as the concentration of Ln(TPP)L increases, more charge can be trapped by the TPP. This is observed in the turn-on voltages of devices of Yb(TPP)acac blended in MEH-PPV which increases from 4 to 5 V in 5 mol% to 20 mol% Yb(TPP)acac, respectively. This is a clear indication of charge trapping in the doped system. However, the opposite trend is observed in devices made with Yb(TPP)L blended in PPP-OR11 where the turn-on voltage decreases from 6 V to 4 V for 5 mol% and 15 mol% Yb(TPP)TP in PPP-OR11, respectively. This may simply be due to the detector sensitivity since devices

containing a large amount of Yb(TPP)TP irradiate more near-infrared output at a given voltage. Further studies using longer detector integration times may clarify this observation.

Charge hopping between lanthanide porphyrin complexes is another possibility for charge transport if the lanthanide complexes are in close proximity to each other. It has been shown for ZnTPP complexes dispersed in poly(2-vinylpyridine) that charges hop between ZnTPP complexes when the average separation between complexes is 1.1 nm.¹⁵² To estimate the spacing between lanthanide porphyrin complexes in PPP-OR11, the following equation was used:

$$\frac{1}{D} = \left[\frac{1}{\chi_{Yb} V_{Yb} + (1 - \chi_{Yb}) V_{PPP}} \right]^{\frac{1}{3}} \quad 3-4$$

where χ is the mole fraction of the molecule and V is its volume. This equation assumes a random dispersion of the Ln(TPP)L complex. Wegner determined that the interchain spacing of poly(2,5-di-n-dodecyl-1,4-phenylene) in solid films was 6.9 Å.¹⁵³ Assuming this is the radius of a sphere of a PPP-OR11 repeat unit, the volume of a PPP-OR11 repeat unit is 1375 Å³. (This is an overestimation of the true volume.) From x-ray crystallography data, the volume of Yb(TPP)TP is 3203 Å³. Therefore, at 5 and 15 mol% concentration, it is estimated that each Yb(TPP)TP molecule is separated on an average of 1.5 and 1.1 nm, respectively. Since electrochemical data of largely conjugated guest dyes suggest that charge transport would be a more significant driving force than Förster energy transfer on EL device efficiency, it is suspected that charge transport between lanthanide porphyrin complexes occurs in the 15 mol% Ln(TPP)L/PPP-OR11 devices.

Recently, the energy transfer processes of devices containing tris(2-phenylpyridine) iridium [Ir(ppy)₃] or PtOEP blended into poly[9,9'-di-*n*-hexyl-2,7-fluorene-alt-1,4-(2,5-di-*n*-hexyloxy)phenylene] (PFHP), a polymer with a similar structure to PPP-OR11, have been explored.¹⁵⁴ It was shown that PFHP readily aggregated preventing dopant molecules from being in close proximity with host molecules thereby inhibiting singlet and triplet energy transfer processes. The EL spectra of 2wt% Ir(ppy)₃ in PFHP was dominated by PFHP emission. When the Ir(ppy)₃ concentration was increased to 8 wt% EL emission from Ir(ppy)₃ dominated. In addition, TEM showed aggregates of Ir(ppy)₃ in PFHP. (Films containing 8 wt% Ir(ppy)₃ in PVK lacked such aggregates.) Thus direct charge trapping and recombination on the dye molecule was suspected.

For the 5 mol% Yb(TPP)L/PPP-OR11 device, even though the estimated separation between porphyrin molecules is greater than 1.1 nm, charge transport between lanthanide porphyrin complexes may occur due to aggregation in the film. As stated earlier, the equation used that the lanthanide porphyrin complexes are non-interacting spheres homogenous dispersed in the polymer matrix. In reality, aggregation of PPP-OR11 or Yb(TPP)L or both may play an important role in the device efficiency. At the concentrations that Yb(TPP)L is blended into PPP-OR11, it is probable that either aggregation of PPP-OR11 and Yb(TPP)L occurs (Figure 3-37). TEM images of the films could show if Yb(TPP)L is aggregated. Thus, the average distance between Yb(TPP)L may be smaller than originally estimated and charge hopping between Yb(TPP)L molecules may occur.

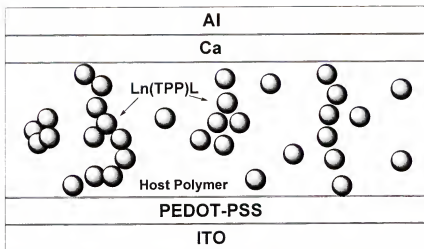


Figure 3-37. When $\text{Ln}(\text{TPP})\text{L}$ is dispersed into PPP-OR11, it may aggregate allowing charge hopping between $\text{Ln}(\text{TPP})\text{L}$ complexes to occur at lower concentrations (5 mol%) than estimated (15 mol%).

There are several examples of near-infrared emitting OLEDs known. One of the first examples of a near-infrared emitting small molecule OLED involved phthalocyanine as the active layer. Phthalocyanines are typically thought of as good hole transport materials because of their low ionization potentials. However, a device was prepared where metal-free phthalocyanine co-deposited with 4-(di-cyanomethylene)-2-methyl-6-(*p*-dimethylaminostyryl)-4H-pyran (DCM) as the active layer of a device has been shown to emit in the near-infrared at 77K.¹⁵⁵ The device possessed a broad emission from 700-1,000 nm and an operating voltage around 18 V. No EL quantum efficiency or voltage-current data was given for the device. The first example of a near-infrared emitting conjugated polymer in an electroluminescent device involved a cyano-substituted thienylene phenylene vinylene polymer. Upon applying a potential, the device emitted a broad emission from 650 - 1000 nm with a peak efficiency of 0.2% at 50 mA cm⁻². In both cases the phthalocyanine and conjugated polymer devices emit broad emission just beyond the visible region. Near-infrared lanthanide complexes offer several advantages

over purely organic materials including sharp spectral transitions and emission well beyond 1000 nm.

Several groups including ours have fabricated near-infrared OLEDs containing Nd^{3+} , Er^{3+} , Yb^{3+} ions. Some of the earliest work erbium work used the Er^{3+} analog of AlQ_3 to generate near-infrared emission at 1.5 μm at room temperature.^{135,156} These vapor-deposited devices were characterized with turn-on voltages of 12 V but possessed irreproducible electroluminescence spectra. Epstein and others prepared a device made of $\text{Er}(\text{acac})_3\text{phen}$ (phen = 1, 10-phenanthroline) blended with poly(*N*-vinylcarbazole), poly(methyl-methacrylate) or poly[2-methoxy, 5-(3',7'-dimethyl-octyloxy)]-*p*-phenylenevinylene which showed near-infrared emission from Er^{3+} at 1.54 μm with a turn-on voltage of approximately 10 V.^{157,158} Our attempts of near-infrared electroluminescent devices consisted of $\text{Er}(\text{TPP})\text{acac}$ in MEH-PPV devices which displayed near-infrared emission at 1.5 μm , similar turn-on voltages to others EL devices (~13 V) and good reproducibility. No quantitative data has yet been reported however it is expected to be low. The low quantum yield of Er^{3+} complexes, both EL and PL, is mainly attributed to rapid deactivation of the excited state by vibronic coupling to C-H bonds. To increase the EL efficiency, this fundamental problem could be lessened by moving the C-H bonds away from the lanthanide and binding the lanthanide to atoms with low vibrational bond energies. Since near-infrared emission of GaAs doped with Er^{3+} is known, the possibility exists that blending $\text{Er}:\text{GaAs}$ nanocrystals with a conjugated polymer may provide a new and more efficient methods of near-infrared electroluminescence.¹⁵⁹ A similar idea using a combination of InAs-ZnSe semiconductor

nanocrystals and conjugated polymers has been reported where a tunable near-infrared PLEDs was created which exhibit external quantum efficiencies approaching 0.5 %.¹⁶⁰

Neodymium emission has been observed by several investigators. Usually Nd-containing small molecules are vapor deposited onto ITO as the active layer. For example, a vapor deposited neodymium-containing *tris*-(8-hydroxyquinoline) complex sandwiched between ITO and Mg/Ag began emitting at the three near-infrared emissive transitions of Nd^{3+} ($^4\text{F}_{3/2} \rightarrow ^4\text{I}_{9/2}$, $^4\text{F}_{3/2} \rightarrow ^4\text{I}_{11/2}$ and $^4\text{F}_{3/2} \rightarrow ^4\text{I}_{13/2}$) when 13 V was applied.¹⁶¹ A neodymium containing near-infrared device has also been fabricated using a blend of poly(dioctylfluorene-co-benzothiadiazole) and lissamine-functionalized Nd^{3+} complex.⁵⁸ It produced a weak near-infrared emission at 850 nm which has been ascribed to the Nd^{3+} transition when a large voltage was applied (31 V). Our group has shown that near-infrared emission from Nd(TPP)TP in PPP-OR11 can be generated at little as 6 V. The improved performance of our devices is possibly due to the improved charge transporting properties of the porphyrin ligand compared to the lissamine-functionalized Nd^{3+} complex used.

Yanagida *et al.* vapor deposited Er^{3+} , Nd^{3+} , or Yb^{3+} *tris*-(dibenzoylmethanato) monobathophenanthroline complexes to prepare near-infrared devices.^{59,133} Their work is one of the few that has estimated the near-infrared efficiencies of lanthanide containing OLEDs. The quantum yields reported were based on comparisons to analogous Eu^{3+} devices with EL quantum efficiencies of 3×10^{-4} , 7×10^{-5} , and 1×10^{-6} for Yb^{3+} , Nd^{3+} , and Er^{3+} containing devices, respectively. We have been able to directly measure the Yb(TPP)L devices directly using a calibrated silicon CCD and a calibrated silicon photodiode and report near-infrared efficiencies up to 3×10^{-4} for unoptimized devices of

Yb(TPP)TP in polystyrene. (Recent work of Garry Cunningham has shown that device efficiencies up to 1.3×10^{-3} can be obtained by blending AlQ₃ with Yb(TPP)L(OEt)₃ into polystyrene.)

Conclusion

Electroluminescent devices have been prepared by blending near-infrared emitting lanthanide complexes into conjugated and non-conjugated polymer hosts. The wavelengths of near-infrared electroluminescence can be varied by changing the lanthanide metal center. In addition, mixing two different near-infrared emitters allows for greater variations in near-infrared luminescence. In general, devices prepared using lanthanide porphyrin complexes perform better in terms of near-infrared power output ($\sim 10 \mu\text{W cm}^{-2}$) and quantum efficiencies ($\sim 3 \times 10^{-4}$) than devices prepared with lanthanide *tris*- β -diketonates.¹³⁶ The comparison of devices prepared using MEH-PPV to PPP-OR11 indicates that spectral overlap between the polymer fluorescence and the dopant's absorption spectra may play an important role in device performance. Experiments with polystyrene show that charge transport along the porphyrin ring, particularly at high dopant concentrations, plays a major role in carrier transport, trapping, and recombination.

Experimental

Lanthanide *tris*- β -diketonate and tetraphenylporphyrin complexes were prepared by Tim Foley or Alison Knefley according to literature procedures.^{53,56,162} MEH-PPV was either provided by Prof S. Ramakrishnan or purchased from R. W. Sands and used as received. PPP-OR11 was synthesized by Mohammed Bouguettaya.

ITO Etching

Electroluminescent devices were prepared by masking, then etching the ITO glass (Delta Technologies, $R_s = 8-12/\square$) by exposure to aqua regia vapor. The ITO glass was first cut into 1 inch by 1 inch squares using a diamond tipped glass cutter. The ITO glass was rinsed with isopropyl alcohol to remove any fingerprints or other residual oils and then was allowed to air-dry. Scotch™ packing tape was placed over the entire piece of ITO glass. Care was taken to prevent any bubbles or ridges in the tape. Using a black marker, the areas where tape would be removed were drawn on the ITO as shown in (Figure 3-38).

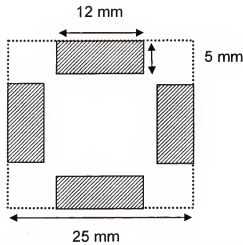


Figure 3-38. Darker areas indicated areas where ITO will be etched away when exposed to aqua regia vapors. Lighter areas represent areas masked by Scotch™ packing tape.

After marking the tape, a razor blade was used to gently cut the tape along the marked edges. A metal spatula was then used to gently remove the small rectangular pieces of tape. The remaining edges were pressed to ensure good contact between the ITO and tape. Now, the masked ITO glass was placed onto a beaker which contained a freshly prepared aqua regia (3:1 v:v HCl:HNO₃) solution. A 25 mL beaker was cut to

approximately 2 inches in height to minimize the amount of aqua regia used (~5 mL). The masked ITO was exposed to the aqua regia vapors for 6 minutes then removed. After removal, a cotton-tipped stick was wiped across the exposed area and then an ohmmeter was used to check the resistivity. There should be very high ($>1\text{M}\Omega$) resistance. If a lower resistance is measured, then the ITO was exposed for 4 additional minutes. After the ITO has been etched, the tape was removed revealing a sharp contrast between the colorless etched regions and purple unetched regions of ITO. The ITO was immediately rinsed multiple times with isopropyl alcohol to remove the dissolved ITO and aqua regia present.

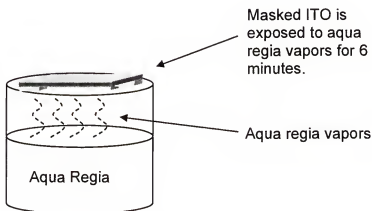


Figure 3-39. Masked ITO is suspended over aqua regia vapors for 6 minutes to etch away the exposed ITO.

Cleaning ITO

The etched ITO slide was then placed into a custom built holder for cleaning in a sonicator. The teflon holder as shown in Appendix Figure B-1 prevented multiple pieces of ITO from rubbing against one another. The ITO glass in the holder was sequentially cleaned by sonication for ten minutes in each of the following solvents: a solution of 20

mg sodium dodecyl sulfate (SDS) per 500 mL water (SDS, Fisher), Milli-Q water, acetone, and isopropyl alcohol. After rinsing the ITO glass was air-dried.

Spin Coating Hole Transport and Active Layers

PEDOT-PSS (Bayer Baytron P VP Al 4083) was used as a hole transport layer. The PEDOT-PSS was first filtered through a 0.2 micron polysulfone filter to remove any particulate matter. Approximately 0.5 mL of PEDOT-PSS was then spin-coated onto 1 inch by 1 inch squares of ITO coated SiO₂ (Delta Technologies, Product Number CG-50IN-1515) at 4000 rpm and subsequently dried in a vacuum oven at 150°C for 4 hr to remove residual water.

Solutions of desired concentration of the Ln complexes were pipetted in solutions containing 2 mg MEH-PPV or PPP-OR11 dissolved in 1 mL CHCl₃. Lanthanide complex concentrations ranged from 1 mol% to 20 mol%. The concentration (mol%) of the lanthanide complex dissolved in PPP-OR11 is based on the mole ratio of the lanthanide complex relative to the polymer repeat unit. These solutions were spin coated onto the substrate at 800 rpm.

Metal Electrode Deposition

The films were placed glass side down onto the inverted stage built for the thermal metal evaporator as shown in Figure 3-40. The stage was custom design to fit into the chamber of the Denton Vacuum DV-502A system. (Appendix Figure B-2). The ITO was then covered with a stainless steel mask with the pattern of the electrodes desired. The masked devices is then placed in the thermal metal evaporator chamber and pumped down to 10⁻⁶ torr for a minimum of 4 hours at room temperature.

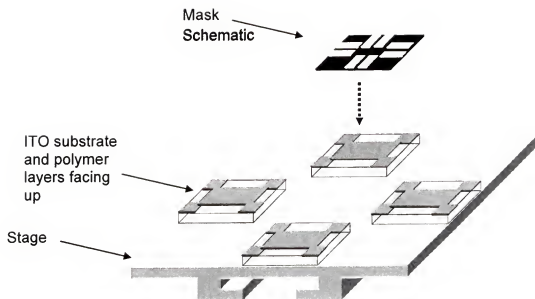


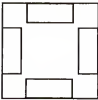

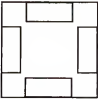

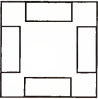

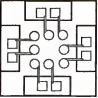
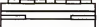


Figure 3-40. ITO coated with polymer layers are placed face up on the inverted stage for electrode deposition. A stainless steel mask is placed squarely onto the polymer film and held in place with a paper binder clip.

Calcium and aluminum layers were sequentially deposited by thermal evaporation at $1-10 \times 10^{-6}$ torr without breaking the vacuum between metal depositions. The thicknesses of the Ca and Al layers were determined to be 50 Å and 2000 Å, respectively, using an oscillating quartz crystal thickness monitor. After 30 minutes, the chamber is purged with nitrogen and the devices were encapsulated with epoxy (Loctite quick set epoxy) under an argon atmosphere in order to minimize exposure to oxygen and moisture.

The process of fabricating a device can be summarized in five steps shown in Table 3-5. After the metal deposition step, devices can be tested with or without an encapsulating layer. If an encapsulating layer is used, the epoxy covers the circular electrode and the bridge up to the square portion of the electrode.

Table 3-5. Summary of electroluminescent device fabrication.

Step	Top View	Side View
1. A clean 1 inch by 1 inch square of ITO on a glass substrate is used for etching.		
2. ITO is etched. Lighter areas indicate area where ITO was removed (See ITO Etching). The ITO is then cleaned (See Cleaning ITO).		
3. PEDOT-PSS is spin coated onto the etched ITO surface and then vacuum dried (See Spin Coating Hole Transport and Active Layers).		
4. The lanthanide/polymer blend is spin coated on top of the PEDOT-PSS layer (See Spin Coating Hole Transport and Active Layers).		
5. The metal electrodes are vapor deposited on top of the lanthanide/polymer blend (See Metal Electrode Deposition).		

Electroluminescent Device Measurements

Visible and near-infrared (up to 1100 nm) electroluminescence spectra were recorded on an ISA-SPEX Triax 180 spectrograph fitted with a liquid N₂ cooled CCD detector (EEV CCD, 1024 x 128 pixels, 400 - 1100 nm). To accomplish this a freshly prepared device was placed into the EL device holder such that electrical contact between

the vapor deposited electrodes and the gold pins of the device were made and then mounted on a stage attached to a x-y stage as shown in Figure 3-41. (See Appendix Figure B-3 and B-4 for device holder schematics.)

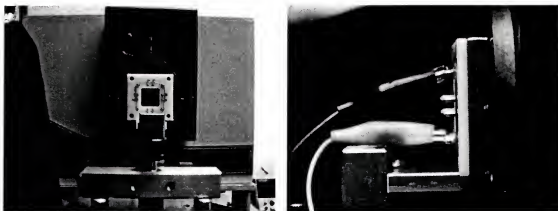


Figure 3-41. Front and side view of device holder mounted on XY stage setup for EL device measurements on the Triax 180/CCD system.

The device was placed as close as possible to the Triax 180. At this distance, the device is 4.8 cm from the entrance slit of the monochromator. Using the x-y stage, the electrode to be measured is aligned with the center of the monochromator opening. Power for electroluminescence measurements was supplied using a Keithley 228 voltage/current source. Positive bias was applied to one of the four corners of the device. Negative bias was applied to the metal electrode. A primary standard tungsten lamp was used to calibrate the CCD detector. The details of calibration and quantitative calculation of the external quantum efficiencies can be found in Appendix A. For measurements in the 1000-1550 nm region, a Fluorolog-2 fluorescence spectrophotometer (Jobin Yvon Inc.) equipped with a liquid N₂ cooled InGaAs photodiode was used. It is important that the room lights are off when using the InGaAs detector to minimize stray light. Also, an RG850 filter in the emission path helps to minimize second order scattering. For very weak signals from EL devices, the xenon lamp may need to be turned off.

CHAPTER 4 CONCLUSIONS

In the previous chapters, detailed examinations of several near-infrared emitting systems were presented. Several general conclusions and highlights from which future experiments may yield interesting results will be presented.

Near-Infrared Photoluminescence

Near-infrared emitting lanthanides complexes containing Yb^{3+} , Nd^{3+} , and Er^{3+} have been shown to photoluminescence in the near-infrared. The porphyrin ligand plays the lead role in controlling the absorption properties of the complexes while the lanthanide directs the emissive properties by accepting energy from the porphyrin ligand and generating near-infrared luminescence. In general, lanthanide tetraphenylporphyrin complexes have higher near-infrared quantum yields than their β -diketonate analogs. For example, $\text{Yb}(\text{TPP})\text{TP}$ has been shown to have a quantum yield of 3.2×10^{-2} which is ten times larger than $\text{Yb}(\text{TTFA})_3\text{phen}$ that is considered to be one of the most efficient near-infrared lanthanide *tris*- β -diketonate complexes known. This improvement in quantum efficiency may be due to the lower triplet energy of the porphyrin and the effective shielding of the axial capping ligand from water molecules. Figure 3-1 shows two proposed ligands which may improve the quantum efficiency. The first proposed ligand shown in Figure 3-1 is a tripodal amine tetrafluoronated phenol ligand which would coordinate first to zinc through the four nitrogen atoms. The remaining three oxygen

atoms would coordinate to the lanthanide and two of them would also be shared with zinc. This podand-framework would protect the lanthanide from solvent accessing the metal and should help to improve the quantum efficiency.

A general trend observed is that the quantum yields of the near-infrared photoluminescence decreases with increasing emission wavelength. This is due to the excited state energies of the lanthanide more closely matching the non-radiative vibrational modes of C-H bonds. In addition there is strong support in the literature that O-H and C-H bonds in close proximity to the lanthanide metal center result in higher non-radiative decay rates of the lanthanide excited state. One possibility to combat this problem is to bond the lanthanide to atoms with lower bond vibrational energies. The second ligand shown in Figure 3-1 is analogous to the β -diketonate ligands previously used and should coordinate in a similar manner once the nitrogen proton is removed. Replacing C=O and C-H bonds with S=O and C-F bonds should reduce the non-radiative rate via bond vibrational deactivation significantly resulting in improved photoluminescent quantum yields.

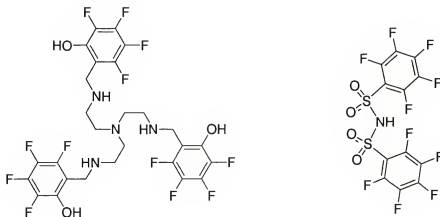


Figure 4-1. Proposed ligands for coordination to lanthanides.

Near-Infrared Electroluminescence

Near-infrared electroluminescent devices were prepared using near-infrared emitting lanthanide complexes blended into conjugated and non-conjugated polymer hosts. The near-infrared wavelength can be tuned by changing the lanthanide metal center. In addition, mixing two different near-infrared emitters allows for greater variations in near-infrared luminescence. In general, devices prepared using lanthanide porphyrin complexes perform better in terms of near-infrared power output (approximately $10 \mu\text{W cm}^{-2}$) and quantum efficiencies ($\sim 3 \times 10^{-4}$) than devices prepared with lanthanide *tris*- β -diketonates.

While photoluminescence studies of lanthanide/polymer blends suggested that Förster energy transfer was occurring, the electroluminescence data supported another dominant mechanism for charge transfer. Experiments with polystyrene show that charge transport along the porphyrin ring, particularly at high dopant concentrations, plays a major role in carrier transport, trapping, and recombination. Thus, if more efficient improvements in near-infrared output or quantum efficiency are desired, then exploring the chemistry of the lanthanide complexes may be a more productive pursuit. This could be done by changing the redox properties of the porphyrin ring and see the effect on the electroluminescence quantum efficiency.

Since the electroluminescence (EL) quantum efficiency is the product of the electron-hole recombination and the photoluminescence quantum yield, increasing either factor will improve the EL quantum efficiency. Ideas for improving the photoluminescence quantum yields were discussed either. Improving the electron-hole injection balance could be done by blending in electron transport materials such as AlQ_3 .

APPENDIX A
CALCULATION OF EXTERNAL
ELECTROLUMINESCENT QUANTUM EFFICIENCIES

This appendix outlines the experimental steps and calculations needed to quantitatively measure the energy and photon output of an electroluminescent (EL) device. Before measuring the energy output of an EL device, the responsivity of the detector must be measured.

Preparing the Detector

6. Turn on the Triax 180 Monochromater and CCD controller.
7. Start SPECTRAMAX on the computer.
8. After initialization is complete, select *Experiment* mode in the Instrument Control Center.
9. Select from the menubar, *Experiment... RTD*. This will finish the initialization of the CCD detector.
10. In the Instrument Control Center, select *Visual Instrument Setup*
11. Click on the box labeled CCD. The temperature of the CCD is shown in degrees Kelvin.
12. ***Warning! Liquid nitrogen is extremely cold. Take protective measures to prevent contact with liquid nitrogen during transfer between dewars.*** Fill the CCD dewar with approximately 1 L of liquid nitrogen to cool the CCD to 140 K. The cooling process should take 45-60 minutes.
13. Place a mercury vapor lamp along the optical axis of the Triax 180 250 cm from the entrance slit.
14. In the Real Time Display (RTD), set the following experiment parameters:

- a. Wavelength: 700 nm
 - b. Integration Time: 0.1 sec
 - c. Entrance Slit: 0.1 mm
15. Measure the spectrum of the lamp. A sharp peak at 546 ± 1 should be observed which corresponds with the 546.074 nm spectral line of mercury. If it not at the correct wavelength, see Appendix A of the SPECTRAMAX manual under the subheading *Entering Your System's Parameters* for the procedure to wavelength calibrate the detector.

Calibrating the Detector

The method developed for calibrating the CCD detector is based on a procedure in the literature.¹⁶³ A 100 W quartz tungsten halogen (QTH) lamp of known irradiance was used to determine the responsivity of the detector. The QTH lamp was purchased from The Eppley Laboratory, Inc. (Serial Number EH-156; Calibrated on September 18, 2002). The irradiance values supplied by the manufacturer are graphically displayed in Figure A-1 along with the photon irradiance plotted using the supplied data.

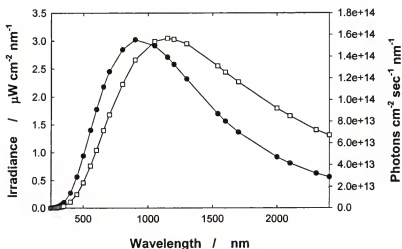


Figure A-1. Irradiance (solid circles) at 50 cm from the detector of a 100 W QTH (S/N: EH-156) calibrated on September 18, 2002. Photon irradiance (open squares) was calculated using the irradiance values and equation A-1.

To convert the irradiance values, $E_0(\lambda)$, supplied by the manufacturer to photonic units, $NP(\lambda)$, equation A-1 was used.

$$NP(\lambda) = \frac{E_0(\lambda)\lambda}{hc} \quad \text{A-1}$$

16. Place the QTH Lamp 250 cm along the optical axis from the entrance slit. Note: NIST and Eppley Laboratory recommend the lamp be placed 50 cm from the detector. Because of the extremely sensitive nature of the detector, this distance is too small and will saturate the detector. Moving the lamp to 250 cm will decrease the lamp intensity by 1/25 according to the inverse square law.
17. Place a 1% transmittance filter to further attenuate the lamp intensity. The fraction of light transmitted by the filter is shown in Figure A-2.

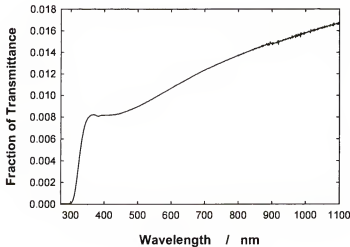


Figure A-2. Fractional transmittance of 1% neutral density filter.

18. In the Experiment Setup, set the following experiment parameters:
 - a. Wavelength: 700 nm
 - b. Integration Time: 0.1 sec

c. Entrance Slit: 0.1 mm

19. Collect the emission spectrum of the 100 W QTH Lamp. An example of the lamp intensity is shown in Figure A-3.

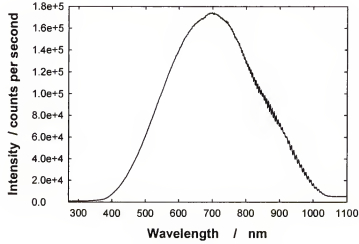


Figure A-3. Raw data collected by the CCD detector of 100 W QTH Lamp placed 250 cm away from 0.1 mm entrance slit width of monochromator. A 1% transmittance filter was placed immediately before the entrance slit.

Placing the lamp at 250 cm from the entrance slit and a 1% transmittance filter between the lamp and entrance slit attenuates the lamp irradiance. Therefore, the energy, $E(\lambda)$ entering the entrance slit can be calculated using equation A-2, where A is the area of the entrance slit, d_0 is 50 cm, d is the distance from the lamp to the entrance slit, $F(\lambda)$ is the fraction transmittance of the neutral density filter, and $E_0(\lambda)$ is the irradiance of the 100 W QTH lamp.

$$E(\lambda) = A \left(\frac{d_0}{d} \right)^2 F(\lambda) E_0(\lambda) \quad \text{A-2}$$

The responsivity, $S(\lambda)$ of the detector can be found using equation A-3 where $E(\lambda)$ is the irradiance of the lamp and $I(\lambda)$ is the response of the detector. The responsivities of the CCD detector in $\mu\text{watts count}^{-1}$ and $\text{photons sec}^{-1} \text{count}^{-1}$ are shown in Figure A-4.

$$S(\lambda) = \frac{E(\lambda)}{I(\lambda)} \quad \text{A-3}$$

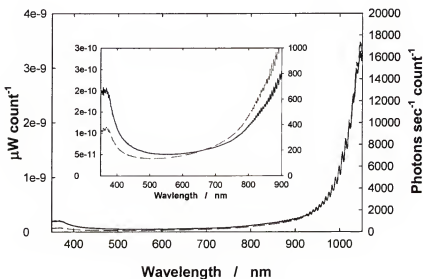


Figure A-4. Correction factors for ISA-SPEX Triax 180 spectrograph equipped with a liquid N_2 cooled CCD detector (Hamamatsu CCD, 1024x64 pixel, 400-1100nm). Correction factors for power (solid line) and photon density (dashed line) are shown.

Measuring the Irradiance of an Electroluminescent Device

1. Place the device in the device holder flush against the external cover of the monochromator entrance slit. This corresponds to 4.8 cm from the entrance slit of the Triax 180.
2. Center the emitting electrode at the entrance slit of the Triax 180.
3. Attach the positive electrode from the power supply to the contact that connects with ITO.
4. Attach the negative electrode from the power supply to the contact that contacts the metal electrode.

5. Cover the device with a black cloth to minimize stray light.
6. Apply the desired voltage.
7. Record the emission spectrum using the following experimental parameters:
 - a. Wavelength: 700 nm
 - b. Entrance Slit: 0.2 mm
 - c. Integration Time: 0.1, 1.0, or 10.0 sec depending on the expected intensity of the EL device.

Assuming the EL device emits isotropically, the irradiance should be equal at all points along a hemispherical distance from the EL device.¹⁶⁴ (A hemisphere is used rather than a sphere because it is assumed that no light is emitted from the backside of the device.) In reality only a small portion of the EL device emission is collected by the detector. This is accounted for by determining the fraction of the sphere sampled by the detector.

Placing the device a distance, r , (4.8 cm as mention in step 1) from the slit, the fraction of light collected by an entrance slit with an area, A_{slit} , of 0.02 cm^2 is 1.38×10^{-4}

$$\text{Fraction of Light Collected} = \frac{A_{\text{slit}}}{2\pi r^2} \quad \text{A-4}$$

The radiant power of the EL device, $P(\lambda)$ can be determined by equation A-5.

$$P(\lambda) = \frac{2\pi r^2}{A_{\text{slit}}} S(\lambda) I(\lambda) \quad \text{A-5}$$

The total power output of the device, P , can be calculated by integrating the radiant power as shown in equation A-6

$$P = \frac{2\pi r^2}{A_{dir}} \int S(\lambda) I(\lambda) d\lambda \quad \text{A-6}$$

The irradiance of the device, E , (commonly reported in units of $\mu\text{W cm}^{-2}$ or mW cm^{-2}) can then be calculated by dividing the total power measured by the physical area of the EL device, A_d (Equation A-7). (For a circular electrode of 0.3 cm in diameter, the area is 0.0707 cm^2 .)

$$E = \frac{P}{A_d} \quad \text{A-7}$$

Electroluminescence Quantum Efficiency

By definition, the external electroluminescence quantum efficiency, Φ_{EL} is the number of photons emitted by the device, NP , divided by the total number of electrons injected (Equation A-8) where J is the current in amps and C is the charge of an electron ($1.602 \times 10^{-19} \text{C}$).

$$\Phi_{EL} = \frac{NP}{J/C} \quad \text{A-8}$$

The number of photons emitted can be calculated using the radiant power of the device. Thus, the number of photons, NP , emitted by the device can be calculated using equation A-9.

$$NP = \frac{2\pi r^2}{A_{slit}} \int \frac{S(\lambda)I(\lambda)\lambda}{hc} \quad \text{A-9}$$

APPENDIX B
DRAWINGS

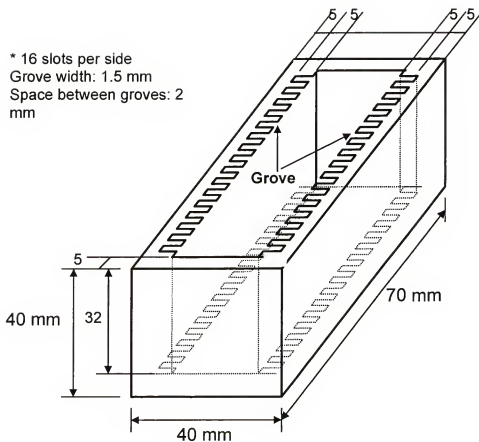


Figure B-1. Dimensions of a Teflon holder for ITO glass during cleaning. The holder was made of five separate sides held together by screws. The groves were 1.5 mm wide (width enough to accommodate the ITO glass). There was 5 mm of Teflon between each grove.

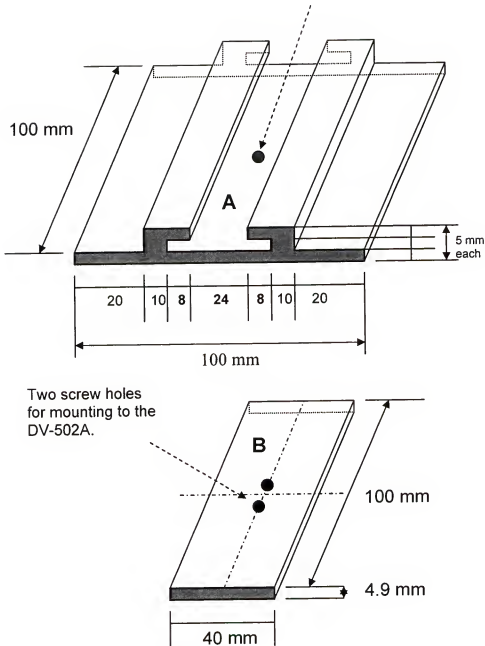


Figure B-2. Mounting stage for metal vapor deposition. All pieces are made of aluminum. Part B is attached to the two mounting screws in the DV-502A. Part A will slide over Part B. (Note: Overtime It has been found that these two pieces start stick together. Making Part B out of Teflon might alleviate the problem.)

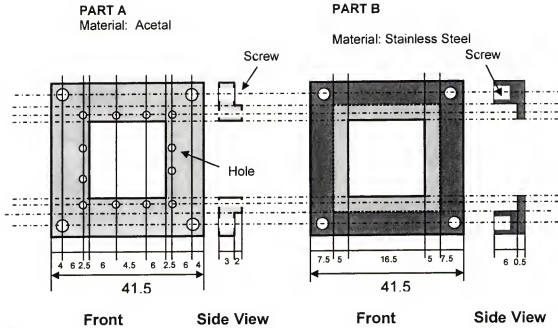


Figure B-3. Drawing of EL device holder. In each hole of part A, receptacles (Interconnect Devices, Inc.; Part Number 300106-000-5000, Description: R-SS-100-WW .420) and gold contact pins (Interconnect Devices, Inc.; Part Number 100165-003-952, Description: GSS-3-3.8-G S/C W/Hole) were used.

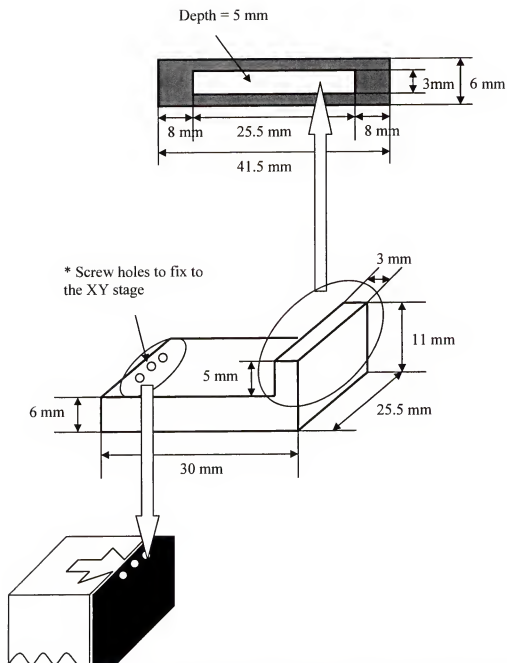


Figure B-4. Mount for device holder to XY stage. A 5 mm groove is made into the device holder in Figure B-3 as shown at the top of this figure. The mount was made of aluminum.

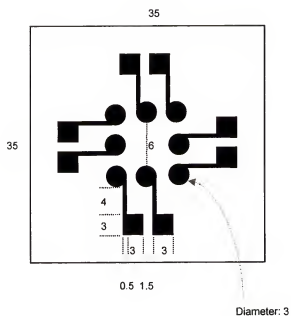


Figure B-5. Mask for metal deposition of electrodes. The mask is made of stainless steel and is 1 mm thick. All dimensions are in millimeters.

APPENDIX C

ELECTROLUMINESCENT DATA PROCESSING

Because of the large amount of data produced while characterizing the electroluminescent devices prepared, an Excel workbook was prepared to expedite the data processing portion of electroluminescent device analysis. In order to use this workbook, the user must have the data in sequentially numbered files in the ASCII format. The Excel file, ELCalculator.xls, contains seven worksheets: RawDataExtract, Table Summary, Radiance Integrator, Photon Integrator, Radiance Data, Photon Data, Correction Factors. In addition to the worksheets, three macros were prepared to automatic the data extraction and processing.

Using the RawDataExtract worksheet, the user enters the directory where the files can be found. (Data that the user must supply is blue in color.) Next, any file name text that remains constant which precedes the incrementing variable is included. The start and ending numbers are next entered. Finally, any constant text and filename extensions after the incrementing numbers are entered in their respective boxes. Once everything is entered, the user simply presses the Step 1 box.

Step 1 runs the macro labeled *DataExtractor*. This macro extracts the data from the file and places it into the excel spreadsheet eventually making a single X and many Y table of raw data. (See Worksheet: RawDataExtract for an example. The macro then generates the equations for multiplying the raw data by two different correction factors

which are found on worksheet *CorrectionFactors*. The calibrated radiance and photon data can be found on worksheets labeled *RadianceData* and *PhotonData*, respectively.

Step 2 runs the macro labeled *DataExtractorIntegrator*. Numerical integration of the data is done using Simpson's Rule. Simpson's rule can be used for approximating the area under the curve within a given interval [a,b] as shown in equation C-1. This method requires an even number, n, of evenly spaced intervals, Δx . Examples of the numerical integration are shown in worksheets *Radiance Integrator* and *Photon Integrator*. The total area of the entire spectrum is also shown on the worksheet.

$$\int_a^b f(x)dx \approx \frac{\Delta x}{3} [f(x_0) + 4(f(x_{n-1}) + 2f(x_n) + 2 \sum_{k=1}^{n/2-1} 2f(x_{2k-1}) + f(x_{2k}))] \quad \text{C-1}$$

Step 3 compiles the data into a table by running the macro *TableSummary*. This table has the most commonly used values for data analysis including irradiance and external electroluminescence efficiency. (The user must enter in the rows labeled voltage and current their data to complete efficiency data.) The visible radiance and electroluminescence efficiency cover the spectral region from 350 to 850 nm. The near-infrared radiance and efficiency encompass the spectral region from 800-1050 nm.

Worksheet: RawDataExtract

Example

			15Yb4-4	15Yb4-5	15Yb4-6
		273.08	-0.2	0.7	1.6
Location		273.91	0.4	0.9	3.0
c:\user2002\101102\		274.75	0.0	0.8	2.0
		275.59	0.1	0.9	3.4
Example		276.42	0.6	0.6	2.8
d:\usr\bsh\030101\		277.26	0.2	0.5	3.6
\\ccdc\clusr\bsh\030101\		278.09	-0.2	0.6	1.8
		278.93	-0.2	1.0	2.8
Filename Before Numbers		279.77	0.1	0.7	2.6
15Yb4-		280.6	0.3	0.4	3.2
		281.44	0.3	0.9	1.6
Beginning Number		282.27	0.1	0.8	2.4
	4	283.11	0.5	0.9	2.6
		283.94	0.3	0.5	2.8
Ending Number		284.78	0.5	0.8	2.0
	11	285.62	-0.1	1.1	1.2
		286.45	0.1	1.2	2.4
After Numbers (leave blank if nothing)		287.29	0.0	0.7	1.4
		288.12	0.1	0.9	2.0
		288.96	0.2	0.9	2.2
Extension		289.79	0.3	0.9	2.0
prn		290.63	0.4	0.6	2.2
		291.47	0.1	0.8	2.2
		292.3	0.3	0.9	2.4
		293.14	0.1	0.3	1.8
		293.97	0.1	0.8	2.4
		294.81	0.3	0.9	2.2
Number of Data Points		295.65	-0.2	0.7	1.6
	1024	296.48	0.5	0.8	1.4
Number of Data Sets		297.32	0.3	0.5	2.2
		298.15	-0.2	0.7	1.6
Step 1. Click Here to Extract the Data		298.99	0.2	0.5	2.0
		299.82	0.6	0.4	2.0
		300.66	0.3	0.8	1.6
Step 2. Click Here to Integrate the Data		301.5	-0.3	0.5	1.4
		302.33	0.2	0.7	2.0
		303.17	0.1	0.5	1.4
		304	0.1	0.6	1.4
Step 3. Click Here to Create a Table Summary of the Data		304.84	0.2	0.9	1.6
		305.67	0.1	0.8	1.8
		306.51	0.2	0.3	1.4
		307.35	0.3	0.9	2.2

Worksheet: Radiance Data

Example

			15Yb4-4	15Yb4-5	15Yb4-6
		273.08	-5.6E-09	-2.8E-09	1.41E-12
THIS DATA IS IN		273.91	4.01E-10	0	2.81E-09
RADIANCE UNITS		274.75	-5.6E-10	-2.8E-10	1.12E-09
		275.59	-2.6E-10	0	4.73E-09
		276.42	1.24E-09	-9.3E-10	3.71E-09
uW cm-2 nm-1		277.26	2.97E-14	-1.2E-09	5.93E-09
		278.09	-1.3E-09	-1E-09	6.69E-10
		278.93	-1.4E-09	3.49E-10	4.19E-09
		279.77	-3.5E-10	-6.9E-10	3.46E-09
		280.6	3.74E-10	-1.9E-09	5.98E-09

Worksheet: Photon Data

Example

			15Yb4-4	15Yb4-5	15Yb4-6
		273.08	-7719.6	-3860.19	1.929996
		273.91	550.479	0	3853.435
		274.75	-771.211	-385.625	1542.885
		275.59	-363.278	0	6539.535
		276.42	1711.461	-1283.64	5134.811
Photons cm-2 sec-1 nm-1		277.26	0.04121	-1648.4	8241.991
		278.09	-1865.47	-1399.22	933.2464
		278.93	-1954.43	488.6308	5864.059
		279.77	-484.968	-970.081	4850.163
		280.6	525.7382	-2628.43	8411.495

Worksheet: Radiance Integrator

Formula: ='Radiance Data'!B2+4*'Radiance Data'!B3+'Radiance Data'!B4

Delta x: =C3-C2

Example

Formula	0	273.08	-4.6E-09	-3.1E-09	1.23E-08
Delta x	0.83	273.91			
		274.75	-3.8E-10	-1.2E-09	2.38E-08
	Total	275.59			
Col 1	0.0962	276.42	-1E-10	-6.7E-09	2.81E-08
Col 2	0.4745	277.26			
Col 3	1.1146	278.09	-7.3E-09	-3E-10	2.09E-08
		278.93			
		279.77	1.56E-09	-8.2E-09	2.74E-08
		280.6			

Worksheet: Photon Integrator

Formula: ='Photon Data'!B2+4*'Photon Data'!B3+'Photon Data'!B4

Delta x: =C3-C2

Example

Formula	0	273.08	-6288.89	-4245.81	16958.56
Delta x	0.83	273.91			
		274.75	-512.864	-1669.26	32835.84
	Total	275.59			
Col 1	4.74E+11	276.42	-153.841	-9276.45	39036.02
Col 2	2.33E+12	277.26			
Col 3	4.50E+12	278.09	-10168.1	-414.774	29239.64
		278.93			
		279.77	2195.292	-11483.8	38496.14
		280.6			

Worksheet: Correction Factors

Example

Energy Correction	nm	$\mu\text{W cm}^{-2} \text{ sr}^{-1} \text{ sec}^{-1}$ count-1	Photon Correction	nm	photons $\text{cm}^{-2} \text{ count}^{-1}$ $\text{sr}^{-1} \text{ sec}^{-1}$
Factor for CCD	272.27	1.40991E-08	Factor for CCD	272.27	1.93E+04
	273.1	2.00448E-09	Factor	273.1	2.75E+03
to Convert	273.94	2.79991E-09	to Convert	273.94	3.86E+03
Counts/sec	274.77	2.6299E-09	Counts/sec	274.77	3.63E+03
into	275.61	3.08778E-09	into	275.61	4.28E+03
$\mu\text{W cm}^{-2} \text{ sec}^{-1}$	276.44	2.96508E-09	photons $\text{cm}^{-2} \text{ sec}^{-1}$	276.44	4.12E+03
	277.28	3.34553E-09		277.28	4.66E+03
	278.11	3.49461E-09		278.11	4.89E+03
Assuming	278.95	3.45932E-09	Assuming	278.95	4.85E+03
device area of	279.78	3.73718E-09	device area of	279.78	5.26E+03
0.0707 cm^2	280.62	4.09147E-09	0.0707 cm^2	280.62	5.77E+03
	281.45	4.09493E-09		281.45	5.79E+03
Slit of 1 $\text{cm} \times 0.02 \text{cm}$	282.29	4.45258E-09	Slit of 1 $\text{cm} \times 0.02 \text{cm}$	282.29	6.32E+03
	283.13	4.55924E-09		283.13	6.49E+03
These Correction	283.96	4.85186E-09	These Correction	283.96	6.93E+03
Factors were lasted	284.8	4.9187E-09	Factors were lasted	284.8	7.04E+03
changed	285.63	5.00163E-09	changed	285.63	7.18E+03
10/10/2002	286.47	5.48351E-09	10/10/2002	286.47	7.90E+03
	287.3	5.75494E-09		287.3	8.31E+03
	288.14	5.85676E-09		288.14	8.49E+03
	288.97	6.08041E-09		288.97	8.83E+03
	289.81	6.44134E-09		289.81	9.39E+03
	290.65	6.91394E-09		290.65	1.01E+04
	291.48	7.11838E-09		291.48	1.04E+04
	292.32	7.43535E-09		292.32	1.09E+04
	293.15	8.10093E-09		293.15	1.19E+04

Worksheet: Table Summary

Example

File Name	15Yb4-4	15Yb4-5	15Yb4-6
Voltage (V)	4	5	6
Current (mA)	1.11	2.6	6.1
Current Density (mA cm ⁻²)	15.70014	36.77511	86.28006
Electron Density (electrons cm ⁻²)	9.8E+16	2.3E+17	5.39E+17
Visible Radiance (uW cm ⁻²)	0.001309	0.00768	0.024096
Visible Photon Density (photons cm ⁻² s ⁻¹)	2.92E+10	1.68E+11	5.21E+11
Visible Q.E.	2.98E-07	7.32E-07	9.68E-07
NIR Radiance (uW cm ⁻²)	0.094919	0.466921	1.090591
NIR Photon Density (photons cm ⁻² s ⁻¹)	2.95E+12	1.45E+13	3.39E+13
NIR Q.E.	3.01E-05	6.32E-05	6.29E-05
Visible Power Efficiency	2.08E-08	4.18E-08	4.65E-08
NIR Power Efficiency	1.51E-06	2.54E-06	2.11E-06
Total Irradiance (uW cm ⁻²)	0.09621	0.474526	1.11457
Total Photon Density (uW cm ⁻² sr ⁻¹)	2.98E+12	1.47E+13	3.44E+13
Total Q.E.	3.04E-05	6.39E-05	6.39E-05
Total Power Efficiency	0.001532	0.002581	0.002153

Macro: DataExtractor

```

Sub DataExtractor()
'
' Data Extractor
' Macro written 3/14/2001 by Benjamin Harrison
'

    i = Range("A14")
    Directory = Range("A4")
    Filename = Range("A11")
    Afters = Range("A20")
    extension = Range("A23")

    For i = Range("A17") To Range("A14") + 1 Step -1
        filelocation = Directory & Filename & i & Afters & "." & extension

        With ActiveSheet.QueryTables.Add(Connection:= _
            "TEXT;" & filelocation, Destination:=Range("C2"))
            .TextFileColumnDataTypes = Array(9, 1)
            .Refresh BackgroundQuery:=False
            Range("C1") = Filename & i & Afters
        End With

        Next i

        i = Range("A14")
        filelocation = Directory & Filename & i & Afters & "." & extension
        With ActiveSheet.QueryTables.Add(Connection:= _
            "TEXT;" & filelocation, Destination:=Range("C2"))
            .Refresh BackgroundQuery:=False
            Range("D1") = Filename & i & Afters
        End With

        Range("C1026") = Null 'removes the character at the end of the first column
                               'this assumes there is only 1024 points of data

        Range("A30") = "=COUNT(R2C4:R2000C4)"
        Range("A32") = "=COUNT(R2C4:R2000C21)/COUNT(R2C4:R2000C4)"

        Let datapoints = Sheets("RawDataExtract").Range("A30") + 1
        Let datasets = Sheets("RawDataExtract").Range("A32")

    For PL Data

```

```

Sheets("RawDataExtract").Select
Range("C2", "C" & datapoints).Select
Selection.Copy
Sheets("Photon Data").Select
Range("C2").Select
ActiveSheet.Paste

```

```

Sheets("RawDataExtract").Select
Range(Cells(1, 4), Cells(1, datasets + 3)).Copy
Sheets("Photon Data").Select
Range(Cells(1, 4), Cells(1, datasets + 3)).PasteSpecial

```

```

For J = 1 To datasets
    Cells(2, J + 3).FormulaR1C1 = "=(RawDataExtract!RC-
RawDataExtract!R40C)*Correction Factors!RC8" 'Added baseline correction 2/19/03
Next J
    Range(Cells(2, 4), Cells(2, datasets + 3)).Copy
    Range(Cells(2, 4), Cells(datapoints, datasets + 3)).PasteSpecial

```

'For EL Data

```

Sheets("RawDataExtract").Select
Range("C2", "C" & datapoints).Select
Selection.Copy
Sheets("Radiance Data").Select
Range("C2").Select
ActiveSheet.Paste

```

```

Sheets("RawDataExtract").Select
Range(Cells(1, 4), Cells(1, datasets + 3)).Copy
Sheets("Radiance Data").Select
Range(Cells(1, 4), Cells(1, datasets + 3)).PasteSpecial

```

```

For J = 1 To datasets
    Cells(2, J + 3).FormulaR1C1 = "=(RawDataExtract!RC-
RawDataExtract!R40C)*Correction Factors!RC4" 'Added baseline correction 2/19/03
Next J
    Range(Cells(2, 4), Cells(2, datasets + 3)).Copy
    Range(Cells(2, 4), Cells(datapoints, datasets + 3)).PasteSpecial
    Sheets("RawDataExtract").Select
End Sub

```

Macro: DataExtractorIntegrator

```

Sub DataExtractorIntegrator()
'
' Data Extractor
' Macro written 10/10/2002 by Benjamin Harrison
'
Let datapoints = Sheets("RawDataExtract").Range("A30") + 1
Let datasets = Sheets("RawDataExtract").Range("A32")

Sheets("Radiance Data").Select
Range("C2", "C" & datapoints).Select
Selection.Copy
Sheets("Radiance Integrator").Select
Range("C2").Select
ActiveSheet.Paste

Sheets("Radiance Integrator").Range("B2").Select
Selection.Copy
Range(Cells(2, 4), Cells(2, datasets + 3)).Select
Range(Cells(2, 4), Cells(2, datasets + 3)).PasteSpecial
Range(Cells(2, 4), Cells(3, datasets + 3)).Copy
Range(Cells(2, 4), Cells(datapoints, datasets + 3)).PasteSpecial

Sheets("Photon Data").Select
Range("C2", "C" & datapoints).Select
Selection.Copy
Sheets("Photon Integrator").Select
Range("C2").Select
ActiveSheet.Paste

Sheets("Photon Integrator").Range("B2").Select
Selection.Copy
Range(Cells(2, 4), Cells(2, datasets + 3)).Select
Range(Cells(2, 4), Cells(2, datasets + 3)).PasteSpecial
Range(Cells(2, 4), Cells(3, datasets + 3)).Copy
Range(Cells(2, 4), Cells(datapoints, datasets + 3)).PasteSpecial

Sheets("RawDataExtract").Select

End Sub

```

Macro: TableSummary

```

Sub TableSummary()
'
' Table Summary()
' Macro written 10/10/2002 by Benjamin Harrison
'
Let datapoints = Sheets("RawDataExtract").Range("A30") + 1
Let datasets = Sheets("RawDataExtract").Range("A32")

Sheets("Table Summary").Select

Range("B3").Formula = "=Radiance Data!D1"
Range("B6").Formula = "=B5/0.0707"
Range("B7").Formula = "=0.001*B6/1.602176e-19"
Range("B8").Formula = "=SUM('Radiance Integrator'!D96:D694)*('Radiance Integrator'!$B$3/3)"
Range("B9").Formula = "=2*3.1415*SUM('Photon Integrator'!D96:D694)*('Photon Integrator'!$B$3/3)"
Range("B10").Formula = "=B9/B7"

Range("B11").Formula = "=SUM('Radiance Integrator'!D694:D1024)*('Radiance Integrator'!$B$3/3)"
Range("B12").Formula = "=2*3.1415*SUM('Photon Integrator'!D694:D1024)*('Photon Integrator'!$B$3/3)"
Range("B13").Formula = "=B12/B7"

Range("B16").Formula = "=(0.001*B8)/(B4*B6)"
Range("B17").Formula = "=(0.001*B11)/(B4*B6)"

Range("B20").Formula = "=SUM('Radiance Integrator'!D2:D1024)*('Radiance Integrator'!$B$3/3)"
Range("B21").Formula = "=2*3.1415*SUM('Photon Integrator'!D2:D1024)*('Photon Integrator'!$B$3/3)"
Range("B22").Formula = "=B21/B7"
Range("B23").Formula = "=B20/(B6*B4)"

Range("B3").Copy
Range(Cells(3, 2), Cells(3, datasets + 1)).PasteSpecial

Range("B6:B23").Copy

```

```
Range(Cells(6, 3), Cells(23, datasets + 1)).PasteSpecial
```

```
'Formats Table with Color
```

```
'Yellow for File Name
```

```
Range(Cells(3, 1), Cells(3, datasets + 1)).Select
```

```
With Selection.Interior
```

```
.ColorIndex = 6
```

```
.Pattern = xlSolid
```

```
.PatternColorIndex = xlAutomatic
```

```
End With
```

```
With Selection.Font
```

```
.Name = "Arial"
```

```
.FontStyle = "Bold"
```

```
End With
```

```
'Blue for user data to be entered
```

```
Range(Cells(4, 1), Cells(5, datasets + 1)).Select
```

```
With Selection.Interior
```

```
.ColorIndex = 37
```

```
.Pattern = xlSolid
```

```
.PatternColorIndex = xlAutomatic
```

```
End With
```

```
'Grey and White for Data
```

```
For x = 6 To 22 Step 2
```

```
Range(Cells(x, 1), Cells(x, datasets + 1)).Select
```

```
With Selection.Interior
```

```
.ColorIndex = 15
```

```
.Pattern = xlSolid
```

```
.PatternColorIndex = xlAutomatic
```

```
End With
```

```
Next x
```

```
'Put Grids Around
```

```
Range(Cells(3, 1), Cells(23, datasets + 1)).Select
```

```
Selection.Borders(xlDiagonalDown).LineStyle = xlNone
```

```
Selection.Borders(xlDiagonalUp).LineStyle = xlNone
```

```
With Selection.Borders(xlEdgeLeft)
```

```
.LineStyle = xlContinuous
```

```
.Weight = xlThin
```

```
.ColorIndex = xlAutomatic
```

```
End With
```

```
With Selection.Borders(xlEdgeTop)
    .LineStyle = xlContinuous
    .Weight = xlThin
    .ColorIndex = xlAutomatic
End With
With Selection.Borders(xlEdgeBottom)
    .LineStyle = xlContinuous
    .Weight = xlThin
    .ColorIndex = xlAutomatic
End With
With Selection.Borders(xlEdgeRight)
    .LineStyle = xlContinuous
    .Weight = xlThin
    .ColorIndex = xlAutomatic
End With
With Selection.Borders(xlInsideVertical)
    .LineStyle = xlContinuous
    .Weight = xlThin
    .ColorIndex = xlAutomatic
End With
With Selection.Borders(xlInsideHorizontal)
    .LineStyle = xlContinuous
    .Weight = xlThin
    .ColorIndex = xlAutomatic
End With

End Sub
```

LIST OF REFERENCES

1. Dieke, G. H. *Spectra and Energy Levels of Rare Earth Ions in Crystals*; Interscience: New York, 1968.
2. France, P. W. In *Fluoride Glass Optical Fibers*; France, P. W., Ed.; CRC Press: Boca Raton, FL, 1990, pp 132-185.
3. Görrler-Walrand, C.; Binnemans, K. In *Handbook on the Physics and Chemistry of Rare Earths*; Gschneidner, K. A., Eyring, L., Eds.; Elsevier North-Holland: New York, 1998; Vol. 25, pp 101-262.
4. Weissman, S. I. "Intramolecular Energy Transfer. The Fluorescence of Complexes of Europium" *J. Chem. Phys.* **1942**, *10*, 214-217.
5. de Sa, G. F.; Malta, O. L.; Donega, C. D.; Simas, A. M.; Longo, R. L.; Santa-Cruz, P. A.; da Silva, E. F. "Spectroscopic Properties and Design of Highly Luminescent Lanthanide Coordination Complexes" *Coord. Chem. Rev.* **2000**, *196*, 165-195.
6. Veiopoulou, C. J.; Lianidou, E. S.; Ioannou, P. C.; Efstathiou, C. E. "Comparative Study of Fluorescent Ternary Terbium Complexes. Application in Enzyme Amplified Fluorimetric Immunoassay for Alpha-Fetoprotein" *Anal. Chim. Acta* **1996**, *335*, 177-184.
7. Gao, X. C.; Cao, H.; Huang, C. H.; Umitani, S.; Chen, G. Q.; Jiang, P. "Photoluminescence and Electroluminescence of a Series of Terbium Complexes" *Synth. Met.* **1999**, *99*, 127-132.
8. Edwards, A.; Claude, C.; Sokolik, I.; Chu, T. Y.; Okamoto, Y.; Dorsinville, R. "Photoluminescence and electroluminescence of new lanthanide-(methoxybenzoyl)benzoate complexes" *J. Appl. Phys.* **1997**, *82*, 1841-1846.
9. Meshhova, S. B.; Topilova, Z. M.; Bolshoy, D. V.; Belyukova, S. V.; Tsvirko, M. P.; Venchikov, V. Y. "Quantum Efficiency of the Luminescence of Ytterbium(III) beta-Diketonates" *Acta Physica Polonica A* **1999**, *95*, 983-990.
10. Tsvirko, M. P.; Meshhova, S. B.; Venchikov, V. Y.; Bolshoy, D. V. "Determination of Contributions of Various Molecular Groups to Nonradiative Deactivation of Electronic Excitation Energy in beta-Diketonate Complexes of Ytterbium(III)" *Opt. Spec.* **1999**, *90*, 669-673.

11. Voloshin, A. I.; Sahavaleev, N. M.; Kazakov, V. P. "Luminescence of Praseodymium (III) Chelates from Two Excited States (3P_0 and 1D_2) and its Dependence on Ligand Triplet State Energy" *Journal of Luminescence* **2001**, *93*, 199-204.
12. Yanagida, S.; Hasegawa, Y.; Murakoshi, K.; Wada, Y.; Nakashima, N.; Yamanaka, T. "Strategies for Enhancing Photoluminescence of Nd(III) in Liquid Media" *Coord. Chem. Rev.* **1998**, *171*, 461-480.
13. Yanagida, S.; Hasegawa, Y.; Iwamuro, M.; Kawamura, Y.; Wada, Y. "Luminescence of Neodymium(III) in Organic Media: Ligand Designs for the Remarkable Luminescence and Their Evolution" *J Syn Org Chem Jpn* **2000**, *58*, 945-955.
14. Vögtle, F.; Gorka, M.; Vincelli, V.; Ceroni, P.; Maestri, M.; Balzani, V. "A Dendritic Antenna for Near-Infrared Emission of Nd(III) Ions" *Chem. Phys. Chem.* **2001**, *2*, 769-773.
15. Vicinelli, V.; Ceroni, P.; Maestri, M.; Balzani, V.; Gorka, M.; Vögtle, F. "Luminescence Lanthanide Ions Hosted in a Fluorescent Polylysin Dendrimer. Antenna-Like Sensitization of Visible and Near-Infrared Emission" *J. Am. Chem. Soc.* **2002**, *124*, 6461-6488.
16. Hebbink, G. A.; Reinhoudt, D. N.; van Veggel, F. C. J. M. "Increased Luminescent Lifetimes of Ln(III) Complexes Emitting in the Near-Infrared as a Result of Deuteration" *Eur. J. Org. Chem.* **2001**, 4101-4106.
17. Klink, S. I.; Alink, P. O.; Grave, L.; Peters, F. G. A.; Hofstraet, J. W.; Geurts, F.; van Veggel, F. C. J. M. "Fluorescent Dyes as Efficient Photosensitizers for Near-infrared Nd(III) Emission" *Perkin Trans. 2* **2001**, 363-372.
18. Klink, S. I.; Hebbink, G. A.; Grave, L.; Peters, F. G. A.; van Veggel, F. C. J. M.; Reinhoudt, D. N.; Hofstraet, J. W. "Near-Infrared and Visible Luminescence from Terphenyl-Based Lanthanide(III) Complexes Bearing Amido and Sulfonamido Pendant Arms" *Eur. J. Org. Chem.* **2000**, *10*, 1923-1931.
19. Klink, S. I.; Keizer, H.; Hofstraet, H. W.; van Veggel, F. C. J. M. "Transition Metal Complexes as a New Class of Photosensitizers for Near-Infrared Lanthanide Luminescence" *Synth. Met.* **2002**, *127*, 213-216.
20. Klink, S. I.; Grave, L.; Reinhoudt, D. N.; van Veggel, F. C. J. M.; Werts, M. H.; Geurts, F. A. J.; Hofstraet, J. W. "A Systematic Study of the Photophysical Processes in Polydentate Triphenylene-Functionalized Eu(III), Tb(III), Nd(III), Yb(III), and Er(III) Complexes" *J. Phys. Chem. A* **2000**, *104*, 5457-5468.

21. Wolbers, M. P. O.; van Veggel, F. C. J. M.; Peters, F. G. A.; van Beelen, E. S. E.; Hofstraat, J. W.; Geurts, F.; Reinhoudt, D. N. "Sensitized Near-Infrared Emission from Nd(III) and Er(III) Complexes of Fluorescein-Bearing Calix[4]arene Cages" *Chem. Eur. J.* **1998**, *4*, 772-780.
22. Hofstraat, J. W.; Wolbers, M. P. O.; van Veggel, F. C. J. M.; Reinhoudt, D. N.; Werts, M. H.; Verhoeven, J. W. "Near-IR Luminescence Rare Earth Ion-Sensitizer Complexes" *J. Fluorescence* **1998**, *8*, 301-308.
23. Sato, S.; Shinkai, S. "Energy-Transfer Luminescence of Lanthanide Ions Encapsulated in Sensitizer-Modified Calix[N]Arenes" *Perkin Trans. 2* **1993**, 621-624.
24. Shevchuk, S. V.; Rusakova, N. V.; Turianskaya, A. M.; Korovin, Y.; Nazarenko, N. A.; Gren, A. I.; Shapiro, Y. E. "Novel Ytterbium Complexes of Two Calix[4]resorcinarenes" *Anal. Commun.* **1997**, *34*, 201-203.
25. Shevchuk, S. V.; Rusakova, N.; Turianskaya, A. M.; Korovin, Y.; Nazarenko, N. A.; Gren, A. I. "Infrared Luminescence of Ytterbium Ion in Complexes with Calix[4]resorcinarenes" *J. Fluorescence* **1998**, *8*, 225-228.
26. Shevchuk, S. V.; Rusakova, N. V.; Turianskaya, A. M.; Korovin, Y. V.; Nazarenko, N. A.; Gren, A. I. "Luminescence of Neodymium Ion in Complexes with Calix [4] resorcinarenes" *Asian. J. Spec.* **2000**, *3*, 155-160.
27. Korovin, Y.; Rusakova, N. "Infrared 4f-luminescence of Lanthanides in the Complexes with Macrocyclic Ligands" *Rev. Inorg. Chem.* **2001**, *21*, 299-329.
28. Korovin, Y. U.; Shevchuk, S. V.; Bacherikov, V. A.; Rusakova, N. V.; Alexeeva, E. A.; Gren, A. I. "Sensitization of Infrared Luminescence of Neodymium and Ytterbium Ions in Binuclear Complexes with 4-tert-Butylcalix[8]arene" *Russ. J. Inorg. Chem* **2000**, *45*, 1383-1387.
29. Dickens, R. S.; Aime, S.; Batsanov, A. S.; Beeby, A.; Botta, M.; Bruce, J.; Howard, J. A. K.; Love, C. S.; Parker, D.; Peacock, R. D.; Puschmann, H. "Structural, Luminescence, and NMR Studies of the Reversible Binding of Acetate, Lactate, Citrate, and Selected Amino Acids to Chiral Diaqua Ytterbium, Gadolinium, and Europium Complexes" *Journal of the American Chemical Society* **2002**, *124*, 12697-12705.
30. Beeby, A.; Faulkner, S.; Parker, D.; Williams, J. A. G. "Sensitized luminescence from phenanthridine appended lanthanide complexes: analysis of triplet mediated energy transfer processes in terbium, europium and neodymium complexes" *Perkins Trans. 2* **2001**, 1268-1273.

31. Beeby, A.; Dickins, R. S.; Fitzgerald, S.; Govenlock, L. J.; Maupin, C. L.; Parker, D.; Riehl, J. P.; Siligardi, G.; Williams, J. A. G. "Porphyrin Sensitization of Circularly Polarised Near-IR Lanthanide Luminescence. Enhanced Emission with Nucleic Acid Binding" *Chem. Comm.* **2000**, 1183-1184.
32. Beeby, A.; Dickins, R. S.; Faulkner, S.; Parker, D.; Williams, J. A. G. "Luminescence from ytterbium(III) and its complexes in solution" *Chem Commun* **1997**, 1401-1402.
33. Beeby, A.; Clarkson, I. M.; Dickins, R. S.; Faulkner, S.; Parker, D.; Royle, L.; de Sousa, A. S.; Williams, J. A. G.; Woods, M. "Non-radiative deactivation of the excited states of europium, terbium and ytterbium complexes by proximate energy-matched OH, NH and CH oscillators: an improved luminescence method for establishing solution hydration states" *Perkin Trans. 2* **1999**, 493-503.
34. Batsanov, A. S.; Beeby, A.; Bruce, J. I.; Howard, J. A. K.; Kenwright, A. M.; Parker, D. "Direct NMR and luminescence observation of water exchange at cationic ytterbium and europium centres" *Chem Commun* **1999**, 1011-1012.
35. Horrocks, W. D.; Wong, C. P. "Lanthanide Porphyrin Complexes: Evaluation of Nuclear Magnetic Resonance Dipolar Probe and Shift-Reagent Capabilities" *J. Am. Chem. Soc.* **1976**, 98, 7157-7162.
36. Gouterman, M.; Schumaker, C. D.; Srivastava, T. S.; Yonetani, T. "Absorption and Luminescence of Yttrium and Lanthanide Octaethylporphyrin Complexes" *Chem. Phys. Lett.* **1976**, 40, 456-461.
37. Korovin, Y.; Zhilina, Z.; Rusakova, N.; Kuz'min, V.; Vodzinsky, S.; Ishkov, Y. "Spectral-Luminescent Effects in Heterometallic Complexes of Crown-Porphyrins" *J. Porphyrins Phthalocyanines* **2001**, 5, 481-485.
38. Pyatossin, V. E.; Tsvirko, M. P.; Solovov, K. N.; Kachura, T. F. "Laser Photophysics of Complexes of Etioporphyrin I with Rare-Earth Elements" *Zh. Prikl. Spekt.* **1981**, 35, 268-271.
39. Pyatossin, V. E.; Tsvirko, M. P.; Solovov, K. N.; Kachura, T. F. "Study of the Photophysics of Complexes of Porphyrins with the Lanthanides by Nanosecond Absorption Spectroscopy" *Opt Spektrosk* **1982**, 52, 269-275.
40. Tsvirko, M. P.; Soloviev, K. N.; Piskarskas, A. S.; Pyatossin, V. E.; Krasauskas, V. V.; Kachura, T. F. "Pico-Second Kinetics of Intramolecular Energy-Transfer in Porphyrin Complexes of Rare-Earth Elements" *Dokl Akad Nauk SSSR* **1984**, 279, 1118-1122.

41. Tsvirko, M. P.; Stelmakh, G. F.; Pyatosin, V. E.; Solovyov, K. N.; Kachura, T. F.; Piskarskas, A. S.; Gadonas, R. A. "Fast Electronic Relaxation in Lanthanide Porphyrins" *Chem. Phys.* **1986**, *106*, 467-476.
42. Solovev, K. N.; Tsvirko, M. P.; Pyatosin, V. E.; Kachura, T. F. "Studying the Mechanism of Photophysical Processes in Complexes of Rare-Earth Elements by Methods of Luminescence and Kinetic Absorption-Spectroscopy" *Izv an Sssr Fiz+* **1982**, *46*, 242-248.
43. Solovev, K. N.; Tsvirko, M. P.; Kachura, T. F. "Intramolecular Energy Migration in Complexes of Lanthanides with Porphyrins" *Opt Spektrosk+* **1976**, *40*, 684-690.
44. Shushkevich, I. K.; Dvornikov, S. S.; Kachura, T. F.; Solovev, K. N. "Spectral Luminescence Properties of Porphyrin Complexes of Neodymium and Ytterbium" *Zh. Prik. Spek.* **1981**, *35*, 647-653.
45. An, Y.; Schramm, G. E.; Berry, M. T. "Ligand-to-Metal Charge-Transfer Quenching of the Eu(III) (3D_1) State in Europium-Doped tris(2,2,6,6-tetramethyl-3,5-heptanedionato)Gadolinium (III)" *J. Lumin.* **2002**, *97*, 7-12.
46. Wong, C. P.; Venteicher, R.; Horrocks, W. D. "Lanthanide Porphyrin Complexes - Potential New Class of Nuclear Magnetic-Resonance Dipolar Probe" *J. Am. Chem. Soc.* **1974**, *96*, 7149-7150.
47. Wong, C. P. In *Inorg. Syn.*, 1983; Vol. 22, p 156.
48. Spyroulias, G. A.; de Montauzon, D.; Maisonat, A.; Poilblanc, R.; Coutsolelos, A. G. "Synthesis, UV-visible and electrochemical studies of lipophilic and hydrophilic lanthanide(III) bis(porphyrinates)" *Inorg. Chem. Acta* **1998**, *276*, 182-191.
49. Spyroulias, G. A.; Coutsolelos, A. G.; Raptopoulou, C. P.; Terzis, A. "Synthesis, Characterization, and X-Ray Study of a Heteroleptic Samarium(III) Porphyrin Double-Decker Complex" *Inorg. Chem.* **1995**, *34*, 2476-2479.
50. Jiang, J. Z.; Mak, T. C. W.; Ng, D. K. P. "Isolation and Spectroscopic Characterization of Heteroleptic, Anionic and Neutral (phthalocyaninato)(tetra-4-pyridylporphyrinato)lanthanide(III) Double-deckers" *Chem. Ber.* **1996**, *129*, 933-936.
51. Schaverien, C. J. "Octaethylporphyrin-Yttrium-Methyl Chemistry: Preparation and Selective Activation of Dioxygen by (OEP)Y(Mu-Me)₂AlMe₂" *Chem. Comm.* **1991**, 458-460.

52. Schaverien, C. J.; Orpen, A. G. "Chemistry of (Octaethylporphyrinato)Lutetium and (Octaethylporphyrinato)Yttrium Complexes - Synthesis and Reactivity of (Oep)Mx Derivatives and the Selective Activation of O₂ by (Oep)Y(Mu-Me)₂alme₂" *Inorg. Chem.* **1991**, *30*, 4968-4978.
53. Wong, W. K.; Hou, A. X.; Guo, J. P.; He, H. S.; Zhang, L. L.; Wong, W. Y.; Li, K. F.; Cheah, K. W.; Xue, F.; Mak, T. C. W. "Synthesis, Structure and Near-infrared Luminescence of Neutral 3d-4f Bi-metallic Monoporphyrinate Complexes" *Dalton Trans.* **2001**, 3092-3098.
54. Wong, W. K.; Zhang, L.; Xue, F.; Mak, T. C. W. "Synthesis, Characterization and Crystal Structures of Neutral Mono- and Di-nuclear Lanthanide(III) Porphyrinate Complexes" *Dalton Trans.* **1999**, 3053-3062.
55. Wong, W. K.; Zhang, L. L.; Wong, W. T.; Xue, F.; Mak, T. C. W. "Synthesis and Crystal Structures of Cationic Lanthanide(III) Monoporphyrinate Complexes" *Dalton Trans.* **1999**, 615-622.
56. Foley, T. J.; Abboud, K. A.; Boncella, J. M. "Synthesis of Ln(III) Chloride Tetraphenylporphyrin Complexes" *Inorg. Chem.* **2002**, *41*, 1704-1706.
57. Harrison, B. S.; Foley, T. J.; Bouguettaya, M.; Boncella, J. M.; Reynolds, J. R.; Schanze, K. S.; Shim, J.; Holloway, P. H.; Padmanaban, G.; Ramakrishnan, S. "Near-infrared Electroluminescence from Conjugated Polymer/lanthanide Porphyrin Blends" *Appl. Phys. Lett.* **2001**, *79*, 3770-3772.
58. Slooff, L. H.; Polman, A.; Cacialli, F.; Friend, R. H.; Hebbink, G. A.; van Veggel, F. C. J. M.; Reinhoudt, D. N. "Near-Infrared Electroluminescence of Polymer Light-Emitting Diodes Doped with a Lissamine-Sensitized Nd(III) Complex" *Appl. Phys. Lett.* **2001**, *78*, 2122-2124.
59. Kawamura, Y.; Wada, Y.; Yanagida, S. "Near-Infrared Photoluminescence and Electroluminescence of Neodymium(III), Erbium(III), and Ytterbium(III) complexes" *Jpn. J. Appl. Phys.* **2001**, *40*, 350-356.
60. Hong, Z. R.; Liang, C. J.; Li, R. G.; Zang, F. X.; Fan, D.; Li, W. L.; Hung, L. S.; Lee, S. T. "Infrared and visible emission from organic electroluminescent devices based on praseodymium complex" *Appl. Phys. Lett.* **2001**, *79*, 1942-1944.
61. Henry, C. M. "Noninvasive Glucose Monitoring" *C & E News* **2002**, *80*, 41-43.
62. Burmeister, J. J.; Arnold, M. A.; Small, G. W. "Noninvasive Blood Glucose Measurements by Near-infrared Transmission Spectroscopy Across Human Tongues" *Diabetes Technology & Therapeutics* **2000**, *2*, 5-16.

63. Zhang, L.; Small, G. W.; Arnold, M. A. "Calibration Standardization Algorithm for Partial Least-Squares Regression: Application to the Determination of Physiological Levels of Glucose by Near-Infrared Spectroscopy." *Anal. Chem.* **2002**, *74*, 4097-4108.
64. Boyer, A. E.; Lipowska, M.; Zen, J. M.; Patonay, G.; Tsang, V. C. W. "Evaluation of Near Infrared Dyes as Labels for Immunoassays Utilizing Laser Diode Detection: Development of Near Infrared Dye Immunoassay (NIRDIA)" *Anal. Lett.* **1992**, *25*, 415-428.
65. Daneshvar, M. I.; Peralta, J. M.; Casay, G. A.; Narayanan, N.; Evans, L.; Patonay, G.; Strekowski, L. "Detection of Biomolecules in the Near-Infrared Spectral Region via a Fiber-Optic Immunosensor" *Immun. Meth.* **1999**, *226*, 119-128.
66. Chien, J. C. W. "Correlation of Electronic Spectra of Metalloporphyrins and Metalloproteins" *J. Am. Chem. Soc.* **1978**, *100*, 1310-1313.
67. Gouterman, M. In *The Porphyrins*; Dolphin, D., Ed.; Academic Press: New York, 1978; Vol. 3, pp 1-169.
68. Crosby, G. A.; Kasha, M. "Intramolecular Energy Transfer in Ytterbium Organic Chelates" *Spectrochim. Acta* **1958**, *10*, 377-382.
69. Asano-Someda, M.; Kaizu, Y. "Hot bands of (f, f*) emission from ytterbium(III) porphyrins in solution" *J. Photochem. Photobiol. A* **2001**, *139*, 161-165.
70. Auzel, F. "A Relationship for Crystal Field Strength Along the Lanthanide Series; Application to the Prediction of the ($^2F_{7/2}$) Yb(III) Maximum Splitting" *Opt. Mater.* **2002**, *19*, 89-94.
71. Goldner, P.; Pelle, F.; Meichenin, D.; Auzel, F. "Cooperative Luminescence in Ytterbium-doped CsCdBr₃" *J. Lumin.* **1997**, *71*.
72. Quimby, D. J.; Longo, F. "Luminescence Studies on Several Tetra-arylporphyrins and their Zinc Derivatives" *J. Am. Chem. Soc.* **1975**, *97*, 5111-5117.
73. Kaizu, Y.; Asano, M.; Kobayashi, H. "Dual Fluorescence from Two Erbium (III) Porphyrins" *J. Phys. Chem.* **1986**, *90*, 3906-3910.
74. Bajema, L.; Gouterman, M.; Rose, C. B. "Porphyrins 23. Fluorescence of Second Excited Singlet and Qasiline Structure of Zinc Tetrabenzporphrin" *J. Mol. Spectrosc.* **1971**, *39*, 421-.
75. Zaleski, I. E.; Kotlo, V. N.; Sevchenko, A. N.; Solovov, K. N.; Shkirman, S. F. "Polarization of Fluorescence due to Transitions from Upper Excited-Levels" *Dokl Akad. Nauk SSSR* **1974**, *218*, 324-327.

76. Tsvirko, M. P.; Stelmakh, G. F.; Pyatosin, V. E.; Solovyov, K. N.; Kachura, T. F. "Fluorescence from Upper Pi-Pi-Star Electronic States of Lanthanide-Porphyrin Complexes" *Chem. Phys. Lett.* **1980**, *73*, 80-83.
77. Siebrand, W. "Radiationless Transitions in Polyatomic Molecules I. Calculation of Franck-Condon Factors" *J. Chem. Phys.* **1967**, *46*, 440.
78. Pekkarinen, L.; Linschitz, H. "Studies on Metastable States of Porphyrins. II. Spectra and Decay Kinetics of Tetraphenylporphine, Zinc Tetraphenylporphine and Bacteriochlorophyll" *J. Am. Chem. Soc.* **1960**, *82*, 2407-2411.
79. Horrocks, W. D.; Bolendar, P. J.; Smith, W. D.; Supkowski, R. M. "Photosensitized Near Infrared Luminescence of Ytterbium(III) in Proteins and Complexes Occurs via an Internal Redox Process" *J. Am. Chem. Soc.* **1997**, *119*, 5972-5973.
80. Wang, Y. S.; Schanze, K. S. "Photochemical Probes of Intramolecular Electron and Energy-Transfer" *Chem. Phys.* **1993**, *176*, 305-319.
81. Fox, R. B.; Price, T. R.; Cozzens, R. F.; Echols, W. H. "Photophysical Processes in Polymers. VII. Electronic Energy Migration and Trapping in Alternating Copolymers" *Macromolecules* **1974**, *7*, 937-941.
82. Guillet, J. *Polymer Photophysics and Photochemistry: An Introduction to the Study of Photoprocesses in Macromolecules*; Cambridge University Press: Cambridge, U. K., 1987.
83. Miao, Y.-J.; Bazan, G. C. "Photophysics of Main-chain Polychromophores by Acyclic Diene Metathesis Polymerization" *Macromolecules* **1997**, *30*, 7414-7418.
84. Bazan, G. C.; Miao, Y.-J.; Renak, M. L.; Sun, B. J. "Fluorescence Quantum Yield of Poly(p-phenylenevinylene) Prepared via the Paracyclophene Route: Effect of Chain Length and Interchain Contacts" *J. Am. Chem. Soc.* **1996**, *118*, 2618-2624.
85. Peng, K.-Y.; Chen, S.-A.; Fann, W.-S. "Efficient Light Harvesting by Sequential Energy Transfer across Aggregates in Polymers of Finite Conjugational Segments with Short Aliphatic Linkages" *J. Am. Chem. Soc.* **2001**, *123*, 11388-11397.
86. Jenekhe, S. A.; Osaheni, J. A. "Excimers and Exciplexes of Conjugated Polymers" *Science* **1994**, *265*, 765-768.
87. Nguyen, T.-Q.; Doan, V.; Schwartz, B. J. "Conjugated Polymer Aggregates in Solution: Control of Interchain Interactions" *J. Chem. Phys.* **1999**, *110*, 4068-4078.

88. Blatchford, J. W.; Gustafson, T. L.; Epstein, A. J.; Vanden Bout, D. A.; Kerimo, J.; Higgins, D. A.; Barbara, P. F.; Fu, D.-K.; Swager, T. M.; MacDiarmid, A. G. "Spatially and Temporally Resolved Emission from Aggregates in Conjugated Polymers" *Phys. Rev. B* **1996**, *54*, R3683-R3686.
89. Blatchford, J. W.; Jessen, S. W.; Lin, L.-B.; Gustafson, T. L.; Fu, D.-K.; Wang, H.-L.; Swager, T. M.; MacDiarmid, A. G.; Epstein, A. J. "Photoluminescence in Pyridine-based Polymers: Role of Aggregates" *Phys. Rev. B* **1996**, *54*, 9180-9189.
90. Halkyard, C. E.; Rampey, M. E.; Kloppenburg, L.; Studer-Martinez, S. L.; Bunz, U. H. F. "Evidence of Aggregate Formation of 2,5-Dialkyl(p-phenyleneethynylene)s in Solution and Thin Films" *Macromolecules* **1998**, *31*, 8655-8659.
91. Lemmer, U.; Heun, S.; Mahrt, R. F.; Scherf, U.; Hopmeier, M.; Siegner, U.; Göbel, E. O.; Müllen, K.; Bässler, H. "Aggregate Fluorescence in Conjugated Polymers" *Chem. Phys. Lett.* **1995**, *240*, 373-378.
92. Köhler, A.; Grüner, J.; Friend, R. H.; Müllen, K.; Scherf, U. "Photocurrent Measurements on Aggregates in Ladder-Type Poly(p-phenylene)" *Chem. Phys. Lett.* **1995**, *243*, 456-461.
93. Brunner, K.; van Haare, J. A. E. H.; Langeveld-Voss, B. M. W.; Schoo, H. F. M.; Hofstra, J. W.; van Dijken, A. "Mechanistic Study of Excitation Energy Transfer in Dye-Doped PPV Polymers" *J. Phys. Chem. B*, **2002**, *106*, 6834-6841.
94. Halls, J. J. M.; Pichler, K.; Friend, R. H.; Moratti, S. C.; Holmes, A. B. "Exciton Dissociation at a Poly(p-phenylenevinylene) C-60 Heterojunction" *Synth. Met.* **1996**, *77*, 277-280.
95. Levitsky, I. A.; Kim, J.; Swager, T. M. "Energy Migration in a Poly(phenylene ethynylene): Determination of Interpolymer Transport in Anisotropic Langmuir-Blodgett Films" *J. Am. Chem. Soc.* **1999**, *121*, 1466-1472.
96. Virgili, T.; Lidzey, D. G.; Bradley, D. D. "Efficient Energy Transfer from Blue to Red in Tetraphenylporphyrin-Doped Poly(9,9-dioctylfluorene) Light-Emitting Diodes" *Adv. Mater.* **2000**, *12*, 58-62.
97. McGehee, M. D.; Bergstedt, T.; Zhang, C.; Saab, A. P.; O'Regan, M. B.; Bazan, G. C.; Srdanov, V. I.; Heeger, A. J. "Narrow Bandwidth Luminescence from Blends with Energy Transfer from Semiconducting Conjugated Polymers to Europium Complexes" *Adv. Mater.* **1999**, *11*, 1349-1354.
98. Vahlenkamp, T.; Wegner, G. "Poly(2,5-Dialkoxy-p-phenylene)s - Synthesis and Properties" *Macromol. Chem. Phys.* **1994**, *195*, 1933-1952.

99. Child, A. D.; Sankaran, B.; Larmat, F.; Reynolds, J. R. "Charge-carrier Evolution in Electrically Conducting Substituted Polymers Containing Diheterocycle p-Phenylene Repeat Units" *Macromolecules* **1995**, *28*, 6571-6578.
100. Balanda, P. B. In *Department of Chemistry*; University of Florida:Gainesville, 1997, p 243.
101. Miniscalco, W. J. In *Rare Earth Doped Fiber Lasers and Amplifiers*; Dignonnet, M. J. F., Ed.; Marcel Dekker, Inc.: New York, 1993, pp 48-50.
102. Förster, T. "Zwischenmolekulare Energiewanderung und Fluoreszenz" *Ann. Phys.* **1948**, *2*, 55.
103. Morgado, J.; Cacialli, F.; Iqbal, R.; Moratti, S. C.; Holmes, A. B.; Yahsioglu, G.; Milgrom, L. R.; Friend, R. H. "Forster Energy Transfer and Control of the Luminescence in Blends of an Orange-Emitting Poly(p-phenylenevinylene) and a Red-Emitting Tetraphenylporphyrin" *J. Mater. Chem.* **2001**, *11*.
104. Destriau, G.; Ivey, H. F. In *Proceedings IRE*, 1955; Vol. 43, pp 1911-1940.
105. Destriau, G. *J. Chim. Phys.* **1936**, *33*, 587.
106. Helfrich, W.; Schneider, W. G. "Recombination Radiation in Anthracene Crystals" *Phys. Rev. Lett.* **1965**, *17*, 229-231.
107. Pope, M.; Magnante, P.; Kallmann, H. P. "Electroluminescence in Organic Crystals" *J. Chem. Phys.* **1963**, *38*, 2042.
108. Tang, C. W.; Van Slyke, S. A. "Organic Electroluminescence Diodes" *Appl. Phys. Lett.* **1987**, *51*, 913-915.
109. Burroughes, J. H.; Bradley, D. D.; Brown, A. R.; Marks, R. N.; Mackay, K.; Friend, R. H.; Burns, P. L.; Holmes, A. B. "Light-Emitting-Diodes Based on Conjugated Polymers" *Nature* **1990**, *347*, 539-541.
110. Cao, Y.; Parker, I. D.; Yu, G.; Zhang, C.; Heeger, A. J. "Improved Quantum Efficiency for Electroluminescence in Semiconducting Polymers" *Nature* **1998**, *397*, 414-417.
111. Friend, R. H.; Gymer, R. W.; Holmes, A. B.; Burroughes, J. H.; Marks, R. N.; Taliani, C.; Bradley, D. D. C.; Dos Santos, D. A.; Bredas, J. L.; Logdlund, M.; Salaneck, W. R. "Electroluminescence in conjugated polymers" *Nature* **1999**, *397*, 121-128.
112. Dodabalapur, A. "Organic Light Emitting Diodes" *Solid State Commun.* **1997**, *102*, 259.

113. Braun, D.; Heeger, A. J. "Visible-Light Emission From Semiconduction Polymer Diodes" *Appl. Phys. Lett.* **1991**, *58*, 1982-1984.
114. Burn, P. L.; Kraft, A.; Baigent, D. R.; Baigent, D. R.; Bradley, D. D. C.; Brown, A. R.; Friend, R. H.; Gymer, D. A.; Holmes, A. B.; Jackson, R. W. J. "Chemical tuning of the electronic properties of poly(p-phenylenevinylene)-based copolymers" *J. Am. Chem. Soc.* **1993**, *115*, 10117-10124.
115. Burn, P. L.; Bradley, D. D. C.; Friend, R. H.; Halliday, D. A.; Holmes, A. B.; Jackson, R. W.; Kraft, A. "Precursor Route Chemistry and Electronic-Properties of Poly(p-phenylene-vinylene), Poly[(2,5-dimethyl-p-phenylene)vinylene] and Poly[(2,5-dimethoxy-p-phenylene)vinylene]" *Perkin Trans. I* **1992**, 3225-3231.
116. Greenham, N. C.; Moratti, S. C.; Bradley, D. D. C.; Friend, R. H.; Holmes, A. B. "Efficient Light-Emitting-Diodes Based on Polymers with High Electron-Affinities" *Nature* **1993**, *365*, 628-630.
117. Grem, G.; Leditzky, G.; Ullrich, B.; Leising, G. "Blue Electroluminescent Device Based on a Conjugated Polymer" *Synth. Met.* **1992**, *51*, 383-389.
118. Grem, G.; Leditzky, G.; Ullrich, B.; Leising, G. "Realization of a Blue-Light-Emitting Device Using Poly(para-phenylene)" *Adv. Mater.* **1992**, *4*, 36-37.
119. Scherf, U.; List, E. J. W. "Semiconducting Polyfluorenes--Towards Reliable Structure--Property Relationships" *Adv. Mater.* **2002**, *14*, 477-487.
120. Bernanose, A.; Compte, M.; Vouaux, P. *J. Chim. Phys.* **1953**, *50*, 64.
121. Kaneto, K.; Yoshino, K.; Kao, K.; Inuishi, Y. "Electroluminescence in Polyethylene Terphthalate" *Jpn. J. Appl. Phys.* **1974**, *13*, 1023-1024.
122. Wang, D. K.; Hong, Z., Y.; Ma, D. G.; Zhao, X. J.; Wang, L. X.; Lu, S.; Minami, N.; Takada, N.; Ichino, Y.; Yase, K.; Jing, X. B.; Wang, F. S. "Luminescence Enhancement by Blending PVK with Blue PPV Copolymer" *Synth. Met.* **1999**, *102*, 1132-1134.
123. Förster, T. *Discuss. Faraday Soc.* **1959**, *27*, 7.
124. Dogariu, A.; Gupta, R.; Heeger, A. J.; Wang, H. "Time-Resolved Forster Energy Transfer in Polymer Blends" *Synth. Met.* **1999**, *100*, 95-100.
125. Barigelletti, F.; Flamigni, L. "Photoactive Molecular Wires Based on Metal Complexes" *Chem. Soc. Rev.* **2000**, *29*, 1-12.

126. Furue, M.; Yoshida, T.; Nozakura, S.; Kamachi, M. "Intramolecular Energy-Transfer in Covalently Linked Polypyridine Ruthenium(II)/Osmium(II) Binuclear Complexes- Ru(II)(Bpy)MeBpy-(CH₂)_N-MeBpyOs(II)(Bpy)₂ (N=2, 3, 5, and 7)" *Bull. Chem. Soc. Jpn.* **1991**, *64*, 1632-1640.
127. Gholamkhash, B.; Nozaki, K.; Ohno, T. "Evaluation of Electronic Interaction in Matrix Elements for Photoinduced Electron Transfer Processes within Mixed-Valence Complexes" *J. Phys. Chem. B* **1997**, *101*, 9010-9021.
128. Krishnan, C. S. S.; Pamidighantam, R.; Tan, W.-S. *Proceedings of SPIE Optical Wireless Communications IV* **2001**, 104.
129. Tanaka, Y.; Tomioka, K.; Takano, M.; Nakagawa, M. "Wireless CATV Uplink System with Subcarrier Modulation Using Infrared Communications for Apartment Houses" *IEICE Transactions on Communications* **2001**, *E84B(12)*, 3235-3242.
130. Porumb, G. G.; Sterian, A. G.; Spulber, O.; Piscureanu, M. C. *Proceedings of SPIE ROMOPTO 2000 - Sixth Conference on Optics* **2000**, 674.
131. Wemara, L.; Kaoru, S.; Yuxiao, X.; Huangcong, X. *Proceedings of SPIE Optical Sensing, Imaging, and Manipulation for Biological and Biomedical Applications* **2000**, 34.
132. Liddiard, K. C. *Proceedings of SPIE Infrared Technology and Applications XXVI* **2000**, 119.
133. Kawamura, Y.; Wada, Y.; Iwamuro, M.; Kitamura, T.; Yanagida, S. "Near-infrared Electroluminescence from Ytterbium(III) Complex" *Chem Lett* **2000**, 280-281.
134. Hong, Z. R.; Liang, C. J.; Li, R. G.; Zhao, D.; Fan, D.; Li, W. L. "Infrared Electroluminescence of Ytterbium Complexes in Organic Light Emitting Diodes" *Thin Solid Films* **2001**, *391*, 122-125.
135. Curry, R. J.; Gillian, W. P. "Infra-red and Visible Electroluminescence from ErQ based OLEDs" *Synth. Met.* **2000**, *111-112*, 35-38.
136. Kang, T.-S.; Harrison, B. S.; Bouguettaya, M.; Foley, T. J.; Boncella, J. M.; Schanze, K. S.; Reynolds, J. R. "Near-IR LEDs Based on Poly(phenylene)/Yb-*tris*-beta-Diketonate Complexes" *Adv. Funct. Mater.*, In Press.
137. Foley, T. J.; Harrison, B. S.; Knefely, A. S.; Reynolds, J. R.; Schanze, K. S.; Boncella, J. M. *Inorg. Chem.*, Submitted.

138. Hale, G. D.; Oldenburg, S. J.; Halas, N. J. "Effects of Photo-Oxidation on Conjugated Polymer Films" *Appl. Phys. Lett.* **1997**, *71*, 1483-1485.
139. Nguyen, T.-Q.; Schwartz, B. J.; Schaller, R. D.; Johnson, J. C.; Lee, L. F.; Haber, L. H.; Saykally, R. J. "Near-Field Scanning Optical Microscopy (NSOM) Studies of the Relationship between Interchain Interactions, Morphology, Photodamage, and Energy Transport in Conjugated Polymer Films." *J. Phys. Chem. B* **2001**, *105*, 5153-5160.
140. Shin, S.-H.; Park, J.-S.; Park, J.-W.; Kim, H. K. "Poly(p-phenylene)-based Materials for Light-emitting Diodes: Electroluminescence and Photo-oxidation" *Synth. Met.* **1999**, *102*, 1060-1062.
141. Nguyen, T.-P.; Destruel, P.; Molinie, P. In *Handbook of Advanced Electronic and Photonic Materials and Devices*; Nalwa, H. S., Ed.; Academic Press: San Diego, 2000; Vol. 10.
142. http://www.roithner-laser.com/All_Datasheets/LEDs/LED970-06.pdf. (accessed March 7, 2003).
143. Baldo, M. A.; Adachi, C.; Forrest, S. R. "Transient Analysis of Organic Electrophosphorescence. II. Transient Analysis of Triplet-triplet Annihilation." *Phys. Rev. B* **2000**, *62*, 10967-10977.
144. Kang, T.-S.; Harrison, B. S.; Foley, T. J.; Knefely, A. S.; Boncella, J. M.; Reynolds, J. R.; Schanze, K. S. "Near-Infrared Electroluminescence from Lanthanide Tetraphenylporphyrin:Polystyrene Blends" *Adv. Mater.* **2002**, Submitted.
145. Walters, V. A.; de Paula, J. C.; Jackson, B.; Nutaitis, C.; Hall, K.; Lind, J.; Cardozo, K.; Chandran, K.; Raible, D.; Phillips, C. M. "Electronic Structure of Triplet States of Zinc(II) Tetraphenylporphyrins" *J. Phys. Chem.* **1995**, *99*, 1166-1171.
146. Taccheo, S.; Laporta, P.; Longhi, S.; Svelto, O.; Svelto, C. "Diode-Pumped Bulk Erbium-Ytterbium Lasers" *Appl. Phys. B* **1996**, *B63*, 425-436.
147. Scheps, R. "Upconversion Laser Processes" *Progress in Quantum Electronics* **1996**, *20*, 271-358.
148. Samoc, M.; Samoc, A.; Luther-Davies, B.; Scherf, U. "Linear and Nonlinear Optical Properties of a Ladder Poly(p-phenylene) Polymer" *Synth. Met.* **1997**, *87*, 197-200.
149. Suzuki, H. "Self-enhancement in the Electroluminescence of a Near-infrared Ionic Dye" *Appl. Phys. Lett.* **2000**, *76*, 1543-1545.

150. Pinner, D. J.; Friend, R. H.; Tessler, N. "Analysis of Polymer-based Devices" *Synth. Met.* **2001**, *124*, 41-43.
151. Lane, P. A.; Palilis, L. C.; O'Brien, D. F.; Giebeler, C.; Cadby, A. J.; Lidzey, D. G.; Campbell, A. J.; Blau, W.; Bradley, D. D. C. "Origin of electrophosphorescence from a Doped Polymer Light Emitting Diode" *Phys. Rev. B* **2001**, *63*, 235206.
152. Zhang, J.; Abe, T.; Kaneko, M. "Charge Transfer of Tetraphenylporphyrin Zinc Complexes Incorporated in a poly(2-vinylpyridine) Matrix" *J. Porphyrins Phthalocyanines* **1998**, *2*, 93-99.
153. McCarthy, T. F.; Witteler, H.; Pakula, T.; Werts, M. H. "Structure and Properties of Poly(2,5-di-n-dodecyl-1,4-phenylene) Depending on Chain Length" *Macromolecules* **1995**, *28*, 8350-8362.
154. Noh, Y.-Y.; Lee, C.-L.; Kim, J.-J.; Yase, K. "Energy Transfer and Device Performance in Phosphorescent Dye Doped Polymer Light Emitting Diodes" *J. Chem. Phys.* **2003**, *118*, 2853-2864.
155. Fujii, A.; Ohmori, Y.; Yoshino, K. "An Organic Infrared Electroluminescent Diode Utilizing a Phthalocyanine Film" *IEEE Trans. Elec. Devices* **1997**, *44*, 1204-1207.
156. Curry, R. J.; Gillian, W. P. "1.54 μm Electroluminescence from Erbium (III) tris(8-hydroxyquinoline) (ErQ)-based Organic Light-Emitting Diodes" *Appl. Phys. Lett.* **1999**, *75*, 1380-1382.
157. Sun, R. G.; Wang, Y. Z.; Zhang, Q. B.; Zhang, H. J.; Epstein, A. J. "1.54 μm Infrared Photoluminescence and Electroluminescence from an Erbium Organic Compound" *J. Appl. Phys.* **2000**, *87*, 7589-7591.
158. Koppe, M.; Brabec, C. J.; Saricic, N. S.; Eichen, Y.; Nakhmanovich, G.; Ehrenfreund, E.; Epstein, O.; Heiss, W. "Er(III) Emission from Organic Complexes Embedded in Thin Polymer Films" *Synth. Met.* **2001**, *121*, 1511-1512.
159. Ennen, H.; Schneider, J.; Pomrenke, G.; Axmann, A. "1.54- μm Luminescence of Erbium-Implanted III-V Semiconductors and Silicon" *Appl. Phys. Lett.* **1983**, *43*, 943-945.
160. Tessler, N.; Medvedev, V.; Kazaes, M.; Kan, S.; Banin, U. "Efficient Near-Infrared Polymer Nanocrystalline Light-Emitting Diodes" *Science* **2002**, *295*, 1506-1508.

161. Khreis, O. M.; Curry, R. J.; Somerton, M.; Gillian, W. P. "Infrared Organic Light Emitting Diodes Using Neodymium tris-(8-hydroxyquinoline)" *J. Appl. Phys.* **2000**, *88*, 777-780.
162. Joshi, K. C.; Pathak, V. N. "Studies in Fluorinated Beta-Diketonates and Related Compounds 3. Synthesis of Some New Piperidinium Tetrakis Rare-Earth 1, 3-Diketonates and Their Fluorescence and Infrared Spectral Studies" *J. Inorg. Nucl. Chem.* **1973**, *35*, 3161-3170.
163. He, Y.; Hattori, R.; Kanicki, J. "Light Output Measurements of the Organic Light-Emitting Devices" *Rev. Sci. Instrum.* **2000**, *71*, 2104-2107.
164. Greenham, N. C.; Friend, R. H.; Bradley, D. D. "Angular-Dependence of the Emission from a Conjugated Polymer Light-Emitting Diode -- Implications for Efficiency Calculations" *Adv. Mater.* **1994**, 491-494.

BIOGRAPHICAL SKETCH

Benjamin Scott Harrison was born April 10, 1977 in Pensacola, Florida, as the first of three children of Jeremiah and Glenda Harrison. Two years later he was joined by his brother Micah; and another three years later by his sister Melissa. Ben spent most of his life living just north of Pensacola, Florida in an area that is even now losing its rural characteristics.

Beginning in high school, Ben set his sights on becoming an electrical engineer. However, a brief meeting with Ed Webster changed his thinking. Ed was then a chemistry student at the University of West Florida (UWF) and later received a Ph.D. in chemistry at the University of Florida (UF). Ed's praise of the experience he received at UWF inspired Ben to pursue chemistry at UWF. Ben excelled in the chemistry program, eventually winning the department's highest honor—the Solutia Award (formerly the Monsanto Award), and the Top Undergraduate Award in the College of Science and Technology. Chemistry was not the only thing at UWF that came to Ben's attention. In Organic Chemistry and Calculus III classes, a bright-eyed and cheery girl named Patty Gore introduced herself to Ben. Three years later they were married.

After receiving his B.S. degree, Ben continued his studies at UF to pursue a Ph.D. in Inorganic Chemistry in 1998. On May 13, 2000, Ben and Patty were married in Patty's hometown of Americus, GA. On May 16, 2001, Patty gave birth to their first child, Jackson David. Jackson is a wonderful child with a cute smile and laugh that

people cannot resist. But one was not enough because on February 24, 2003, their daughter Theda Frances was born.

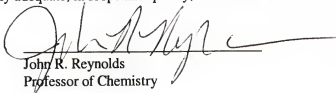
Upon graduation, Ben will be leaving the traditional chemistry field for a while. He and his family are planning to move to Clemson University where Ben will work under the direction of Physics/Materials Science Professor Dave Carroll as a postdoctoral associate. Beyond then, the future has not been written.

I certify that I have read this study and that in my opinion it conforms to acceptable standards of scholarly presentation and is fully adequate, in scope and quality, as a dissertation for the degree of Doctor of Philosophy.



Kirk S. Schanze, Chairman
Professor of Chemistry

I certify that I have read this study and that in my opinion it conforms to acceptable standards of scholarly presentation and is fully adequate, in scope and quality, as a dissertation for the degree of Doctor of Philosophy.



John R. Reynolds
Professor of Chemistry

I certify that I have read this study and that in my opinion it conforms to acceptable standards of scholarly presentation and is fully adequate, in scope and quality, as a dissertation for the degree of Doctor of Philosophy.



David E. Richardson
Professor of Chemistry

I certify that I have read this study and that in my opinion it conforms to acceptable standards of scholarly presentation and is fully adequate, in scope and quality, as a dissertation for the degree of Doctor of Philosophy.



Daniel R. Talham
Professor of Chemistry


I certify that I have read this study and that in my opinion it conforms to acceptable standards of scholarly presentation and is fully adequate, in scope and quality, as a dissertation for the degree of Doctor of Philosophy.



Haniph A. Latchman
Associate Professor of Electrical and Computer
Engineering

This dissertation was submitted to the Graduate Faculty of the Department of English in the College of Liberal Arts and Sciences and to the Graduate School and was accepted as partial fulfillment of the requirements for the degree of Doctor of Philosophy.

May 2003


Dean, Graduate School